1150.

Final Report for the

PRELIMINARY DESIGN OF THE SHUTTLE-C AVIONICS RECOVERY SYSTEM

A design project by students in the Department of Aerospace Engineering at Auburn University under the sponsorship of the NASA/USRA University Advanced Design Program.

Auburn University
Auburn University, Alabama
June 1989

. . . *Continuing Education is Essential* . . .

Final Report for the

PRELIMINARY DESIGN OF THE SHUTTLE-C AVIONICS RECOVERY SYSTEM

A design project by students in the Department of Aerospace Engineering at Auburn University under the sponsorship of the NASA/USRA University Advanced Design Program.

Auburn University
Auburn University, Alabama
June 1989

PRELIMINARY DESIGN OF THE SHUTTLE-C AVIONICS RECOVERY SYSTEM

Submitted to:

Dr. J. O. Nichols
Senior Design III
AE 449

Prepared by:

Morgan Brookfield
Deron Decker
Harold Gilbert
David Moore
Mark Rist

7 May 1989

EXECUTIVE SUMMARY

This report contains the analysis done in developing a recovery system for the Shuttle-C cargo vehicle. This recovery system is comprised of a reentry capsule which houses the venicles avionics. The avionics are contained in a single package which is extracted from the capsule by the parachute recovery system. The Shuttle-C will be able to satisfy NASA's design and mission requirements. Included, is an analysis of the structural, thermal protection, and parachute recovery systems. A discussion of the merits of the proposed system is also included.

TABLE OF CONTENTS

Executive Summary	II
List of Symbols	IV
List of Figures	VII
List of Tables	XI
Introduction	1
Discussion of Recovery Options	2
Mission Profile	6
Payload Requirements	8
Avionics Capsule Reentry Analysis	12
Avionics Capsule Structural Design	25
Avionics Package	29
Thermal Protection System	31
Reaction Control System	37
Three Stage Aerodynamic Decelerator Recovery System	41
Discussion	49
Conclusion	51
List of References	52
Appendix (Figures)	54

LIST OF SYMBOLS

Symbol	Definition	Units
A	Cross sectional area	ft^2
A_e	Nozzle exit area	ft^2
B	Constant in density-altitude relation	ft^{-1}
C_D	Drag coefficient	--
C_D	Pressure drag coefficient	--
C_P	Pressure coefficient	--
C_{Pmax}	Maximum pressure coefficient	--
C_F	Skin friction drag coefficient	--
c	Distant from neutral axis to outermost fiber of beam	in
D	Drag force	lb_f
F_{TS}	Ultimate Tensile Strength	lb_f/in^2
g	Acceleration due to gravity	ft/s^2
H	Altitude	ft
H_f	Altitude at which atmospheric drag becomes appreciable	ft
I	Moment of Inertia	in^4
I_{sp}	Specific Impulse	s
L	Lift Force	lb_f
l	Length	ft
M_u	Ultimate moment	$ft\text{-}lb_f$
M	Freestream Mach number	--
m	Mass	lb_m
$\dot{m}$	Mass flow rate	lb_m/s

LIST OF SYMBOLS (cont)

Symbol	Definition	Units
$\dot{m}_{cp}$	Mass loss rate of carbon phenolic	lb_m/s
N	Normal Force	lb_f
P_a	Atmospheric pressure	lb_f/ft^2
P_{o2}	Stagnation pressure behind normal shock wave	lb_f/ft^2
P_u	Ultimate load	lb_f
P	Freestream static pressure	lb_f/ft^2
Q	Total heat absorbed	btu
$\dot{Q}$	Average heat flow rate	btu/s
R_e	Radius of Earth	ft
r_{co}	Radius of orbit	ft
S	Section Modulus	in^3
T	Thrust provided by engines	lb_f
T_{sl}	Thrust at sea level	lb_f
t	Time	s
t_b	Instantaneous burntime	s
V	Velocity	ft/s
V_{co}	Circular orbital velocity	ft/s
V_e	Nozzle exit velocity	ft/s
V_f	Initial reentry velocity	ft/s
$\dot{V}$	Acceleration of rocket	ft/s^2
V_{cp}	Volume loss rate of carbon phenolic	in^3/s
W	Instantaneous weight	lb_f
W_t	Total weight	lb_f

LIST OF SYMBOLS (cont)

Symbol	Definition	Units
$\dot{W}_{pSRB}$	SRB propellant weight flow	lb/s
$\dot{W}_{pSSME}$	SSME propellant weight flow	lb/s
Δ	Displacement	in
α	Angle of attack of nose cone	deg
γ	Ratio of specific heats of air	---
δ	Angular displacement	deg
θ	Flight path angle, measured from horizontal	deg
θ_a	Flight path angle at maximum heating rate	deg
θ_f	Initial reentry flight path angle	deg
θ^*	Flight path angle at maximum deceleration	deg
ξ	Specific mechanical energy	ft^2/s^3
ρ	Air density	sl/ft^3
ρ_{cp}	Density of carbon phenolic	lbm/in^3
ρ_f	Air density at initial reentry point	sl/ft^3
ρ_0	Air density at sea level	sl/ft^3
ρ^*	Air density at maximum deceleration	sl/ft^3
ϕ	Angle between nose cone surface and relative velocity vector	deg
μ	Gravitational parameter	ft^3/s^2

LIST OF FIGURES

Figure	Title	Page
1	Shuttle-C Launch Configuration.	54
2	Avionics Reentry Capsule and Subsystems.	55
3	Shuttle-C Mission Profile.	56
4	Three Launch Stages to Circular Orbit.	57
5	Thrust of Solid Rocket Motors as a Function of Altitude.	58
6	Thrust of the Space Shuttle Main Engines as a Function of Altitude.	59
7	The Velocity as a Function of Time.	60
8	Thermal Protection System for the Capsule.	61
9	Reentry Capsule Angle of Attack and Coordinate System.	62
10	Approximated Reentry Capsule Geometry.	63
11	The Relationship Between Mach Number and Drag Coefficient for the Avionic Capsule.	64
12	Velocity as a Function of Altitude for Ballistic Reentry at Initial Flight Path Angles Ranging form Five to Ninety Degrees.	65
13	Total Heat Absorbed as a Function of Initial Flight Path Angle for Ballistic Reentry.	66
14	Average Heat Flow Rate per Unit Area as a Function of Initial Flight Path Angle for Ballistic Reentry.	67
15	Altitude at Maximum Heat Flow Rate as a Function of Initial Flight Path Angle for Ballistic Reentry.	68
16	Deceleration Measured in Earth g's as Function of Initial Flight Path Angle for Ballistic Reentry.	69
17	Velocity as a Function of Altitude for Ballistic Reentry at an Initial Flight Path Angle of Five Degrees.	70

LIST OF FIGURES (cont)

Figure	Title	Page
18	Mach Number as a Function of Altitude for Ballistic Reentry at an Initial Flight Path Angle of Five Degrees.	71
19	Average Heat Flow Rate per Unit Area as a Function of Altitude for Ballistic Reentry at an Initial Flight Path Angle of Five Degrees.	72
20	Deceleration Measured in Earth g's as a Function of Altitude for Ballistic Reentry at a Flight Path Angle Equal to Five Degrees.	73
21	Velocity as a Function of Altitude for Reentry with L/D Equal to 0.25 at Initial Flight Path Angles Ranging From three to Fifteen Degrees.	74
22	Total Heat Absorbed as a Function of Initial Flight Path Angle for Reentry With L/D equal to 0.25.	75
23	Average Heat Flow Rate per Unit Area as a Function of Initial Flight Path Angle for Reentry with L/D equal 0.25.	76
24	Flight Path Angle at Maximum Heat Flow Rate as a Function of Initial flight Path Angle for Reentry with L/D equal to 0.25.	77
25	Deceleration Measured in Earth g's as a Function of Initial Flight Path Angle for reentry with L/D equal to 0.25.	78
26	Flight Path Angle at Maximum Deceleration as a Function of Initial Flight Path Angle for Reentry with L/D equal to 0.25.	79
27	Velocity as a Function of Altitude for Reentry with L/D equal to 0.25 at an Initial Flight Path Angle Equal to three Degrees.	80
28	Mach Number as a Function of Altitude for Reentry with L/D equal to 0.25 at an Initial Flight Path Angle Equal to three Degrees.	81

LIST OF FIGURES (cont)

Figure	Title	Page
29	Flight Path Angle as a Function of Altitude for Reentry with L/D equal to 0.25 at an Initial Flight Path Angle Equal to three Degrees.	82
30	Deceleration Measured in Earth g's as a Function of Altitude for Reentry With L/D equal to 0.25 at an Initial Flight Path Angle Equal to three Degrees.	83
31	Average Heat Flow Rate Per Unit Area as a Function of Altitude for Reentry with L/D equal to 0.25 at an Initial Flight Path Angle Equal to three Degrees.	84
32 A-D	Capsule Structural Design With Dimensions: Side View and Sectional Views.	85
33	Plastic Hinge Diagram.	89
34	Capsule Structural Parts Identification.	90
35	Extrusion No. S 851-C Dimensions and Properties.	91
36	Extrusion No. S 851-A Dimensions and Properties.	91
37	Extrusion No. 853-F Dimensions and Properties.	91
38	Avionics Module Cutaway View With Skid Detail and Dimensions.	92
39	Temperature Ranges for the Mercury Capsules Tower Section Over a Five Hour Mission. Peak Temperature During Reentry At 4:45 hrs.	93
40	Thruster and Tank Locations of the Capsule Reaction Control System.	94
41	Location of the Three Stage Parachute Recovery System in the Reentry Capsule.	95
42	Snatch and Opening Forces as a Function of Time.	96
43	Ribbon Hemisflo Drogue and Attaching Bridal.	97

LIST OF FIGURES (cont)

Figure	Title	Page
44	Conical Ribbon Parachute.	98
45	Parachute Reefing System.	99
46	Inflated Ram-air Aerodynamic Decelerator.	100

LIST OF TABLES

Table	Title	Page
1	Shuttle-C Weight Breakdown	10
2	Payload Carrier Subsystem Detail Weight	10
3	Structural Specifications	28
4	Avionics Capsule Component Weight	29
5	Comparison of Three Types of Molybdenum Heat Shields; Looking For Low Weight And Low Skin Temperature	34
6	Weight Breakdown and Thickness of the Secondary Heat Shield for the Top and Sides of Avionics Capsule.	36
7	Weight and Location Breakdown of Avionics Equipment	38
8	Weight Breakdown of the Reaction Control System	40
9	Avionics Package Specifications	41
10	Parachute Recovery System Requirements	42
11	Ribbon Hemisflo Conical Drogue	44
12	Conical Ribbon	45
13	Ram-air Aerodynamic Decelerator	46

INTRODUCTION

The design and development of a shuttle cargo (Shuttle-C) heavy lift vehicle was recommended in the USRA/NASA design proposal submitted Fall quarter 1988. The Shuttle-C design would incorporate existing space technology wherever possible. The vehicle configuration and supporting elements would utilize developed and proven NSTS or other existing hardware, software, and operational procedures to the fullest extent practical. The Shuttle-C vehicle is to be compatible with the NSTS transportation system, launch site facilities, ground support equipment, and launch processing systems, except where deviation is required to satisfy Shuttle-C objectives. Figure 1 illustrates the Shuttle-C launch configuration.

Since the submission of the proposal, NASA has announced plans to begin construction of a prototype, fully expendable Shuttle-C vehicle. However, in order to reduce the life-cycle-cost of the Shuttle-C program, the design team chose to pursue the development of methods of recovering the vehicle's SSME's and avionics. The incorporation of a recovery system will not compromise the Shuttle-C's ability to fulfill NASA's design requirements or mission objectives.

DISCUSSION OF RECOVERY OPTIONS

The relative advantages and disadvantages of four Shuttle-C recovery options are summarized in this section. These options are: recovery of the SSME's by modified boattail atmospheric reentry, recovery of both the SSME's and the avionics by P/A module reentry, recovery of the avionics by EVA and return on a manned shuttle flight, and recovery of the avionics by avionics capsule reentry. Each design option is evaluated in terms of development time, cost, and its compatibility with the existing National Space Transportation System.

P/A Module

The propulsion/avionics module is the most attractive option in that both main engines and avionics are recovered. However, a P/A module requires the complete redesign of the propulsive system's housing and attachment with the payload carrier. Two major obstacles associated with this redesign are: the successful interface of the P/A module with the existing National Space Transportation System and the protection of the avionics from the heat and vibrations generated by the Shuttle-C 's propulsion systems. The development time and cost required to solve these problems eliminates the P/A module as a viable Shuttle-C recovery option.

Mcdified Boattail

Unlike the P/A module, this option calls for minimal redesign of the existing shuttle boattail to ensure compatibility with existing NSTS facilities and reduce development time. The boattail's structure and thermal protection system would both have to be redesigned. Because the boattail's aft cross-sectional area is greater than the cross-sectional area of the boattail-payload carrier interface, an ablative heat shield appended to the front of the boattail provides inadequate thermal protection. The bcattail's reaction control system needs to be reconfigured to both provide attitude control for the separated boattail and to maintain, in conjunction with the nose cone's reaction control system, control over all six degrees of freedom for the entire Shuttle-C vehicle. A secondary avionics package would have to be installed in the boattail to provide autonomous guidance, navigation, and control. Therefore, the money and time required to redesign, develop, test, and evaluate a boattail reentry system exceeds the net return of recovering the SSME's. This conclusion is further strengthened by NASA's announcement that the SSME's life span is rated at ten flights, and that only SSME's with one flight remaining would be used on Shuttle-C missions.

Manned Recovery of the Avionics

Recovery of the avionics by EVA requires only minimal design alterations to NASA's fully expendable, prototype design. Thus, this option is advantageous from a development time and cost standpoint. However, recovery is dependent upon the ability of the manned shuttle program. Since the Challenger accident, the manned program has been pressed to meet the needs of the Defense Department and the scientific community. The addition of a manned shuttle mission designed to recover the Shuttle-C's avionics is inconsistent with the findings of the President's Commission on the Challenger accident. The commission found "the capabilities of the system (the space shuttle program) were stretched to the limit to support the flight rate in winter 1985/1986." (1:176) As a result of this conclusion, manned recovery of the avionics by EVA was abandoned.

Avionics Reentry Module

This recovery option utilizes developed and proven space technology to the fullest extent; conic shaped reentry vehicles have been used since the early manned space programs. The conic nose of the Shuttle-C would be replaced by a conic shaped reentry capsule which would contain the avionics package. The capsule's structure and thermal protection system would have to be designed to accommodate the loads and heating rates experienced during low lift reentry. The reaction control system must maneuver the

capsule away from the payload carrier and maintain attitude control during reentry. The principal merits of this design are: easy integration with the existing NSTS program and a minimal design, development, test, and evaluation period. Therefore, the design team selected to pursue the avionics reentry module option.

The avionics reentry capsule consists of three subsystems: a conic shroud, an avionics package, and a three stage parachute recovery system. Figure 2 displays the reentry capsule and each of these components. A typical mission profile for a Shuttle-C vehicle outfitted with an avionics recovery system follows. (Figure 3)

MISSION PROFILE

I. INTEGRATION OF VEHICLE

A. Cargo vehicle is shipped from production center to Cape Kennedy.
B. Vehicle is "turned on" and the electrical and hydraulic systems are checked.
C. The solid rocket boosters and external fuel tank are mated to the vehicle.
D. The SSME's are mounted into the vehicle.
E. Cargo is integrated into the cargo bay.
F. Vehicle is rolled out to the pad.

II. THE LAUNCH

A. Final vehicle flight readiness checks are made.
B. Weather conditions and launch windows are checked.
C. Vehicle launches.
   a. Main engines ignite.
   b. Vehicle clears tower and control switches from Cape Kennedy to Houston.
   c. Vehicle rolls onto its back.
   d. Vehicle passes through maximum dynamic pressure.
   e. Solid rocket boosters are released.
   f. Main engines are cut off. (MECO)
   g. External tank is jettisoned.
   h. OMS engines burn to place the vehicle in a 28.5 degree 220 nm orbit.

III. EXECUTION OF THE MISSION

A. Vehicle verifies its orbit and corrects for error.
B. Vehicle blows off cargo bay doors to release launch heat and expose cargo.
C. Vehicle maneuvers to a position to deploy cargo or prepares to dock with the space station.
D. Vehicle unloads cargo or docks with space station.
E. Vehicle prepares for deorbit.

IV. DEORBIT

A. Vehicle places itself on a deorbit vector for a specified landing coordinate.
B. Vehicle uses the reaction control system to position itself for retro firing. (Nose pointing opposite the velocity vector)
C. OMS burn reduces the velocity of the vehicle.
D. Electrical system is turned off except to the nose cone in order to prevent fires during separation.

E. Avionics capsule separates from the cargo bay.
   a. Once clear automatic thrusters on the cargo bay will begin a slow tumble of the remainder of the vehicle to ensure burn up.
F. Avionics capsule, using its independent control system, guides itself onto the proper reentry vector.

V. REENTRY

A. Avionics capsule begins to enter the atmosphere.
B. Heating reaches maximum and blackout of communications occurs.
C. Aerodynamic effects help to stabilize the vehicle.
D. Mortar deploys drogue parachute.
E. Second stage parachute deploys and the avionics package is extracted from the capsule.
F. Third stage flexible wing is deployed.
G. Flexible wing is guided to the dry lake bed at Edward's Air Force Base by radio control.
H. Avionics package lands on skids on the dry lake bed.
I. Avionics are removed, refurbished and prepared for the next Shuttle-C flight.

PAYLOAD REQUIREMENTS

The incorporation of the avionics recovery system will not compromise the Shuttle-C's ability to satisfy NASA's mission requirements. This section demonstrates that the Shuttle-C with the additional weight of the recovery system can fulfill the primary payload requirement: the placement of at least 100,000 pounds into a circular 220 nmi low earth orbit with a 28.5 degree inclination. The velocity required to maintain a circular orbit is determined from the following expression. (2:34)

$$V_{cs}^2 = \left(\frac{\mu}{r}\right)^{\frac{1}{2}} \qquad (1)$$

For a 220 nmi circular orbit the required velocity is 25,146.023 ft/s. This required velocity must be attained by the Shuttle-C after its final burn to achieve this circular orbit.

The equation of motion for the Shuttle-C is (2:6)

$$\mathbf{m \times V = T - W} \qquad (2)$$

The drag force is assumed negligible in comparison to the thrust and weight forces. The final velocity of the Shuttle is determined by integrating the equation of motion

$$V = \int_0^{t_b} \left(\frac{g(T - W\sin\theta)}{W} \right) dt \qquad (3)$$

The gravity term in the equation varies inversely as the square of the distance from the center of the earth. (3:380)

$$g = g_0 \left(\frac{R_o}{R_o + H} \right)^2 \qquad (4)$$

The instantaneous weight depends upon the shuttle's stages of flight: initial boost, second stage, or glide stage. In the initial boost stage, the instantaneous weight is given by

$$W = W_t - W_{pSSME}(t_b) - W_{pSRB}(t_b) \qquad (5)$$

The Shuttle-C's total takeoff weight is detailed in Tables 1 and 2. For the second stage, the instantaneous weight is given by equation (5) minus the SRB weight term. During the third stage, the glide stage, the change in velocity is negligible (see figure 4).

Table 1. Shuttle-C Weight Breakdown

		Weight (lbf)	
SRB Propellant	-	1,107,201	
Inert	-	193,155	
Subtotal	-		1,300,356
ET Propellant	-	1,603,431	
Inert	-	67,998	
Subtotal	-		1,671,429
Shuttle-C			
Payload	-	150,000	
Strongback	-	17,448	
Shroud	-	7,682	
Payload Carrier	-	24,181	
Boattail	-	55,197	
Nose Cone	-	11,020	
Subtotal	-		265,528
Total	-		3,237,313

Table 2. Payload Carrier Subsystem Detail Weight

	Weight (lbf)
Structures	23,778
Avionics & Electrical Power System	4,610
Separation Systems	1,043
Induced Environmental Protection	2,249
Contingency (Total)	4,372
Payload Carrier Weight (Dry)	36,052
Payload Carrier Weight On-Orbit (Dry)	24,181

The top main engine is pitched 16.0 degrees and the bottom two main engines are pitched at 13.5 and yawed at 3.5 degrees. (4:2) As with the instantaneous weight, the

thrust depends upon the shuttle's stages of flight. In the initial boost stage the thrust is given by

$$T = 2\,T_{SRB} + T_{SSME}\cos 16^\circ + 2\,T_{SSME}\cos 13.5^\circ \cos 3.5^\circ \qquad (6)$$

In the second stage, the thrust is given by equation (6) minus the SRB's thrust. The third stage thrust is negligible. The thrust terms on the right side of equation (6) are a function of altitude and are calculated from the following equation (5:5)

$$T(x) = T_{sl} + (P_{asl} - P(x))A_e \qquad (7)$$

The thrust of a SSME and a SRB as a function of altitude are shown in Figures 5 and 6.

The solution to equation (3) cannot be readily obtained due to the complexity of the variables, but by using a step-wise integration with a time step of two seconds, the velocity history over the first and second stages is determined and shown in Figure 7. The velocity at the end of the second stage, the final velocity, equals 25,220.2 ft/sec, enabling the Shuttle-C to achieve a stable 220 nmi orbit.

AVIONICS CAPSULE REENTRY ANALYSIS

The avionics capsule is designed for a Mercury type capsule reentry with a carbon phenolic ablative heat shield at the base and a molybdenum-beryllium thermal protection system tapering up the sides (Figure 8). The capsule will reenter the atmosphere at an angle of attack which ensures that the maximum heated zone occurs at the base. Angle of attack is defined as the angle between the relative velocity vector and the x-axis of the capsule, see Figure 9. This angle of attack restriction limits the options for reentry trajectory to: ballistic entry (lift-to-drag ratio equal to zero) at initial flight path angles ranging, from five to 90 degrees and reentry with lift-to-drag ratios between 0.25 and 1.00 at initial flight path angles ranging, from three to 15.0 degrees. (7:6) Lift-to-drag ratios higher than 0.25 require angles of attack that expose the shroud sides to temperature gradients greater than the molybdenum-beryllium thermal protection system can withstand and must be avoided. The reentry parameters; i.e., heat transfer and deceleration force, associated with both types of reentry are examined in the following sections.

Drag Coefficient

Both reentry trajectories depend upon the capsule's drag coefficient. The major contribution to the capsule's drag is pressure drag; skin friction is negligible. For

preliminary drag coefficient calculations, the capsule's geometry is approximated as a conical nose with an spherical base and a sharp, pointed top. (See Figure 10) The variation in drag coefficient with angle of attack is assumed negligible. Thus, the total drag force coefficient is equal to the axial force coefficient at zero angle of attack. The zero lift pressure drag coefficient for bodies of revolution is given by (8:1-3)

$$C_D = \frac{2}{y_{max}^2} \int_0^1 C_p \, y \, \frac{dy}{dx} \, dx \tag{8}$$

For Mach numbers, ranging between two and thirty, the flow field can be modeled with Newtonian theory. (9:484-486) Mach numbers below two are not considered because parachute system deployment is expected around Mach two. The pressure coefficient is given by

$$C_p = C_{p_{max}} \sin^2 \phi \tag{9}$$

where

$$C_{p_{max}} = \frac{2}{\gamma M_\infty^2} \left[\frac{P_{0_2}}{P_\infty} - 1 \right] \tag{10}$$

and

$$\frac{P_{0_2}}{P_\infty} = \left[\frac{(\gamma+1)^2 M_\infty^2}{4\gamma M_\infty^2 - 2(\gamma-1)} \right]^{\frac{\gamma}{\gamma-1}} \left[\frac{1 - \gamma + 2\gamma M_\infty^2}{\gamma+1} \right] \tag{11}$$

For initial design calculations the ratio of specific heats for air will be considered constant and equal to 1.4 at all altitudes. Upon substituting the appropriate geometry into the above relations, the drag coefficient becomes a function of the freestream Mach number alone. The relationship between Mach number and drag coefficient is presented in Figure 11.

Angle of Attack

To generate lift, the capsule must be at a negative angle of attack. The optimum lift-to-drag ratio for the cone is about 0.25. The relationship between lift and drag forces with normal and axial forces is

$$L = N\cos\alpha - A\sin\alpha \tag{12}$$

$$D = N\sin\alpha + A\sin\alpha \tag{13}$$

Assuming that the normal force is negligible, the lift-to-drag ratio is obtained by dividing equation (12) by equation (13).

$$\frac{L}{D} = -\tan\alpha \tag{14}$$

Solving for the angle of attack yields

$$\alpha = -14.0 \text{ degrees}$$

In order to generate a lift-to-drag ratio equal to 0.25, the shroud will enter the atmosphere at an angle of attack equal to negative fourteen degrees.

Ballistic Reentry

A first order velocity and flight path angle solution for ballistic entry (L/D=0) at large initial flight path angles, ranging from five to 90 degrees is given by ref 7:103-104. The flight path angle at any time after reentry is a function of altitude, velocity and the initial reentry state; i.e., initial reentry velocity and flight path angle.

$$\cos\theta = \frac{\cos\theta_f}{1+\left(\frac{1}{BR_0}\right)\left(\frac{gR_0}{V^2}-1\right)\left(1-\frac{\rho_f}{\rho}\right)} \tag{15}$$

Since, $1/BR_o = 1/900$ for earth

$$\left(\frac{1}{BR_0}\right)\left(\frac{gR_0}{V^2}-1\right)\left(1-\frac{\rho_f}{\rho}\right) \ll 1 \tag{16}$$

equation (15) reduces to

$$\cos\theta = \cos\theta_f \tag{17}$$

Thus, for ballistic reentry the flight path angle can be considered to be constant. The instantaneous vehicle

velocity is a function of altitude, the geometrical and aerodynamical characteristics of the reentry vehicle, and initial reentry state.

$$V = \left[V_f^2 \, e^{\left\{ \left(\frac{-C_D A}{m B} \right) (\rho - \rho_f) \frac{1}{\sin \theta_f} \right\}} \right]^{\frac{1}{2}} \tag{18}$$

The deceleration experienced by the vehicle is

$$\frac{dV}{dt} = \frac{B}{2} (\sin \theta) \, V^2 \ln \left[\frac{V^2}{V_f^2} \right] \tag{19}$$

and the maximum deceleration is a function of initial entry conditions alone

$$\left(\frac{dV}{dt} \right)_{max} = \frac{-B}{2e} (\sin \theta_f) \, V_f^2 \tag{20}$$

The maximum deceleration experienced by a reentry vehicle depends solely upon the initial flight path angle and the initial velocity. The altitude density at which the maximum deceleration occurs is

$$\rho^* = \frac{mB}{C_D A} \sin \theta_f + \rho_f \tag{21}$$

and the velocity at maximum deceleration is

$$V_{\left(\frac{dV}{dt} \right)_{max}} = 0.607 \times V_f \tag{22}$$

A generalized aerodynamic convection heating analysis is given in ref 7:182,189-190. The effects of gaseous imperfections and shock wave boundary-layer interactions are neglected. Prandlt number is assumed constant, and Reynolds analogy is applicable. For reentry from low earth orbits, convection is the only meaningful mode of heat transfer. (9:482) Thus, the aerodynamic heating environment of the capsule during reentry can be sufficiently modeled by convection heat transfer analysis alone.

The total heat input into the vehicle is a function of the vehicle's aerodynamic and geometrical properties and its velocity.

$$Q = \frac{m}{4}\left(\frac{C_F S}{C_D A}\right)\left(V_f^2 - V_f\right) \tag{23}$$

The average heat flow rate per unit area is a function of altitude, skin friction coefficient, and vehicle velocity.

$$\frac{\dot{Q}}{A} = \frac{1}{4}\rho V^3 c_F \tag{24}$$

The maximum average heat flow rate per unit area is

$$\left(\frac{\dot{Q}}{A}\right)_{max} = \frac{B}{6e}\frac{C_F}{C_D A} m V_f^3 \sin\theta_f \tag{25}$$

The maximum average heat flow for a given body is a function of the initial reentry state. The altitude at which the maximum average heat flow rate occurs is

$$H = H_f - \frac{1}{B} \ln\left(\frac{3}{2} \frac{C_D \rho_0 A}{B\, m \sin\theta_f}\right) \tag{26}$$

The velocity, maximum deceleration, total heat, maximum average heat flow rate per unit area, and altitude at maximum average heat flow rate are calculated for ballistic reentry for initial reentry flight path angles, ranging from five to 90.0 degrees. Since atmospheric drag does not appreciably effect a spacecraft with a short orbit duration until about 50 nmi (2:153), the initial reentry velocity and density of the capsule are its velocity and density at 50 nmi. Assuming reentry from a circular orbit the velocity of the capsule is obtained from (2:34)

$$V_f = \sqrt{\frac{\mu}{r_{cs}}} \tag{27}$$

$$V_f = 25733.0 \text{ ft/s}$$

The initial reentry density is obtained form (7:12)

$$\rho = \rho_0 e^{-BH} \tag{28}$$

$$\rho_f = 2.333 \times 10^{-9} \text{ slugs/ft}^3$$

The initial reentry velocity and density are both constants; therefore, the initial flight path angle is the only initial reentry state variable. The mass of the avionics recovery vehicle is assumed to be 10,000 lbm and its geometry is based on the approximated geometry used for drag coefficient calculations.

The ballistic reentry results are represented in Figures 12 to 16. Reasonable results are obtained except at altitudes below about 90,000 ft. This results from the variation in drag coefficient associated with Mach numbers below Mach five. However, the general trend in the reentry parameters is displayed and the data extrapolated to the lower altitudes. The maximum deceleration force is directly proportional to the initial reentry flight path angle and ranges from -14 g's to -161 g's; thus, the larger the initial flight path angle the slower the capsule velocity at parachute recovery system deployment. The total heat varies inversely with initial reentry flight path angle while the average heat flow rate varies directly with flight path angle. High initial flight path angles are desired to reduce the weight and size of the capsule's ablative heat shield; however, the penalty in structural size and weight needed to sustain the high deceleration loads offsets this advantage. In fact, due to the high deceleration force associated with ballistic entry, only reentry at an initial flight path angle equal to five degrees is practical. The

relationships between velocity, Mach number, deceleration, and average heating rate with altitude for ballistic reentry at an initial flight path angle equal to five degrees are represented in Figures 17 to 20.

Reentry at Lift-to-Drag Ratios between 0.25 and 1.00

First order solutions for velocity and flight path angles at lift-to-drag ratios between 0.25 and 1.00 at initial flight path angles, ranging from three to 15.0 degrees, is also given in ref 7:74-75. The flight path angle at any time after atmospheric reentry is a function of lift-to-drag ratio, vehicle geometry, and altitude.

$$\theta = \sqrt{\theta_f^2 \left(\frac{L}{D}\right) \left(\frac{C_D A}{m B}\right) (\rho - \rho_f)} \qquad (29)$$

The velocity is a function of the lift-to-drag ratio, flight path angle, and initial reentry state.

$$V = \sqrt{V_f^2 \exp\left(\frac{-2}{L/D} (\theta_f - \theta)\right)} \qquad (30)$$

The vehicles instantaneous deceleration is given by

$$\frac{dV}{dt} = \frac{-B}{L/D} \left(\cos\theta - \cos\theta_f\right) V_f^2 \exp\left(\frac{-2}{L/D} (\theta_f - \theta)\right) \qquad (31)$$

and the maximum deceleration is

$$\left(\frac{dV}{dt}\right)_{max} = \frac{-B}{L/D}\left(\cos\theta^{*} - \cos\theta_f\right) V_f^2 \exp\left(\frac{-2}{L/D}\left(\theta_f - \theta^{*}\right)\right) \tag{32}$$

where

$$\theta^{*} = \frac{L/D}{2}\left[\sqrt{1 + \left(\frac{2}{L/D}\theta_f\right)^2} - 1\right] \tag{33}$$

Therefore, for a given lift-to-drag ratio, the maximum deceleration is a function of initial reentry flight path angle and initial reentry velocity. The velocity at which the vehicle experiences maximum deceleration is

$$V^2_{\left(\frac{dV}{dt}\right)_{max}} = V_f^2 \exp\left[\frac{-2}{L/D}\left(\theta_f - \theta^{*}\right)\right] \tag{34}$$

and the altitude density at maximum deceleration is

$$\rho^{*} = \frac{\cos\theta^{*} - \cos\theta_f}{\left(\frac{1}{2}\right)\left(L/D\right)\left(\frac{C_D A}{m B}\right)} + \rho_f \tag{35}$$

Using the same assumptions as those made for the ballistic aerodynamic heating analysis, a generalized aerodynamic convection heating analysis for reentry at lift-to-drag ratios between 0.25 and 1.00 for initial reentry flight path angles, ranging from three to 15.0

degrees is also given in ref 7:188. The total heat absorbed by the reentry body is a function of the vehicle's geometric and aerodynamic properties and velocity.

$$Q = \frac{C_F S}{C_D A} \frac{1}{4} m\left(V_f^2 - V^2\right) \tag{36}$$

The average heat flow rate per unit area is a function of vehicle geometry, lift-to-drag ratio ,flight path angle, and the initial reentry state.

$$\frac{\dot{Q}}{A} = \frac{1}{2} \frac{C_F}{C_D A} \frac{B m}{L/D} V_f^3 \left(\cos\theta - \cos\theta_f\right) \exp\left[\frac{-3\left(\theta_f - \theta\right)}{L/D}\right] \tag{37}$$

The maximum average heat flow rate per unit area is

$$\left(\frac{\dot{Q}}{A}\right)_{max} = \frac{B m}{6} \frac{C_F}{C_D A} V_f^3 \sin\theta_a \exp\left[\frac{-3\left(\theta_f - \theta_a\right)}{L/D}\right] \tag{38}$$

where

$$\theta_a = \tan^{-1}\left(\frac{3}{L/D}\right) - \sin^{-1}\left[\frac{\cos\theta_f}{\sqrt{1+\left(\frac{L}{3D}\right)^2}}\right] \tag{39}$$

Thus, for a given vehicle and a given lift-to-drag ratio the maximum average heat flow is dependant on the initial reentry state.

The velocity, maximum deceleration, total heat absorbed, average maximum heating rate per unit area, flight

path angle at maximum heat flow rate, and the angle at maximum deceleration are calculated for reentry with L/D equal to 0.25 at initial flight path angles ranging from three to 15.0 degrees. Results of these calculations are represented in Figures 21 through 26. As with ballistic entry, the deceleration and the average heat flow rate both vary directly with initial flight path angle while total heat varies inversely with flight path angle. The difference in both total heat absorbed and average heating rate between reentry with L/D equal to 0.25 and ballistic reentry is negligible. However, the difference in magnitude between the maximum deceleration forces is dramatic. For reentry with L/D equal to 0.25 the maximum deceleration force ranges from around negative three g's to -32 g's. Thus, reentry with L/D equal to 0.25 is preferable to ballistic entry. The difference in total heat absorbed between reentry at large initial flight path angles and reentry at small initial flight path angles is negligible compared to the difference in deceleration forces. Thus, the capsule is designed to enter the earth's atmosphere at an initial flight path angle equal to three degrees with a lift-to-drag ratio of 0.25. This reentry trajectory minimizes the total weight of the avionics recovery vehicle. The relationships between velocity, Mach number, flight path angle, deceleration, and average heating rate with altitude for reentry with L/D equal to 0.25 at an initial flight path

angle equal to three degrees are represented in Figures 27 through 31. The angles at maximum deceleration and maximum heat flow rate and the altitude density at maximum deceleration for reentry with L/D equal to 0.25 at an initial flight path angle of three degrees are:

$$\theta^{*} = 0.603 \text{ deg}$$

$$\theta_{a} = 0.840 \text{ deg}$$

$$\rho^{*} = 0.0002869 \ {}^{\text{slugs}}/_{\text{ft}^3}$$

AVIONICS CAPSULE STRUCTURAL DESIGN

The initial structural design presented here for the avionics reentry vehicle is based upon the structure of the Apollo capsule. Just as in the Apollo capsule, the Shuttle-C capsule has an internal structure of beams and bulkheads covered by an outer skin. The reentry vehicle differs from the Apollo capsule in that it has six rather than four internal formers. It also has more bulkheads due to the larger size of the capsule. (10:VI-1)

The structural design of the capsule section is depicted in Figure 32A-D. The sizing of the major structural components of the capsule is based upon the 4 g maximum reentry load anticipated. The reentry load is selected as the worst case loading because it is the highest load encountered during the mission. The size of the main structural formers in the base of the capsule (Figure 32B) is determined using the plastic hinge method to determine the ultimate moment experienced by these members (Ref. 11).

The plastic hinge method determines ultimate moment by predicting the failure mechanism of a structure. The internal work done by the resisting moment of the beam and the external work done by the load are equated. The equation that results gives the ultimate moment of the beam as a function of the load.

Figure 33 shows the anticipated failure mechanism of the main structural members in section A-A. Several assumptions were made to determine the load P_u. The load is assumed to be one-sixth of the total reentry load because the load is divided equally among the six formers and is assumed to be concentrated along the centerline of the capsule. In addition, the contribution of the skin in resisting the deflection due to the load is neglected. These assumptions present the highest load that could occur on the former. Actual loading will probably be lower since the load is distributed about the base of the capsule and is resisted by the skin.

The internal work done by the deflecting beam and the external work done by the force P_u can be equated to get equation 40.

$$P_u \Delta = M_u 2\delta \tag{40}$$

Using the geometry of the failure mechanism, the displacement and turning angle can be eliminated by substituting equation 41 into 40 to obtain equation 42.

$$\tan\frac{\delta}{2} = \frac{\delta}{2} = \frac{\Delta}{2l} \tag{41}$$

$$M_u = P_u \frac{l}{2} \tag{42}$$

Equation 42 represents the ultimate moment experienced by the beam in terms of the load. With a load of 7333 lbs (i.e. one-sixth of the 4-g reentry load) the ultimate moment

is 26277.8 ft-lbf. Beams in section A-A are selected using this moment as a criteria. The side formers of section A-A through D-D are made of the same material as the base formers. These formers are made this size because they must transmit the moment from the base formers to the bulkheads. Formers from section D-D through F-F are reduced in size to save weight. This reduction can be made without a loss in strength because these formers do not directly resist the reentry load. The formers from section F-F to H-H are again reduced in size because they do not resist the reentry load. In addition, the section from F-F up is a closed volume making it inherently more rigid.

Aluminum alloy 7178-T6 is used for all structural components. This material is chosen because it has a high ultimate strength, and is commonly used for aircraft structures. (12:115)

As stated in the previous section, structural members are sized using ultimate moment as a criterion. The ultimate moment that the I-beam formers can withstand is determined from the following formula. (13:100)

$$M_u = F_{TS} S \tag{43}$$

Where F_{TS} is the ultimate tensile strength and S is the section modulus.

Table 3 lists the structural members, standard specification numbers for the sections used, and the weights of the members. The covering for the conic surface of the capsule is not included in this list because it is part of the thermal protection system. Identification letters for the various parts refer to Figure 34. Figures 35, 36, and 37 show the beam sections used in the formers.

Table 3 Structural Specifications

Member*	Nomenclature	Section I.D.	No.	Weight Each(lb)	Total Weight(lb)
a	Base Plate	.25" plate	1	1055.9	1055.9
b	Release Mechanism	N/A	1	50.0	50.0
c	Base Former	S 851-C[1]**	6	21.9	131.1
d	Main Side Former	S 851-C	6	27.0	162.1
e	Secondary Side Former	S 851-A[2]	6	10.8	64.7
f	Tip Former	853-F[3]	6	0.7	4.2
g	Bulkhead B	.125" plate	1	311.5	311.5
h	Bulkhead C	.125" plate	1	220.2	220.2
i	Bulkhead D	.125" plate	1	148.8	148.8
j	Bulkhead E	.125" plate	1	82.4	82.4
k	Bulkhead F1	.125" plate	1	28.2	28.2
l	Bulkhead F2	.125" plate	1	57.3	57.3
m	Ring Former G	.125" plate	1	4.8	4.8
n	Ring Former H	.125" plate	1	3.7	3.7
o	Avionics Bay Sides	.125" plate	4	72.7	290.9
				TOTAL	2615.7

* Member identification refers to Figure 34.
** See Figure 35[1], 36[2] 37 [3] for section dimensions and properties.

AVIONICS PACKAGE

The Shuttle-C avionics package is housed in the reentry capsule. The avionics package is extracted from the capsule, reducing the weight supported by the parachute recovery system, and glides to a pinpoint landing under the flexible wing. The package is equipped with shock absorbing skids which cushion impact. Figure 38 shows a cutaway view of the proposed avionics package and the avionics package dimensions. Included in Figure 38 is a detail drawing of the skids on the base of the package.

The avionics package contains four batteries for power and a control system for the ram-air decelerator. A projected weight breakdown of the components of the avionics package is located in Table 4.

Table 4. Avionics Module Component Weights

Component	Weight(lbs)
Structure Weight (includes skids)	500
Batteries	600
Avionics	1000
Control System	50
TOTAL	2150

The control system for the avionics package consists of three subsystems: the automatic guidance, navigation, and control system, remote control system, and the servo

actuator system as shown in Figure 38. The automatic guidance system is designed to autonomously place the package in the vicinity of the landing area. After the module is within visual range, a ground operator will guide the package to a soft landing, using the remote control system. The automatic and remote control guidance system gives control input to the flexible wing through the servo actuators. The servo actuators control the flexible wing by reeling in and letting out control lines.

THERMAL PROTECTION SYSTEM

The thermal protection system for the reentry vehicle is divided into two basic parts. The first part is the ablative heat shield which protects the vehicle from the greatest heat transfer. The secondary shield protects the sides and top of the vehicle in areas of lower heat transfer. The capsule shape, a blunt body, conforms to the proper shape for extreme hypersonic aerodynamic conditions. The ablative heat shield is attached to the capsule base. The secondary heat shield covers the remainder of the shroud. Figure 7 shows the shape and dimensions of the capsule. The ablative heat shield and the secondary heat shield characteristics are discussed below.

Ablative Heat Shield

For rapid deceleration in the lower atmosphere ablative thermal protection systems are efficient and effective. (7:200-201) Heat is dissipated in the sublimation of the ablative material and convected away in the resulting gaseous efflux. Plus, as the ablative material burns it leaves behind a char layer that acts as an insulator, further lowering the heat transferred to the interior structure. (14:1-6)

A carbon phenolic shield is chosen as the ablative heat shield because of its low thermal conductivity. Carbon phenolic is 90% carbon, 7% oxygen, and 3% hydrogen. (15:6)

Thus, the density of phenolic carbon is slightly higher than carbon or approximately

$$= 0.085 \ {}^{lbm}/_{in^3}$$

A rough approximation for the volume loss rate and mass loss rate is obtained from data given in ref 16:266-267,269.

$$\dot{m}_{C_p} = 0.0001582 \, lbm/s$$

$$\dot{V}_{C_p} = 0.0019385 \, in^3/s$$

Assuming an effective heating time of about 20 minutes based on the Mercury missions and an average heat shield thickness of 0.32 in. across the base of the capsule, the weight of the carbon phenolic shield is approximately 1000 lbm.

Secondary Thermal Protection System

Based on experiences from the Mercury program, the side wall maximum temperature is estimated to be no greater than 2500 F (16:2). From this assumption, thermal protection systems are examined in terms of their ability to keep the internal structure cool, the weight of the system, and the simplicity in the system. The different thermal protection

systems investigated included silicon tiles, ceramic plates, structurally cooled systems, and insulated molybdenum structures.

The only system that meets all three criteria is the insulated molybdenum system. Figure 7 shows a cross-section view of the lower secondary heat shield. The outer wall is an alloy of coated molybdenum with a thickness of .0320 inches. The selection of molybdenum is based on the metals extremely high melting point of 4734 F. To keep the internal structure cool over the entire time of reentry, the system requires insulation. In experimental tests at Bell Laboratories, the necessary insulation thickness for the system was found to be .75 inches of ADL-17 packaged powder insulation. Following the insulation is .75 inches of airspace. A regenerative water cooling system absorbs any excess heat. The water runs through tubing into the airspace surrounding the aluminum skin. By spraying the water into the airspace, and circulating the water through piping behind the aluminum skin, the internal temperature of the reentry capsule will remain at or below 200 F. At 200 F aluminum retains 98% of its strength. (17:111-121).

The weight of the insulated molybdenum is the next area of concern. In the Bell Laboratories' experiment (see Table 5) three different amounts of insulation were used with varying amounts of water in the coolant system. The test system chosen, as described above, has an overall density of

4.086 lbs/ft^2. Although the .75 inch thick insulation system requires more water than the other two insulation systems, the reduction in insulation weight offsets the weight penalty of the additional water. The total weight of the thermal protection system is then found by multiplying the density of the secondary heat shield by the surface area of the capsule side. The total weight is 2500.0 lbs, including 500 lbs of water for the cooling system.

Table 5 Comparison of three types of molybdenum heat shields; mission requires low weight and low skin temperature.

TEST RUN	INSULATION THICKNESS	DENSITY	WEIGHT	WATER WEIGHT	TOTAL WEIGHT	SKIN TEMP.
1	1.5 in.	3.924	2211.3	0.0	2211.3	1000 F
2	1.5 in.	4.299	2422.4	357.8	2780.3	200 F
3	0.75 in.	3.549	2000.0	485.0	2485.0	200 F

The coolant system requires a titanium water tank. The tank is composed of a .035 inch thick titanium plate rolled into a cylinder capped by two spherical ends (17:138). The radius of the cylinder and the spheres is two feet. The length of the cylinder section is 3.25 feet. The total weight of the water tank is calculated to be 74.7 lbs.

Although, the molybdenum system is not the least dense system available, it is the least complex system to build.

Other systems, such as silica tiles, are less dense but are more costly to manufacture. The molybdenum system offers a quick and easy solution to reentry temperature problems on the side walls of the capsule.

Since weight is a major concern of this project, a different heat shield is used for the uppermost portion of the capsule. As the distance from the base increases, the temperature decreases. Mercury flights discovered (see Figure 39) that at the farthest area from the shock wave during reentry, in this case the tip of the capsule, temperatures were in the range of 1200 F (18:3). The metal selected is beryllium. Beryllium has a melting point of 2300 F, adequate for temperature ranges from 1000 to 2000 F. Although beryllium's melting point is lower than molybdenum's, the low weight of beryllium offsets the loss in safety margin. Beryllium's density is 115 lbs/cubic feet, while molybdenum's is 637.6 lbs/cubic feet. The difference in density results in a weight savings of approximately 628.8 lbs. (19:5101 1-13). The capsule tip will also be cooled using the water system described above. The insulation for the top section will be .75 inches thick with a weight of ten pounds. The total weight of the upper section of the secondary heat shield will be 154.4 lbs. No developmental problems are foreseen with the beryllium casing.

Overall, the secondary heat shield should adequately protect the avionics from the extreme temperatures experienced during reentry. The molybdenum section of the heat shield will take the brunt of the heat on the side walls. During further thermodynamic tests the insulation thickness may be able to be varied to further reduce the weight of the molybdenum section of the heat shield. Table 6 lists a breakdown of the weights for the heat shield. Note the total weight for the entire secondary heat shield is 2,727.7 lbs.

Table 6 Weight breakdown and thickness of the secondary heat shield for the top and sides of the Shuttle-C reentry capsule.

HEAT SHIELD ITEM	DENSITY (lb/ft^2)	AREA (ft^2)	WEIGHT (lb)
Insulated Molybdenum	3.549	563.5	2000.0
molybdenum	1.700	563.5	957.9
insulation	0.750	563.5	422.6
aluminum skin	0.775	563.5	436.7
coolant feed lines	0.324	563.5	182.7
Cooling System	0.861	578.4	573.0
water	0.861	578.4	498.0
tank	0.819	91.1	74.7
Insulated Beryllium	10.65	14.5	154.4
beryllium	9.58	14.5	138.9
insulation	0.75	14.5	10.8
coolant feed lines	0.33	14.5	4.7
TOTAL WEIGHT			2727.1

THE REACTION CONTROL SYSTEM

The Shuttle-C must have full control authority over its six degrees of motion. By incorporating the existing NSTS reaction control system into the Shuttle-C program, the desired maneuverability performance of the vehicle will be attained with low development cost. The next two sections deal with the Shuttle-C avionics, thrusters, and fuel needed.

Guidance, Navigation and Control Avionics

One of the primary requirements of the Shuttle-C system is to " have autonomous GN&C and systems management systems". (16:33,66) Since GN&C is required to control yaw and pitch for successful reentry, certain avionics packages are needed. In order to keep a final recoverable weight around 2000 lbs, certain avionic equipment is deemed expendable. Table 7 lists the location and the weight of the equipment needed. Equipment listed in the avionics package is recoverable. All other equipment will be destroyed during reentry.

Table 7 Weight and Location Breakdown of Avionics Equipment

EQUIPMENT	QUANTITY	LOCATION	WEIGHT (lbs)
GN&C	1	Avionics package	164 total
IMU	3	GN&C	126
Rate Gyros	3	GN&C	30
Accel.	3	GN&C	8
COMMUNICATIONS	1	Avionics package	131 total
S-Band Trans.	2	Communications	30
Signal Processor	2	Communications	30
Power Amp	2	Communications	32
RF combiner	1	Communications	12
Recorder	1	Communications	19
Hemi-Ant	2	Communications	5
Low Gain Antenna	1	Communications	3
DATA MANAGEMENT	1	Avionics package	668 total
Computer	3	Data Management	192
Multiplexers MDM	6	Data Management	224
Signal Conds.	9	Data Management	180
PCMMV/PDI	2	Data Management	37
Timing Unit	1	Data Management	30
Timer Buffer	1	Data Management	5
ELECTRICAL POWER	1	Avionics Capsule	3647 total
Batteries	4	Avionics package	584
Batteries	4	Cargo Bay	584
Power Distr.	-	Capsule	50
Power Distr.	-	Cargo Bay	100
D.C. Distr.	-	Capsule	40
D.C. Distr.	-	Cargo Bay	80
Power Control	1	Avionics package	60
Power Control	1	Cargo Bay	60
Load Distrib.	-	Capsule	35
Distr & Control	1	Avionics package	30
Battery Charger	1	Avionics package	40
Cabling	-	Everywhere	1984

TOTAL EQUIPMENT WEIGHT:	
Avionics package	1700 lbs.
Capsule	325 lbs.
Cargo bay	2300 lbs.

Thrusters and Fuel

Since the Shuttle-C must maintain full authority over all six degrees of motion. The number of thrusters equals the number in the manned orbiter's nose. The only difference is in the forward thruster locations, as shown in Figure 39. Since during reentry the capsule will be an independent vehicle, the thrusters were spaced equally around the capsule for 360 degrees of control. The forward thrusters are placed so after separation of the shroud from the cargo bay, the shroud retains the six degrees of freedom of motion. Six vernier thrusters are incorporated into the capsule in order to allow smooth docking procedures with the space station.

In order to facilitate refueling operations at Kennedy Space Center, the thrusters will use the same fuel as the manned space shuttle. The fuel will be monomethyl hydrazine, and the oxidizer will be nitrogen tetroxide (1:46). The mix ratio will be 1.6 lbs of oxidizer to every one pound of fuel. The weight of the fuel will be determined based upon the on orbit stay time required of the vehicle. The minimum propellant (oxidizer + fuel) will be 302 lbs/module, enough for one day in orbit. The maximum propellant weight will be 2418 lbs./module, enough for eight days in orbit. Helium, stored in a separate tank, will be used to pressurize the propellant system. (18:138) All three of the capsule tanks will be composed of .035 in.

thick titanium. The oxidizer tank will be the largest with a volume of 74.2 cubic feet. Because of its size it will be in a cylindrical shape of 3.25 foot length and 2 foot radius. The fuel tank will be a sphere with a radius of 2 feet. The helium tank will also be a sphere with a radius of 1.6 feet. Figure 40. shows the locations of the tanks in the shroud. (18:138)

Table 8 Reaction Control System and Weight Breakdown

COMPONENT	QUANTITY	WEIGHT (lbs)
OMS Engines	2	2000.0
Primary Thrusters	38	955.0
Vernier Thrusters	6	44.4
Fuel Tank (hydrazine)	3	123.6
Oxidizer Tank	3	224.1
Helium Tank	3	79.2

THREE STAGE AERODYNAMIC DECELERATOR RECOVERY SYSTEM

The primary objective of the recovery system is to extract the avionics package from the capsule and achieve a safe, self reliant landing of the avionics package with no resulting avionics damage. The recovery system is located in the capsule directly above the avionics package. (Figure 41) The data in the following table presents the avionics package parameters needed for this decelerator system.

Table 9. Avionics Package Specifications

Avionics Module	
Height	= 5 ft
Length	= 4 ft
Width	= 4 ft
Weight (recoverable weight)	
Avionics	= 1000 lb
Structure	= 500 lb
4 Batteries	= 600 lb
Control system	= 50 lb
Total Weight	= 2,150 lb
Maximum Acceptable Forward Speed on Landing	= 55 ft/s

The following is a list of the general requirements and specifications selected for the avionics package decelerator subsystems:

Table 10. Parachute Recovery System Requirements

System Reliability
Performance Envelope
Landing Accuracy and Range
Low Recovery System Weight and Simplicity of design
Multiple Reuse
Simplicity of Maintenance and Operation
Environmental Hazards and Storage Capabilities
Low Development, Acquisition and Life Cycle cost

The decelerator subsystem reliability is considered throughout the design phase due to the high cost of the avionics. The performance envelope considered includes supersonic operations, high altitude performance, stability, glide capabilities, and impact attenuation. The relative overall forces acting on the avionics package are considered in designing the recovery system. The *Recovery System Design Guide* showed, from tests, that for a properly reefed recovery system the snatch force experienced by the avionics package is less than the force exerted upon actual opening of the decelerator (Figure 42) (20:236). The recovery system design is kept as simple as possible while cutting cost wherever possible. Hazards from out-gassing and the harsh environment in space require that the individual stages of the recovery system be packed in metal containers.

(20:148) The recovery system packing process is a rather simple method, which reduces long and short range cost. The decelerator is placed in the container and hydraulically pressure packed. (20:144) The expected life cycle of any component of the recovery system is dependent upon previous mission conditions and will be determined on a case by case basis. The recovery system is comprised of three stages: a mortar deployed ribbon hemisflo, a conical ribbon, and a ram-air flexible wing.

Mortar Deployed Ribbon Hemisflo Drogue

The first stage is a mortar deployed ribbon hemisflo drogue which is deployed, at an altitude of 65,000 feet, after the tip of the shroud has been blown off. The drogue stabilizes the capsule and decreases its velocity at second stage deployment. Mortar deployment and a long attaching bridal aid the drogue in overcoming wake effects caused by the capsule (Figure 43) (Ref 21). The ribbon hemisflo drogue can tolerate opening speeds up to Mach three. Design parameters for the ribbon hemisflo drogue are located in Table 11.

Table 11. Ribbon Hemisflo Conical Drogue

Ribbon Hemisflo Conical Drogue	
C_D	= .3
Diameter	= 6 ft
Number of Gores	= 16
Ribbon Strength	= 1000 lb
Weight	= 45 lb
Pack Volume	= 1.89 ft^3
Material	= High Tension Nylon Webbing
Material Weight	= 1.4 ounce per square yard
Drogue Bridal	= Type XXII Coreless Braided Nylon
Bridal Length	= 180 ft

The drogue slows the 10,000 lb capsule to a speed of Mach one at an altitude of 45,000 ft. The drag created by the drogue is used to extract the conical ribbon. At 45,000 ft explosive bolts are fired, freeing the second stage and the avionics package. The avionics package rests on rollers which enhance its vertical movement.

Conical Ribbon

The second stage is a Conical Ribbon that is extracted from the shroud by the drogue. During opening, the conical ribbon extracts the avionics package from the capsule. (Figure 44) (Ref 22) The conical ribbon is designed to reduce the opening speed of the third stage to approximately 135 ft/s. The following table gives specifications for the second stage.

Table 12 Conical Ribbon

Conical Ribbon		
C_D	=	.6
Diameter	=	12 ft
Number of Gores	=	16
Ribbon Strength	=	1000 lb
Weight	=	90 lb
Pack Volume	=	2.69 ft^3
Material	=	High Tension Nylon Ribbon
Material Weight	=	1.4 ounce per square yard

The opening loads and opening shock sustained by the avionics package upon deployment of the second stage are controlled by:

1) deploying the canopy lines first
2) ensuring that the canopy remains in the bag until suspension line tension is achieved thereby assuring more even line loading
3) the use of a reefing system

The reefing system is comprised of a flat circular plate, which the suspension lines pass through. The flat circular plate divides the suspension lines into four separate groups and is attached to the base of the drogue bridal. The drogue bridal passes through a cutter and then through the apex of the conical ribbon (Figure 45). The cutter is activated by lower lateral band tension as the second stage

opens fully. Once the drogue is cut away the conical ribbon forces the flat plate down the suspension lines to the riser stops.

Since the drogue and second stage are detached from the avionics package they may inadvertently be lost. However, 60%-70% of the time they can be recovered. If homing devices are placed on the drogue and second stage, the odds of recovering them increase dramatically.

Ram-Air Inflated Aerodynamic Decelerator

The third and final stage of the avionics recovery system is a ram-air aerodynamic decelerator. The ram-air aerodynamic decelerator (flexible wing) is chosen for the third stage due to its good performance characteristics. The airfoil shape of the flexible wing provides optimal range, varied rates of descent and increased flight performance. The following table presents the flexible wing design specifications.

Table 13. Ram-Air Aerodynamic Decelerator Specifications

Ram-Air Aerodynamic Decelerator		
Span	=	87 ft
Chord	=	28 ft
Aspect Ratio	=	3:1
L/D	=	3.5:1
Weight	=	100 lb
Pack Volume	=	2.89 ft^3
Material	=	Harris F-111 low porosity nylon
Material Weight	=	1.11 ounce per square yard

The third stage is initiated at 40,000 ft when an automatic activation device begins the third stage deployment. The second stage extracts the flexible wing from the top of the avionics package, lines first to ensure even line loading. A freebag, a deployment bag which separates from the flexible wing upon opening, decreases malfunction possibilities. When tension is reached the freebag is opened by a locking stow which allows the flexible wing to be extracted from the freebag. The second stage is then detached from the third stage when the freebag is released. The flexible wing airfoil is comprised of a top skin, bottom skin and vertical cell dividers that are made of a low porosity nylon. The top and bottom skins form the airfoil shape and the cell dividers provide structural integrity (Figure 46). The front of the airfoil is open and the rear of the airfoil is sewn shut allowing ram-air pressurization. Cross porting or holes in each of the vertical cell dividers allows equal pressurization throughout the airfoil. Vertical stabilizers are attached to the outside bottom skin of the airfoil and extend downward adding stability.

The avionics package is attached to the flexible wing by suspension lines. The suspension lines are contained in four groups which pass through a sliding reefing system, a slider. The reefing system is made of the same low porosity material that the flexible wing is made of with one sliding

ring attached to each corner. Each of the four suspension line groups pass through a respective sliding ring. Drag causes the reefing system to remain at the bottom of the airfoil, choking the decelerator, until pressurization forces are sufficient to force the reefing system down the lines (Ref. 23).

The flexible wing airfoil has control lines attached to the both sides of the airfoil tail. When the control lines are pulled simultaneously the tail deflects downward exchanging forward speed for lift, like flaps on an aircraft. To turn left the left control line is pulled and to turn right the right control line is pulled. An automatic control system is incorporated into the recovery subsystem for homing purposes and manual remote controlled flight. The ram-air aerodynamic decelerator can practically zero the rate of descent of the avionics package upon landing; however, the forward velocity remains relatively high. Therefore, skids are placed on the bottom of the avionics package to facilitate any high landing velocities. The third stage is the most complex of the three stages and is designed for multiple missions.

DISCUSSION

The initial Shuttle-C design proposal called for an investigation into the recovery of the space shuttle main engines. However, since the proposal was submitted, NASA has specified that the SSME's have a life span of ten flights. (24:1) Thus, if all Shuttle-C flights are made with SSME's that have already been used on nine previous missions, recovery of the SSME's will be unnecessary.

The cost of the Shuttle-C avionics is estimated to be approximately 150 million dollars. Furthermore, this value is increased by the current shortage of NSTS spare parts. (25:31) Recovery of the avionics will both lower the cost of the Shuttle-C program and help relieve the shortage in spare parts.

Incorporation of the avionics reentry capsule within the Shuttle-C design will not compromise the Shuttle-C 's ability to fulfill NASA's design or mission requirements. The Shuttle-C, including the reentry capsule, will be compatible with the existing National Space Transportation System. To minimize cost and development time, both the Shuttle-C and the avionics reentry capsule will utilize developed and proven space technology to the fullest extent practical. The Shuttle-C with the additional weight of the avionics reentry capsule will be capable of satisfying NASA's primary mission requirement, the placement of at

least 100,000 lb into a 220 nmi low earth orbit with an inclination angle of 28.5 deg.

The avionics capsule is designed for a low lift reentry. Since considerable knowledge and experience has been accumulated on the this type of reentry, development time and cost will be minimized. The capsule utilizes an ablative heat shield for protection against the heat transfer experienced during deceleration through the earth's atmosphere. For low lift reentry, ablative thermal protection systems have proven extremely efficient. The capsule is constructed to withstand a deceleration force of up to four g's; the maximum expected deceleration force is roughly -3.30 g's. An autonomous guidance, navigation, and control system in conjunction with the reaction control thrusters maintain trajectory control during reentry.

The avionics package is extracted from the capsule, reducing the weight supported by the parachute recovery system. The avionics package glides to a pinpoint landing under the ram-air aerodynamic decelerator (flexible wing). The airfoil shape of the flexible wing provides optimal range, varied rates of descent and increased flight performance. The flexible wing can practically zero the rate of descent of the avionics package; however, the forward velocity remains relatively high. Therefore, skids are placed on the bottom of the avionics package to facilitate high landing velocities.

CONCLUSION

The basic purpose of the Shuttle-C program is to provide the United States space program with a low cost, short development, heavy lift launch vehicle. To reduce the life cycle cost of the Shuttle-C program, an avionics recovery system is incorporated into the Shuttle-C vehicle. The incorporation of the recovery system will not compromise the Shuttle-C's ability to satisfy NASA's mission of design requirements.

The capsules's structural is designed to accommodate the high deceleration loads experienced during reentry. An ablative heat shield is used for protection against the severe heat transfer, and an independent guidance and control system is used to provide control authority over all six degrees of freedom. At 65,000 ft. a three stage recovery parachute system is initiated. This three stage system will stabilize the capsule, decelerate the capsule, pull the avionics from the capsule, and land the avionics safely at Edward's Air Force Base. The parachute recovery system can be recovered and used in future missions.

LIST OF REFERENCES

1. The Presidential Commission of the Space Shuttle Challenger Accident. Report of Presidential Commission. Washington: GPO, 1986.

2. Bate, Roger R., Donald D. Mueller, and Jerry White. Fundamentals of Astrodynamics. Dover Publications, New York, 1971.

3. Rosser, J. Barkley, Robert R. Newton, and George L. Gross. Mathematical Theory of Rocket Flight, McGraw-Hill, New York, 1947.

4. Shevell, Richard S., Fundamentals of Flight. Prentice-Hall, Englewood Cliffs, New Jersery, 1983.

5. Rocketdyne Divison of Rockwell International. "Space Shuttle Main Engine".

6. Sutton, George P. Rocket Propulsion Elements. John Wiley & Sons, New York, 5th ed., 1986.

7. Loh, W. H. T. Dynamics and Thermodynamics of Planetary Entry. Prentice Hall, Englewood Cliffs, 1963.

8. "Report on Drag Force Coefficient Evaluation Procedure for Rocket Propelled Missile Configurations, $0 < M < 20$, $0 < H < 400{,}000$ ft. Part B-III (Methods of Evaluation)". Auburn University, 1961.

9. Anderson, John D. Jr. Fundamentals in Aerodynamics. McGraw-Hill, New York, 1986.

10. Chrysler Corp. Space Divison. "Saturn IB Vehicle Handbook, Vol I". Marshall Space Flight Center, Huntsville, Al., July 25, 1966.

11. Cutchins, Malcolm A. AE521 Flight Vehicle Stress Analysis Lecture Notes. Auburn University, Auburn, Al.,Nov. 9, 1989.

12. Brandt, Paul E. "Aluminum and Aluminum Alloys." Methods of Materials Selection. Ed. E. D. Verink, Jr., New York: Gordon and Breach, 1968.

13. Aluminum Company of America. Alcoa Structural Handbook. Pittsburgh, 1960.

14. Gruntfest, I.J. "The Outlook for Ablating Heat Protection Systems". Aerodynamically Heated Structures. ed. Peter E. Glassor. Englewood-Cliffs: Prentice-Hall, 1962.

15. Moss, J. N., E. Vincent Zoby, Kenneth Sutton, and E. Clay Anderson. "Aerothermal Environment for the Pioneer Venus Multiprobe Mission." Progress in Astronautics and Aeronautics. Vol 59, 1978.

16. Kesselring, J. P., R. E. Maurer, K. E. Suchsland, G. J. Hartman and D. L. Perterson. "Arc-Heater Code Validation Tests of Heat Shield Materials." Progress in Astronautics and Aeronautics. Vol 59, 1978.

17. Gruntfest, I. J. "Thermal Protection with a Temperature Capability to 2500 F, for Cool Structures." Aerodynamically Heated Structures. ed. Peter E. Glasser. Englewood Cliffs, Prentice-Hall, 1962.

18. Edwards, P. R. "Development and Testing of the Space Shuttle Reaction Control System." Journal of Engineering for Industry. Vol 103, 1981.

19. Weiss, V.,and J. G. Sessler, ed. "Aerospace Structural Metals Handbook." Directorate of Materials and Processes Air Force Systems Command. Syracuse: Syracuse University, 1963.

20. Irvin Industries Inc. Recovery Systems Design Guide. Air Force Flight Dynamics Laboratory, Wright-Patterson Air Force Base, 1978.

21. Private Communication with Jim Sickle, Santa Ante, Cal. Feb 28, 1989.

22. Private Communication with Manley C. Butler, Jr., California City, Cal. Feb 15, 1989.

23. Private Communication with Bill Coe, Hialeah, Fl. Feb 15, 1989.

24. Dunnavaat, Robert. "NASA Starts Working on Cargo Shuttle." The Birmingham News Dec 19, 1989.

25. Kolcum, Edward H. "Nasa May Delay on Scrub Mission 29 Because of Turbopump Bearing Corrosion." Aviation Week and Space Technology. McGraw-Hill, New York, January 30, 1989.

APPENDIX

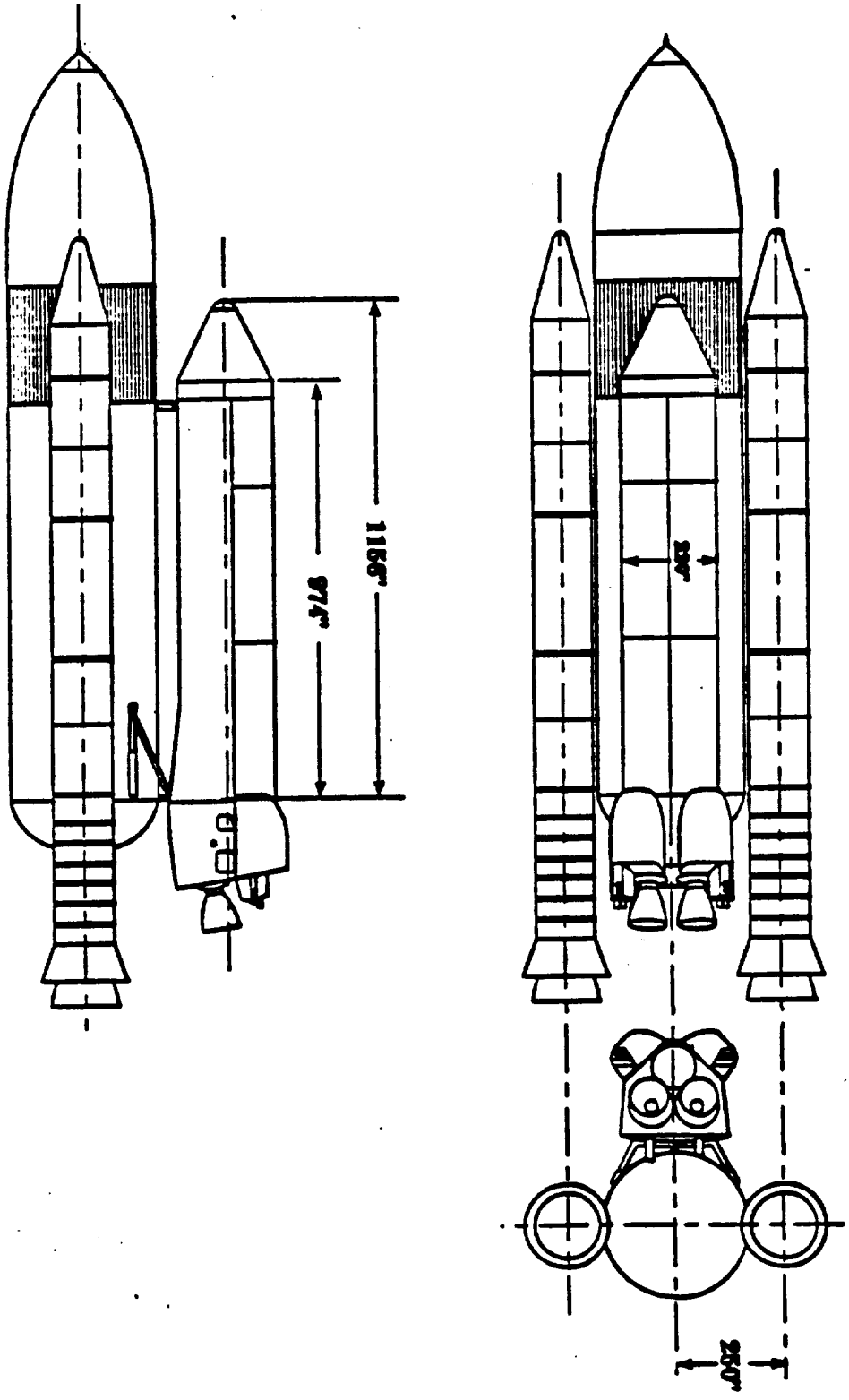

Figure 1. Shuttle-C Launch Configuration.

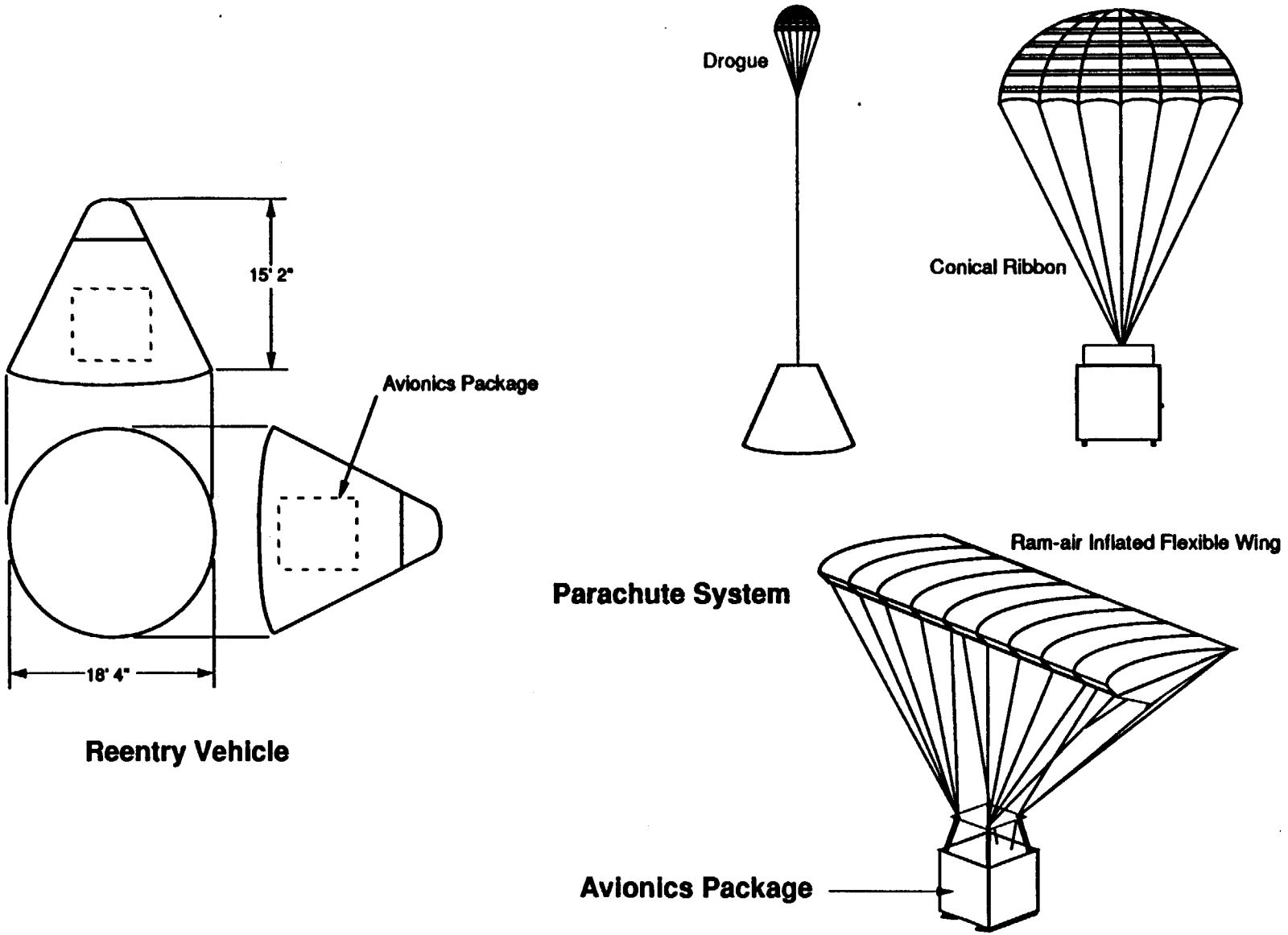

Figure 2. Avionics Reentry Capsule and Subsystems.

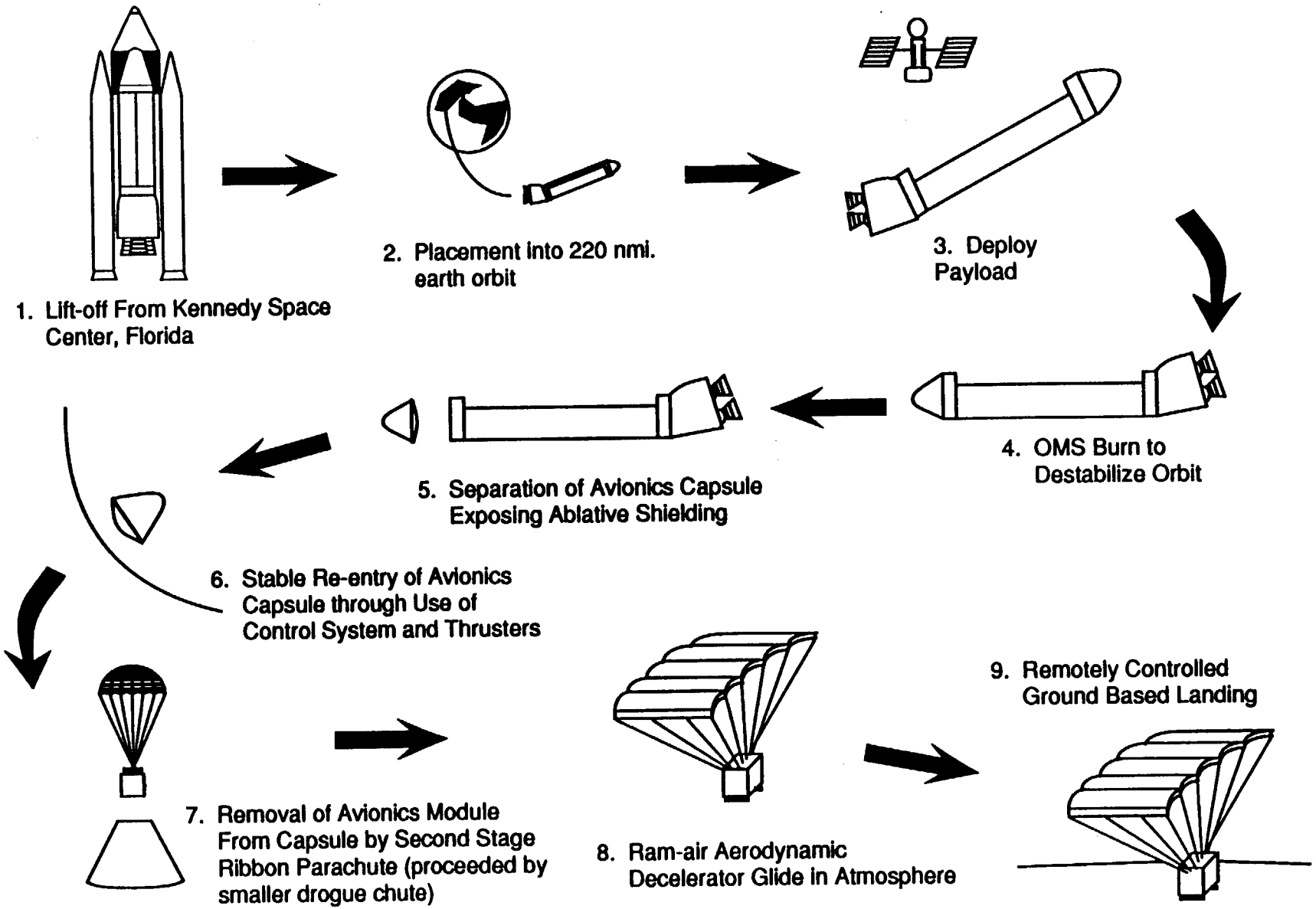

Figure 3. Shuttle-C Mission Profile.

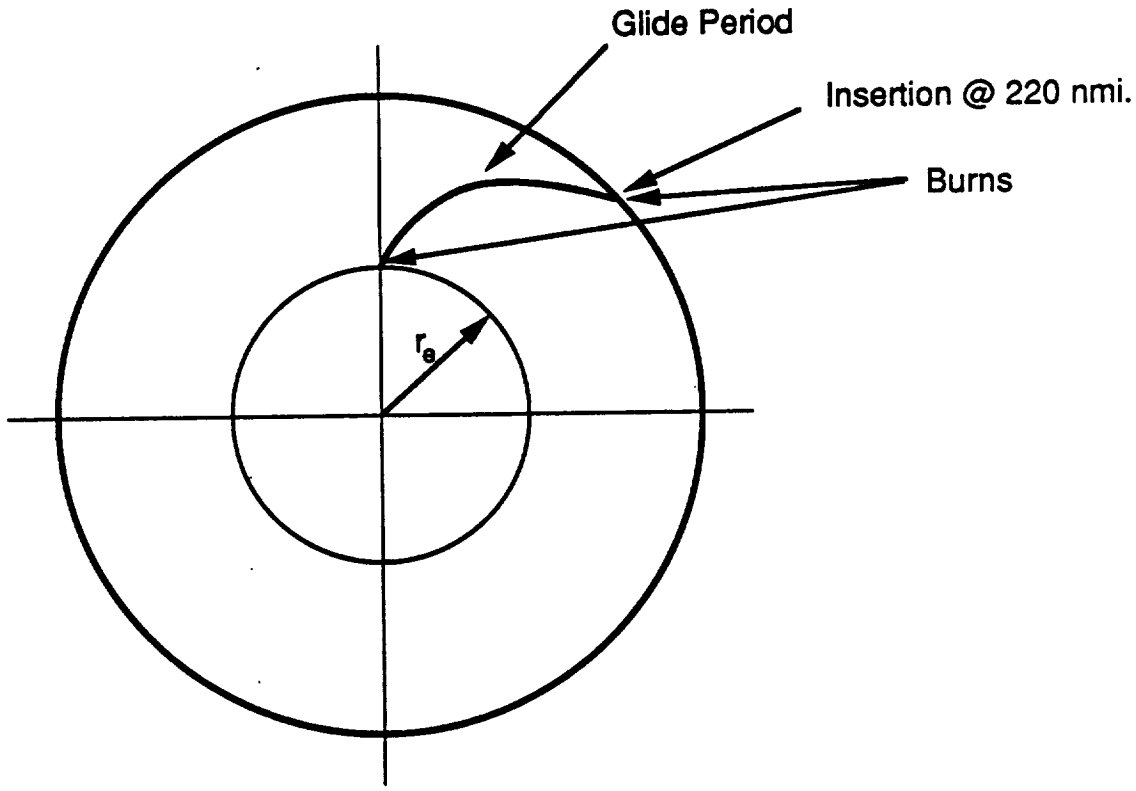

Figure 4. Three Launch Stages to Circular Orbit.

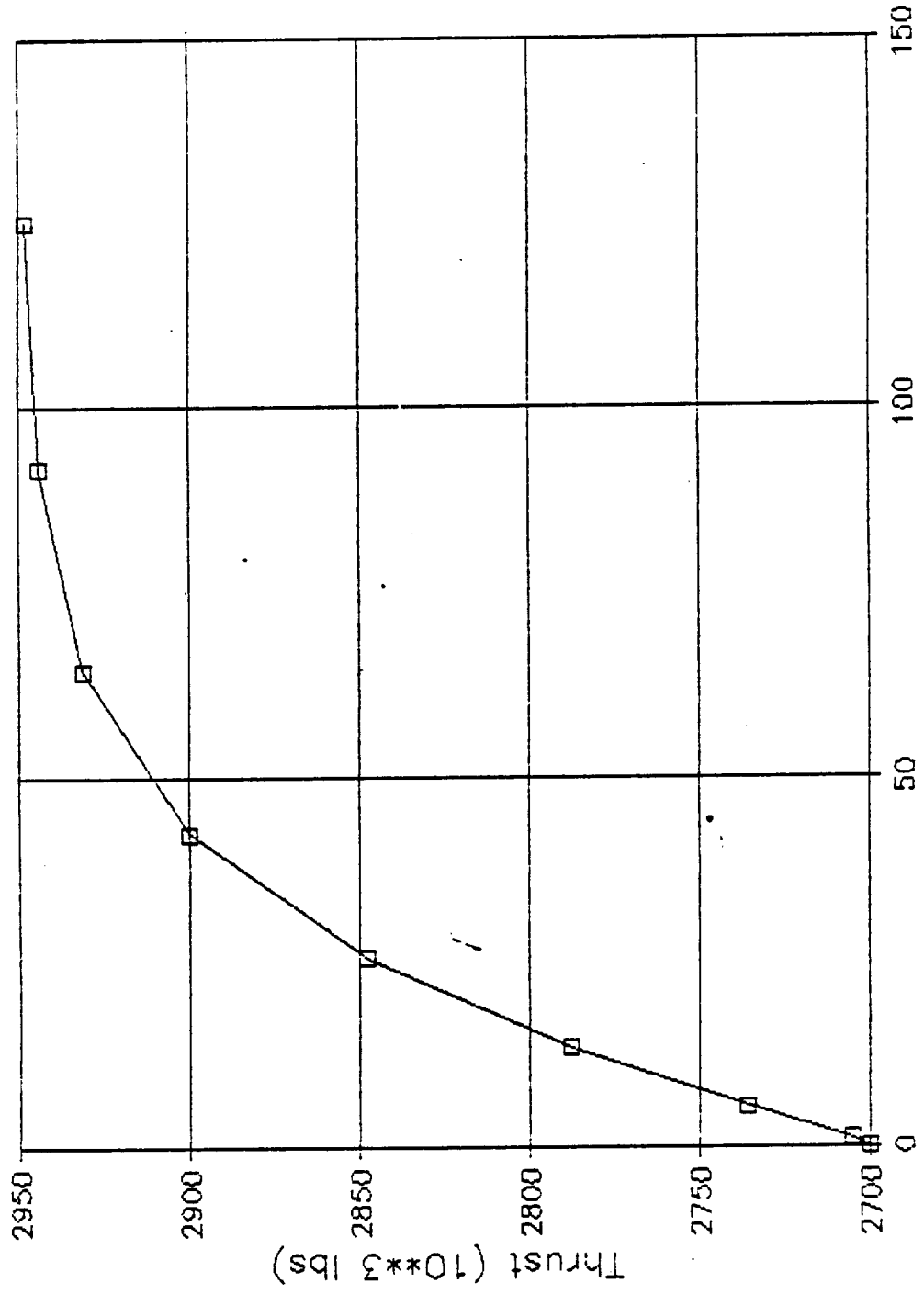

Figure 5. Thrust of Solid Rocket Motors as a Function of Altitude.

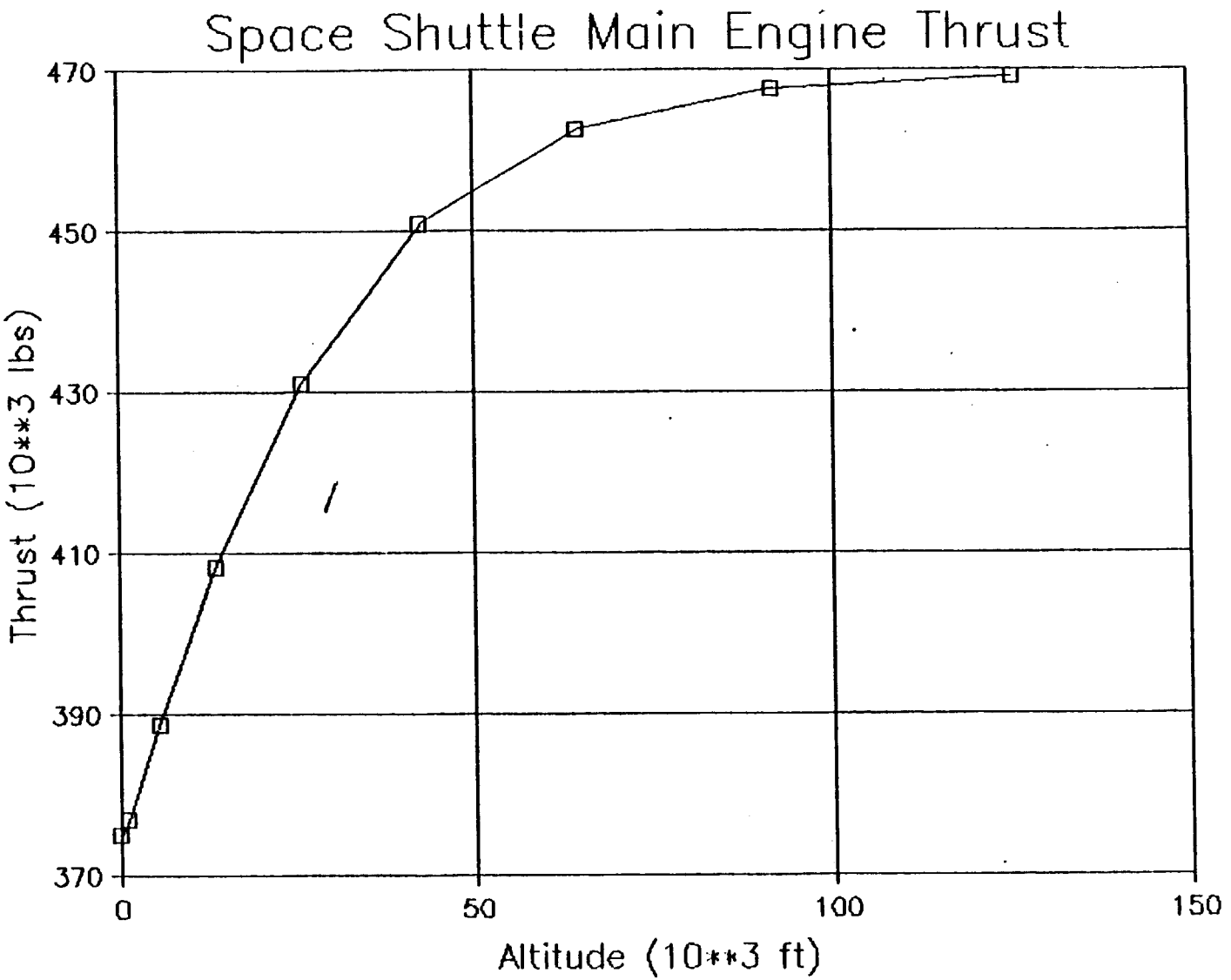

Figure 6. Thrust of the Space Shuttle Main Engines as a Function of Altitude.

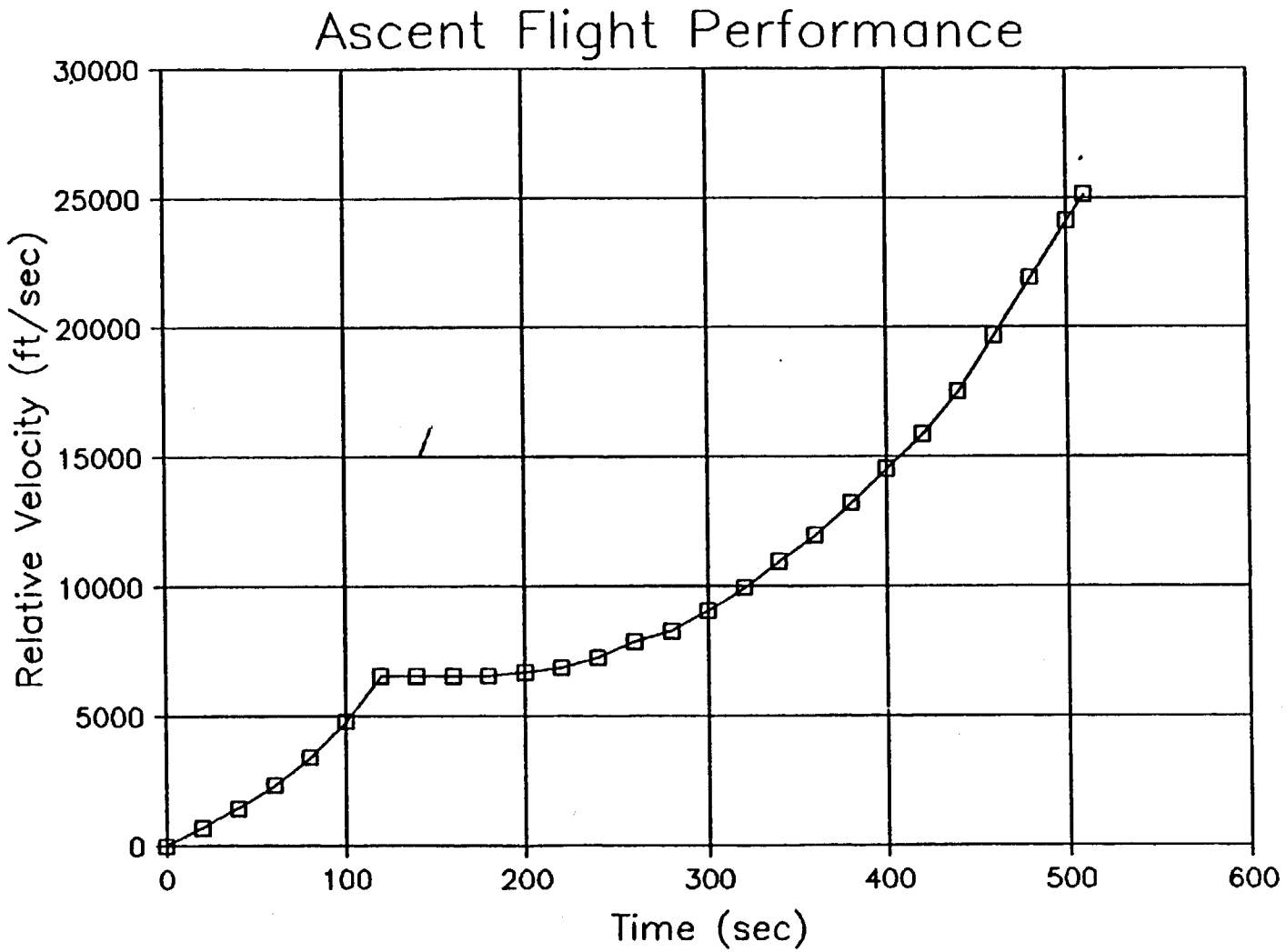

Figure 7. The Velocity as a Function of Time.

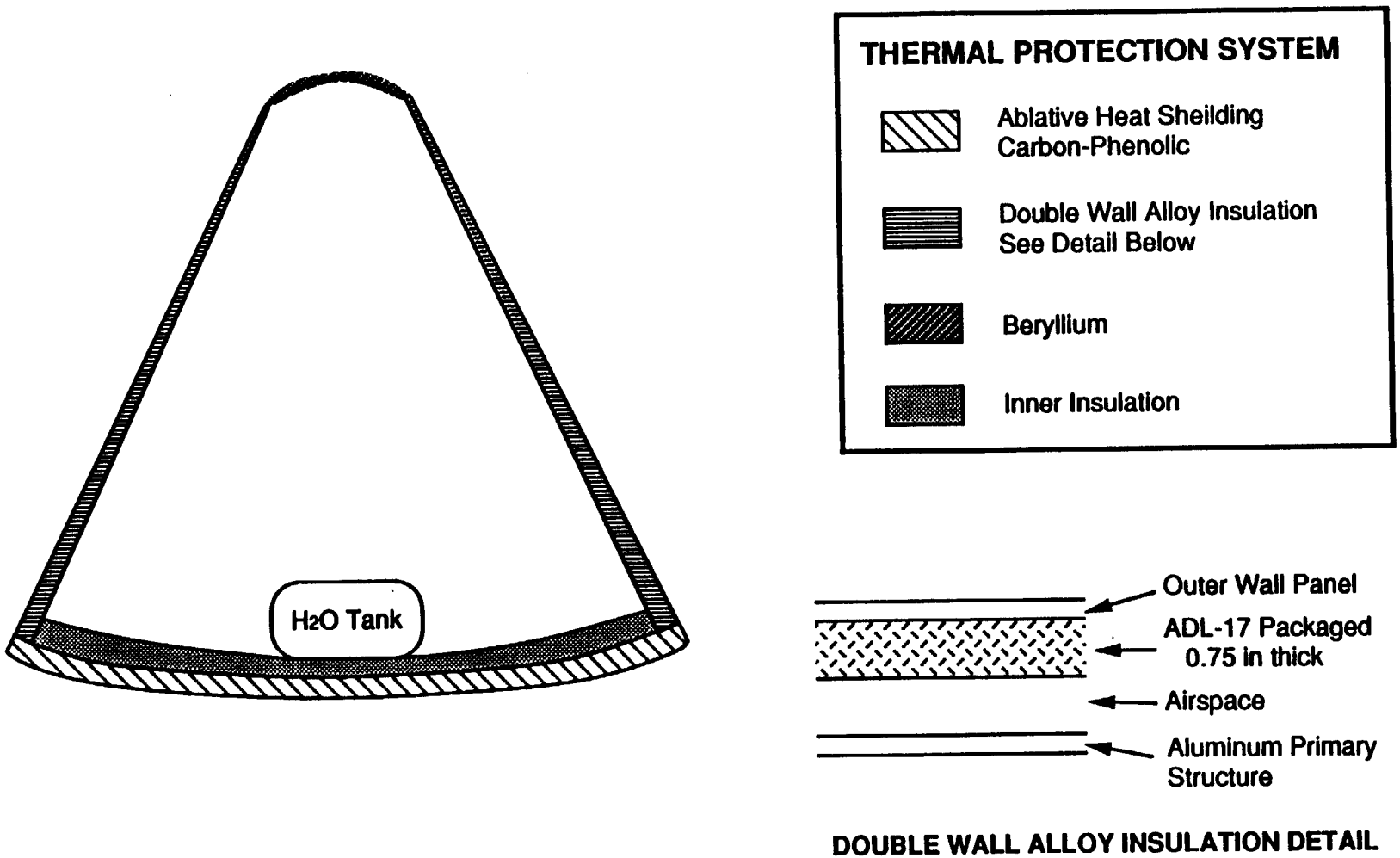

Figure 8. Thermal Protection System for the Capsule.

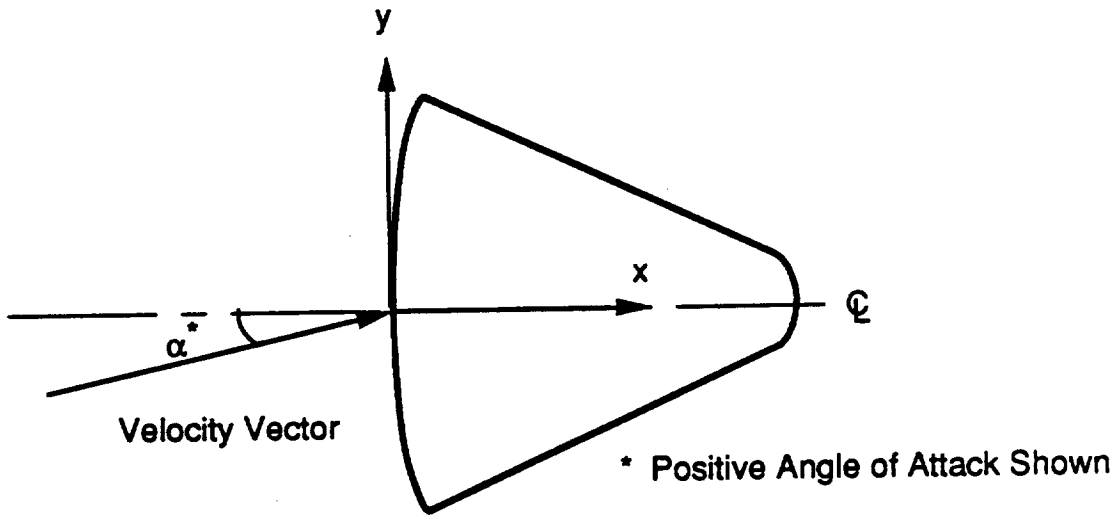

Figure 9. Reentry Capsule Angle of Attack and Coordinate System.

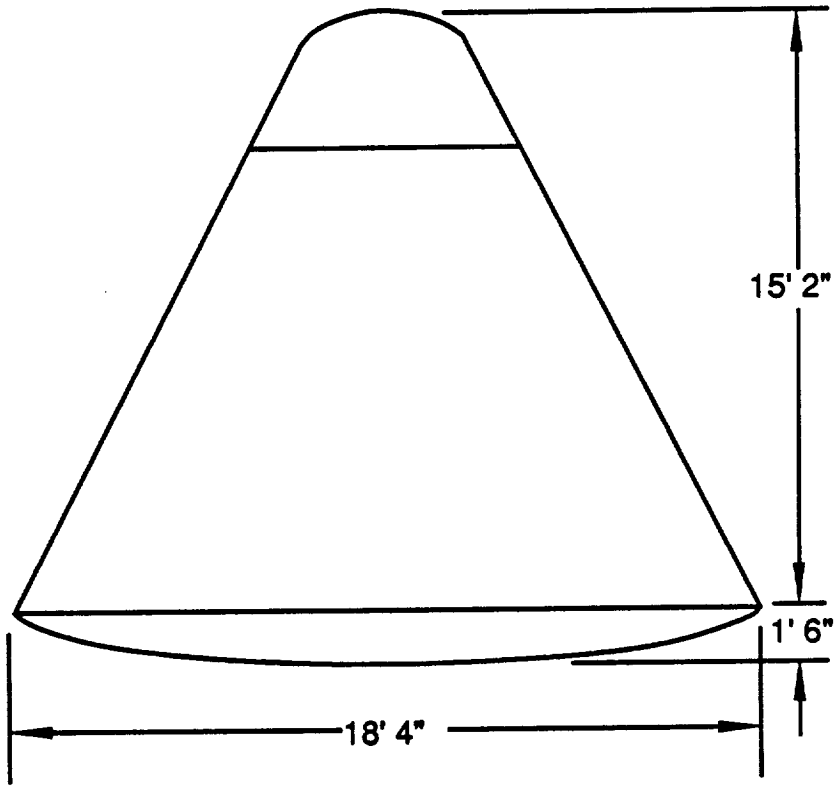

Figure 10. Approximated Reentry Capsule Geometry.

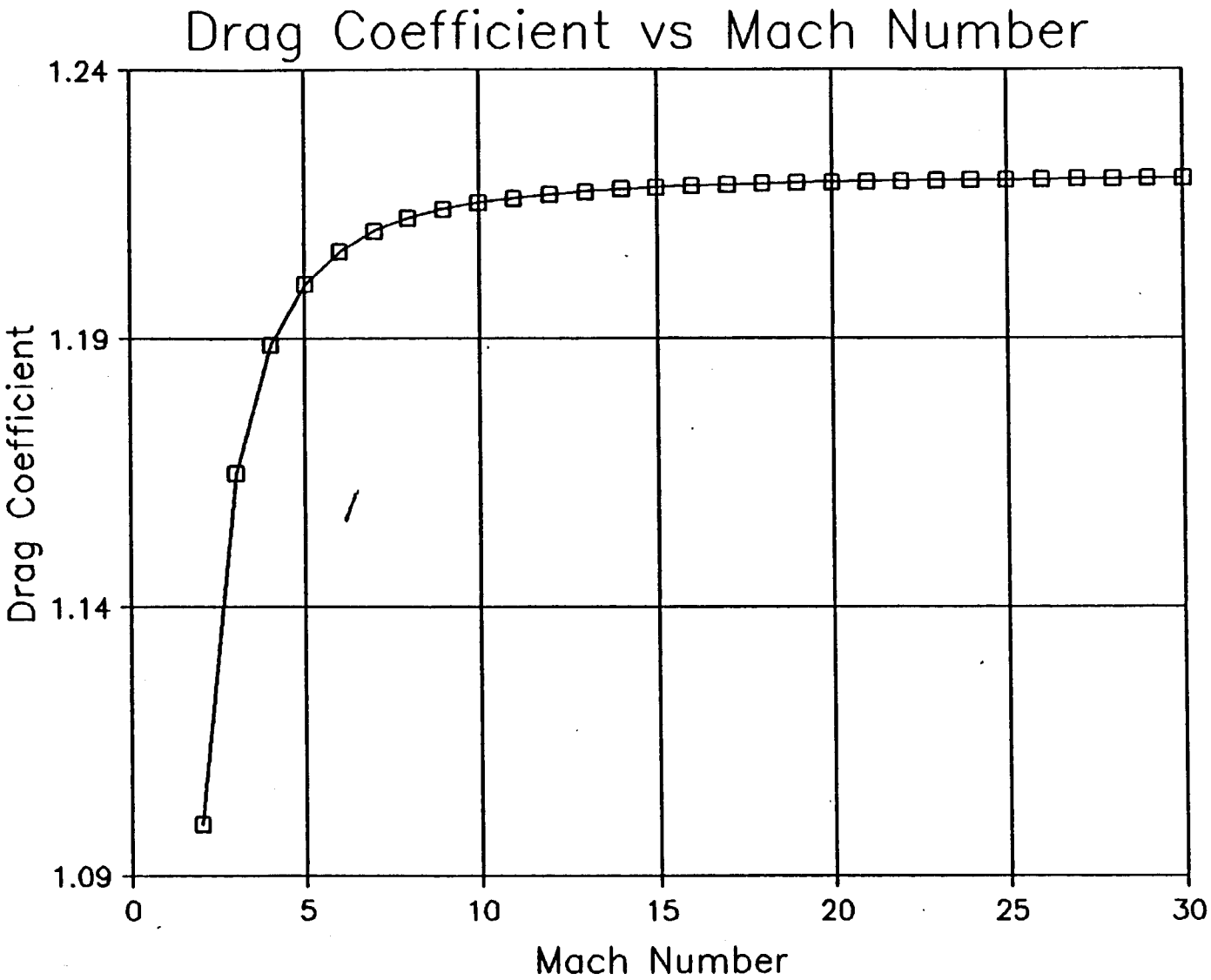

Figure 11. The Relationship Between Mach Number and Drag Coefficient for the Avionic Capsule.

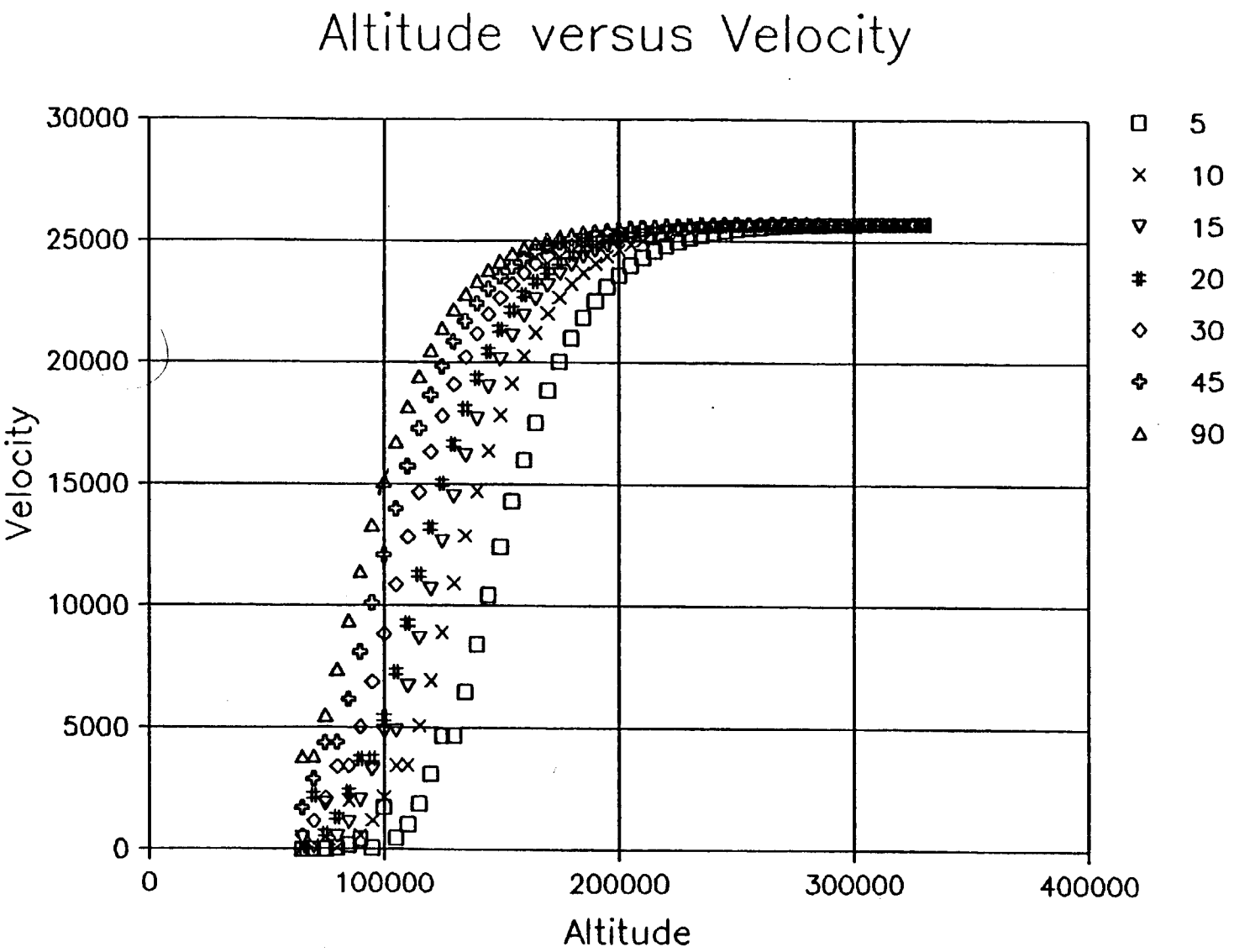

Figure 12. Velocity as a Function of Altitude for Ballistic Reentry at Initial Flight Path Angles Ranging from Five to Ninety Degrees.

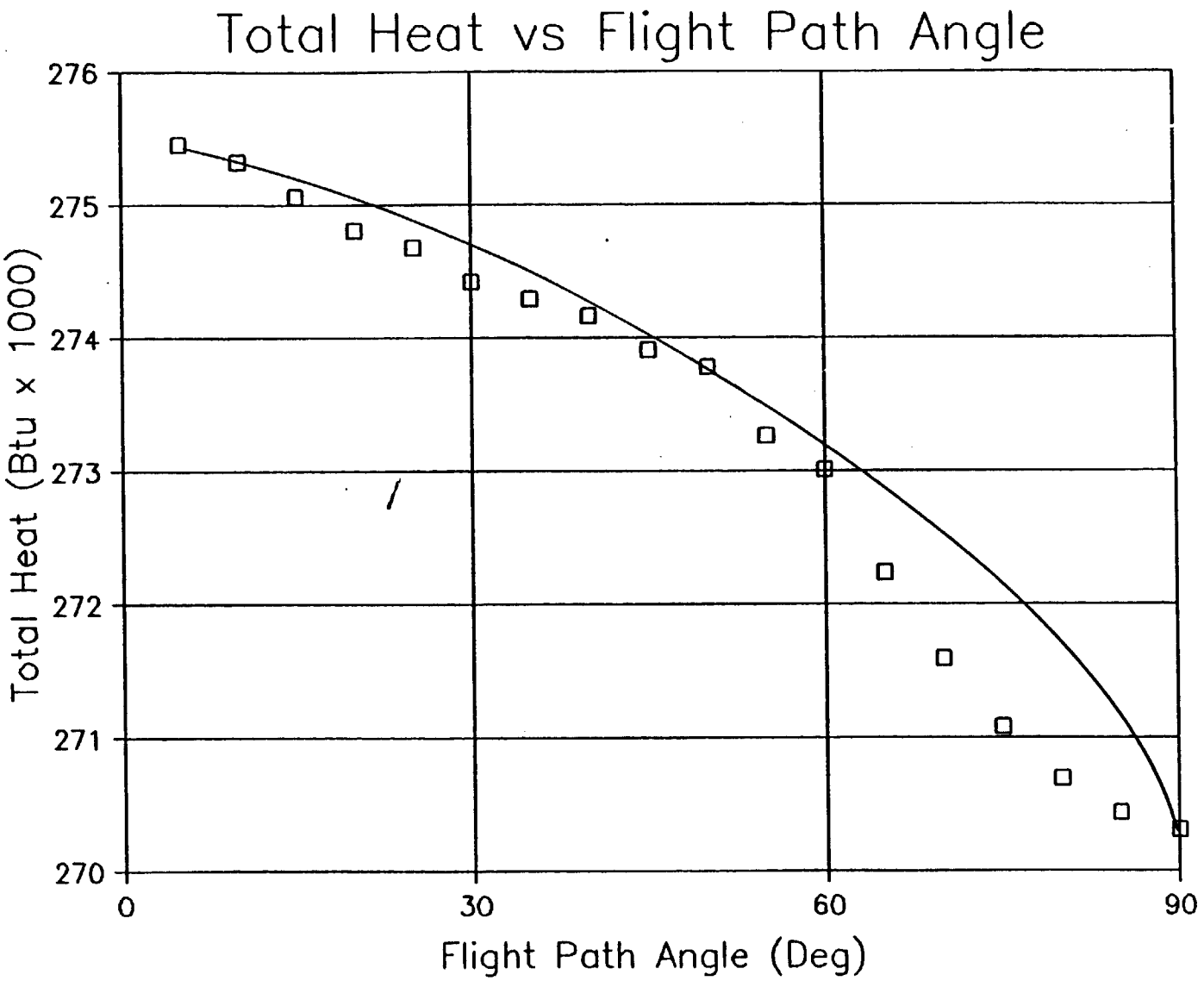

Figure 13. Total Heat Absorbed as a Function of Initial Flight Path Angle for Ballistic Reentry.

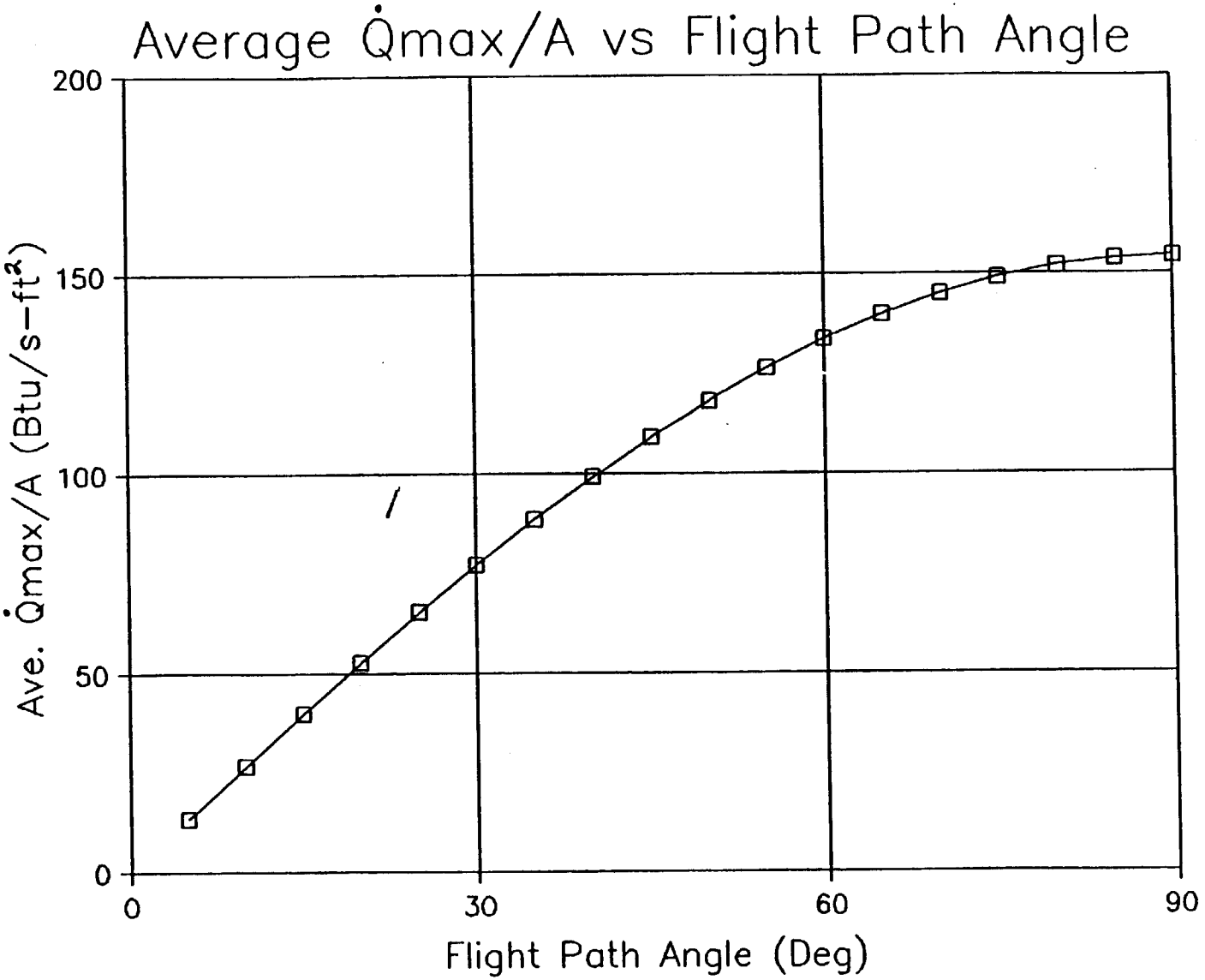

Figure 14. Average Heat Flow Rate per Unit Area as a Function of Initial Flight Path Angle for Ballistic Reentry.

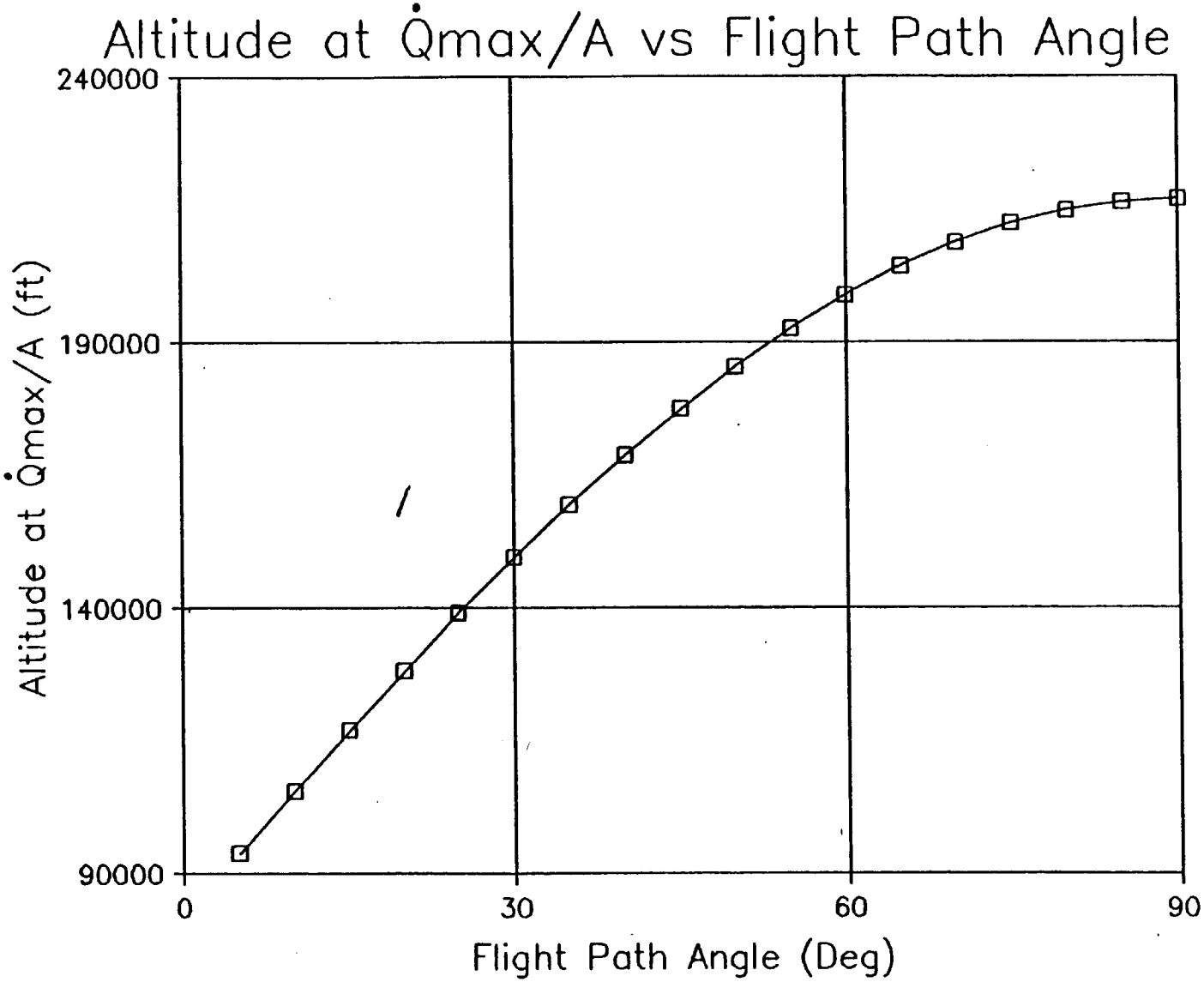

Figure 15. Altitude at Maximum Heat Flow Rate as a Function of Initial Flight Path Angle for Ballistic Reentry.

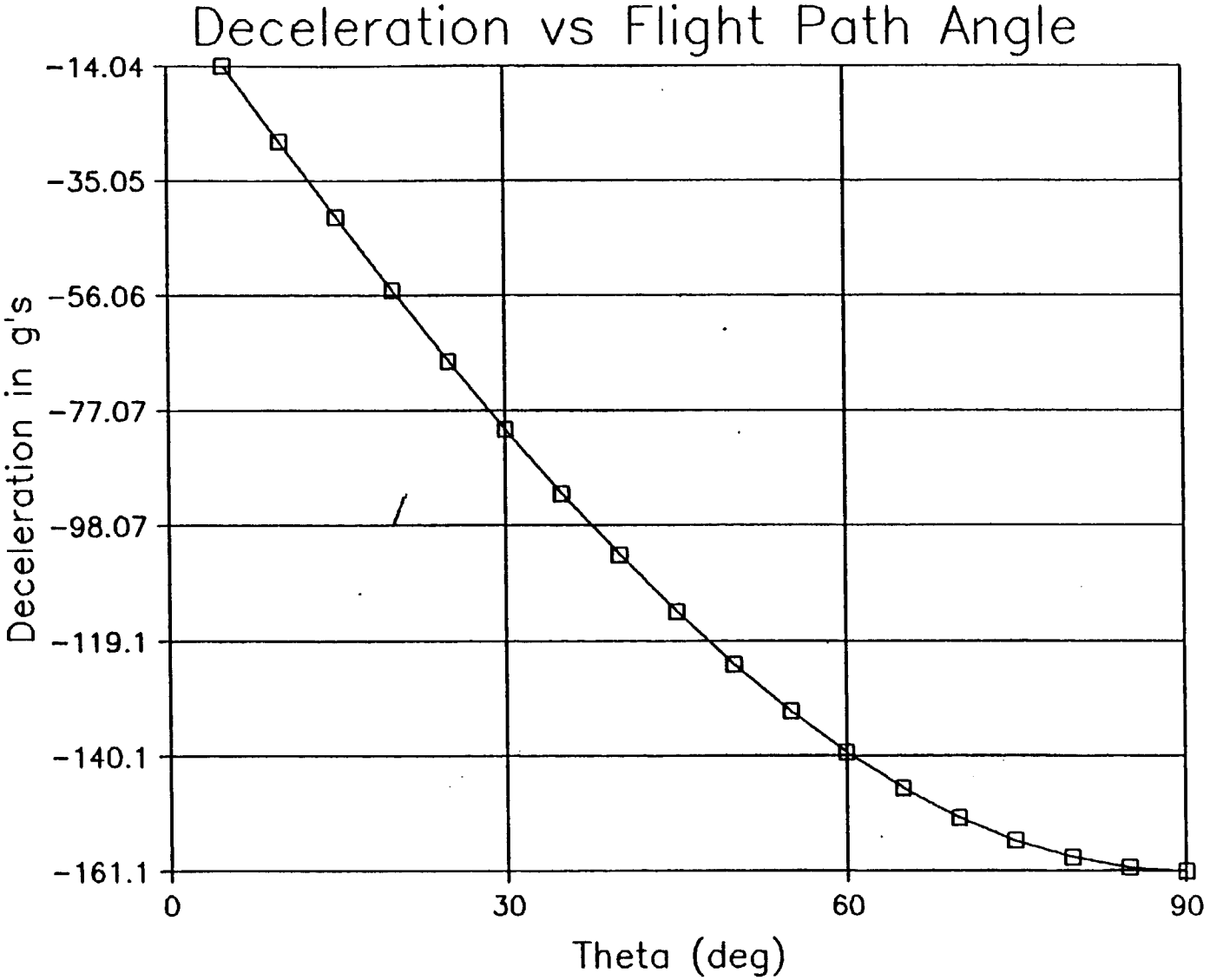

Figure 16. Deceleration Measured in Earth g's as Function of Initial Flight Path Angle for Ballistic Reentry.

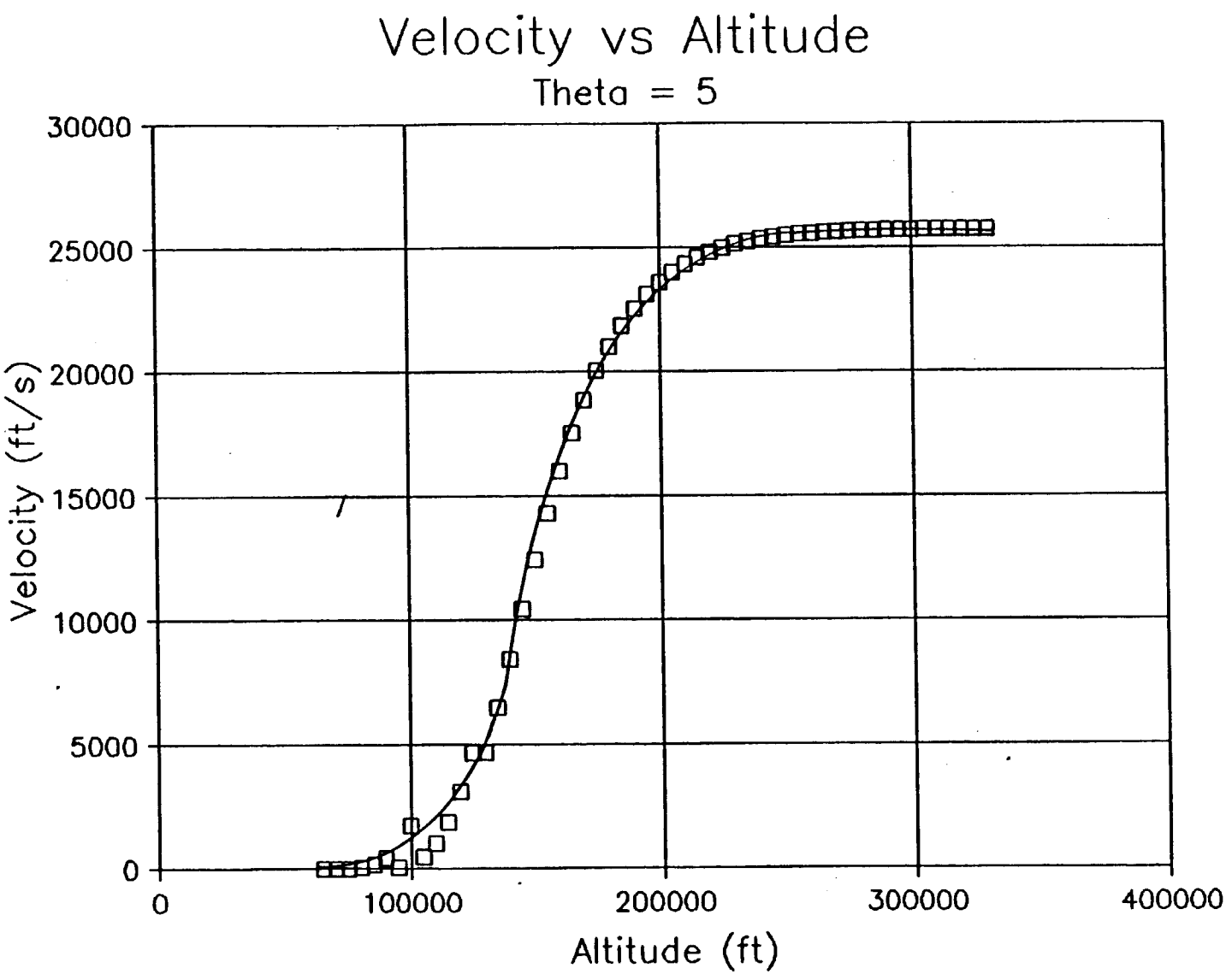

Figure 17. Velocity as a Function of Altitude for Ballistic Reentry at an Initial Flight Path Angle of Five Degrees.

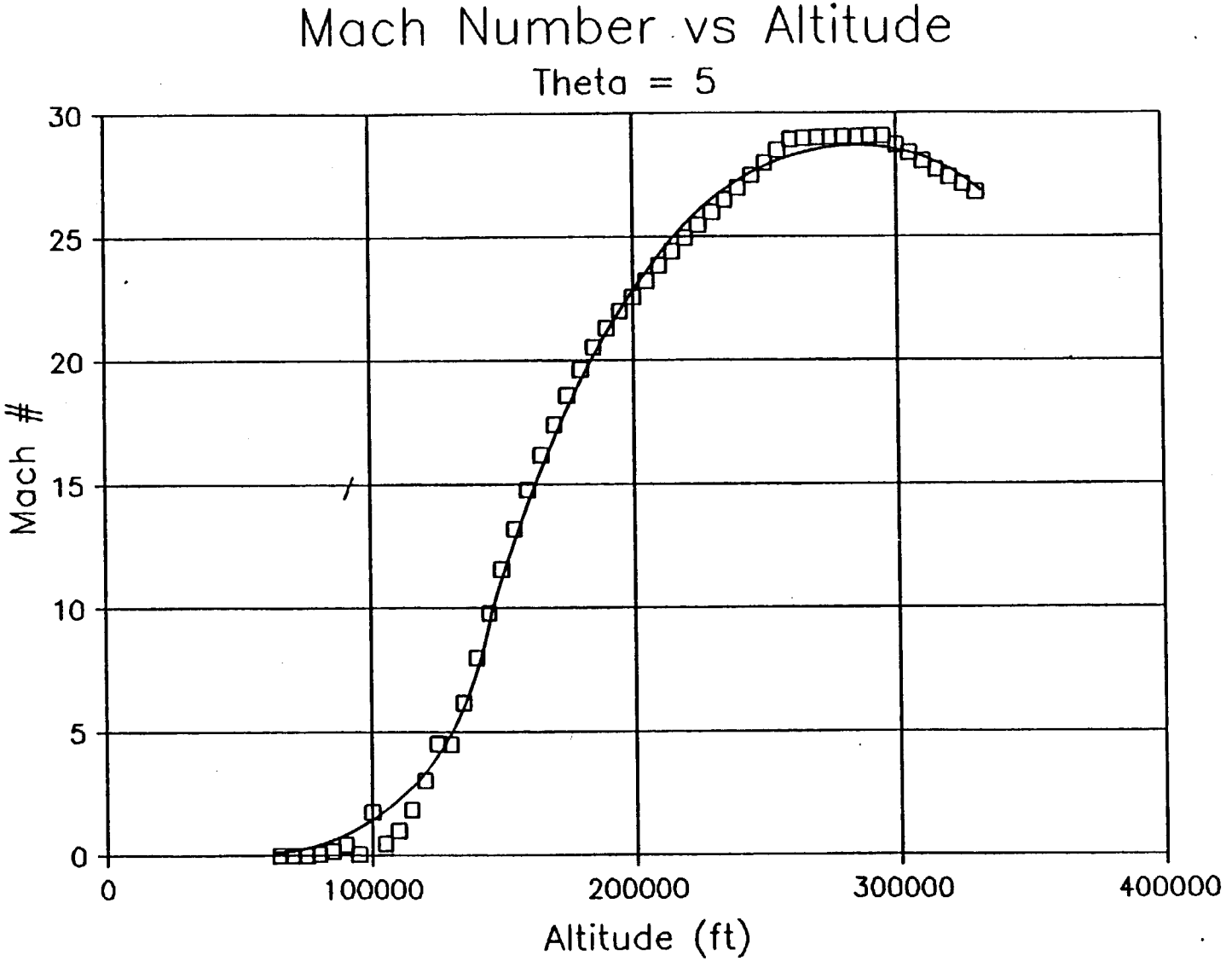

Figure 18. Mach Number as a Function of Altitude for Ballistic Reentry at an Initial Flight Path Angle of Five Degrees.

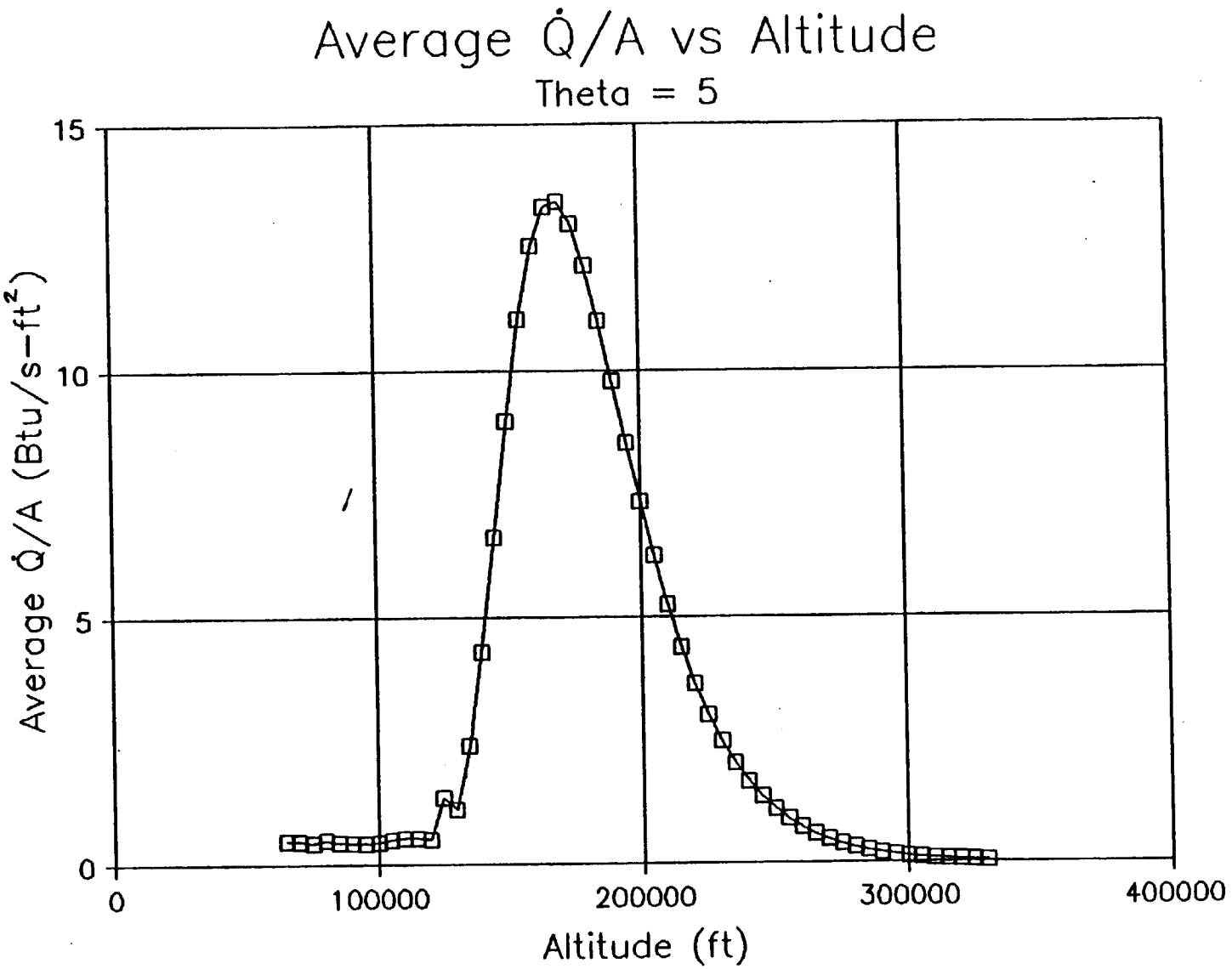

Figure 19. Average Heat Flow Rate per Unit Area as a Function of Altitude for Ballistic Reentry at an Initial Flight Path Angle of Five Degrees.

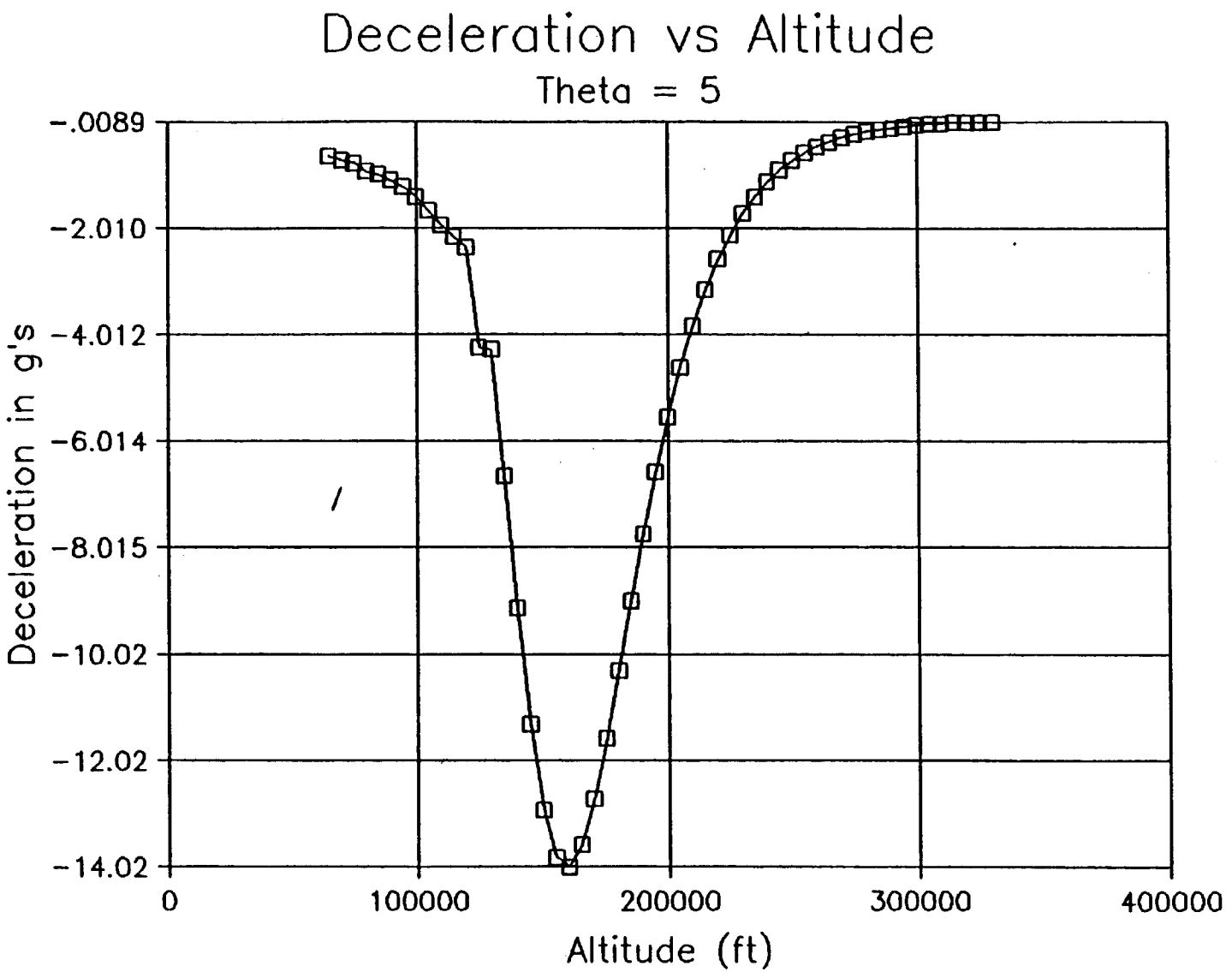

Figure 20. Deceleration Measured in Earth g's as a Function of Altitude for Ballistic Reentry at a Flight Path Angle Equal to Five Degrees.

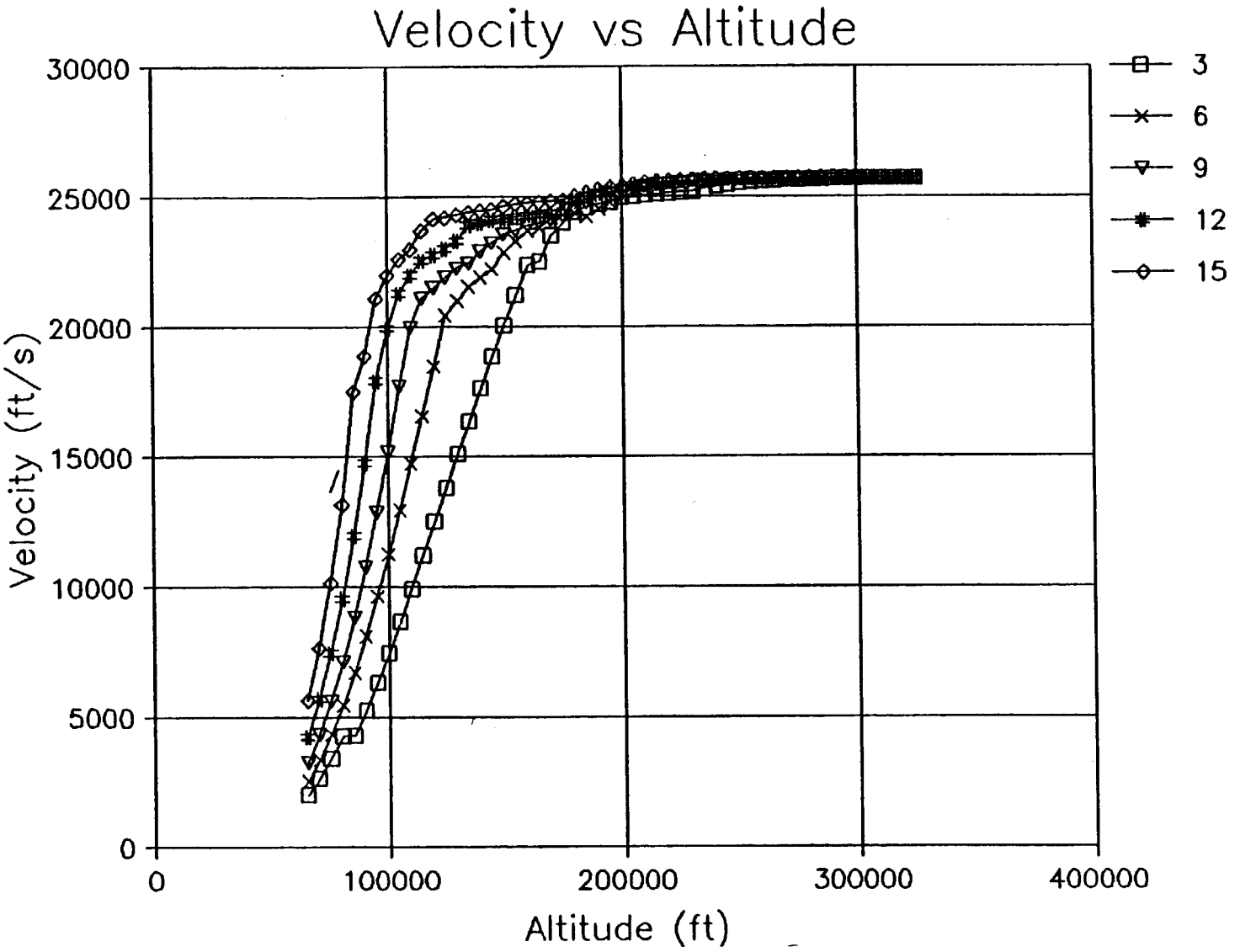

Figure 21. Velocity as a Function of Altitude for Reentry with L/D Equal to 0.25 at Initial Flight Path Angles Ranging From three to Fifteen Degrees.

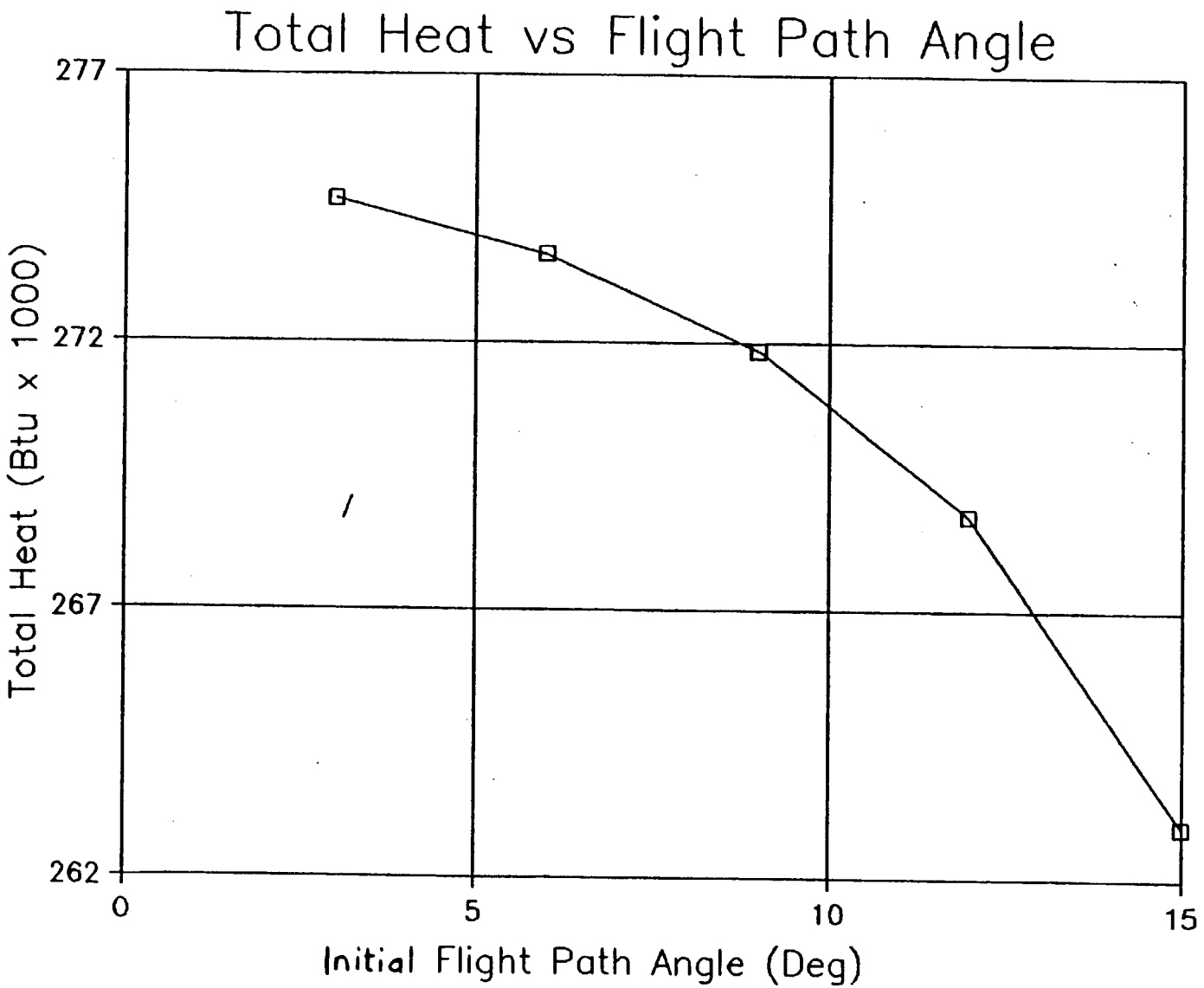

Figure 22. Total Heat Absorbed as a Function of Initial Flight Path Angle for Reentry With L/D equal to 0.25.

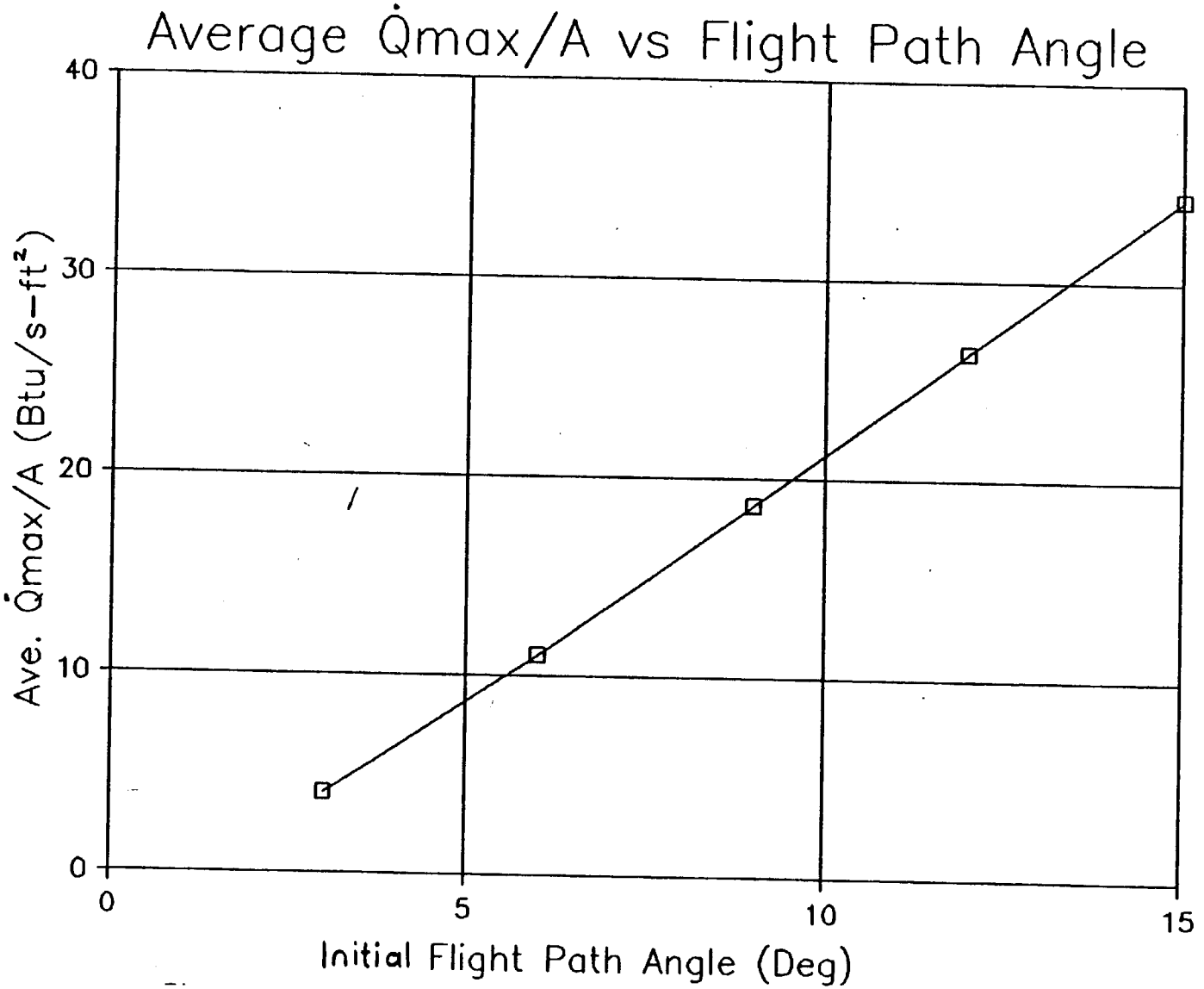

Figure 23. Average Heat Flow Rate per Unit Area as a Function of Initial Flight Path Angle for Reentry with L/D equal 0.25.

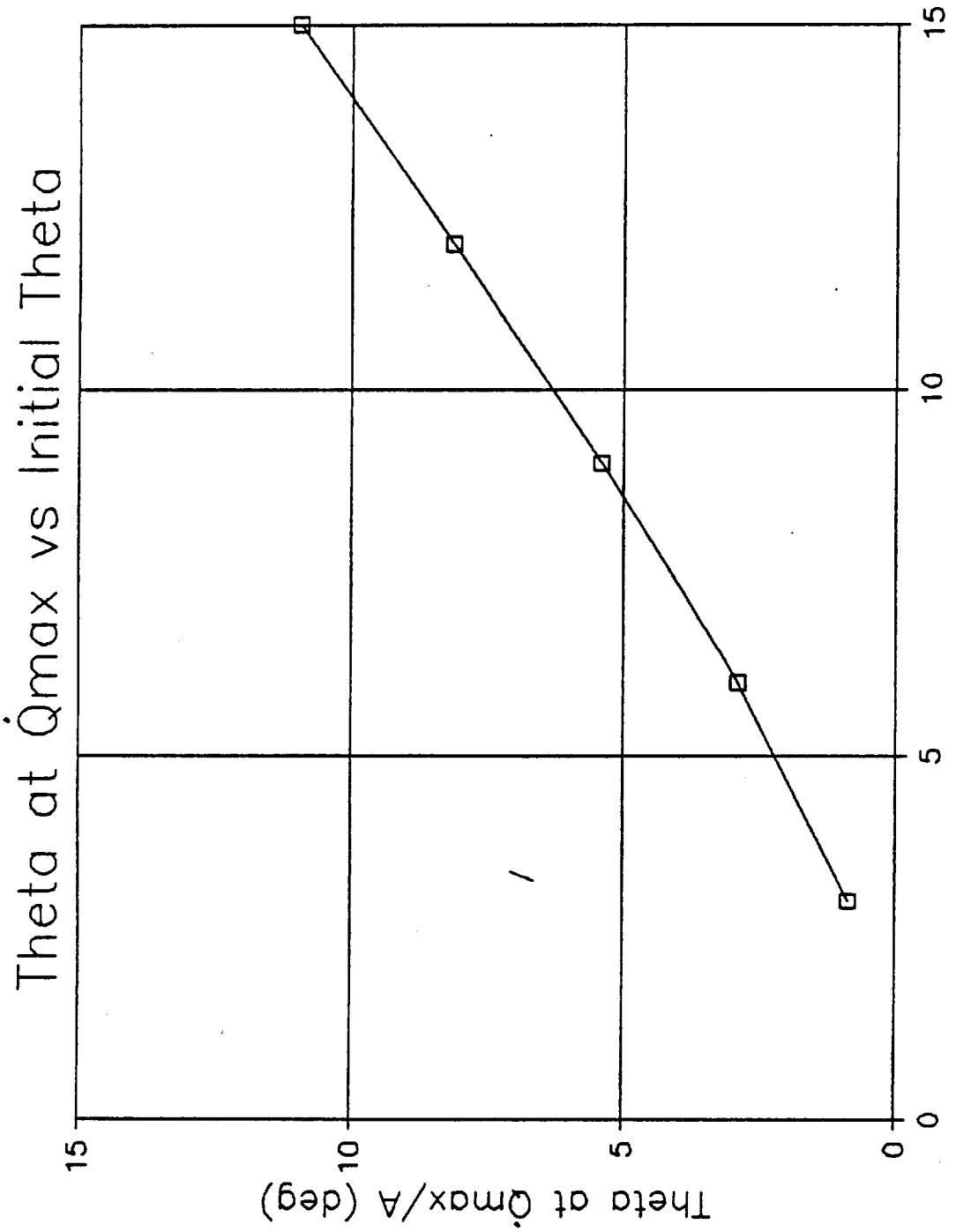

Figure 24. Flight Path Angle at Maximum Heat Flow Rate as a Function of Initial Flight Path Angle for Reentry with L/D equal to 0.25.

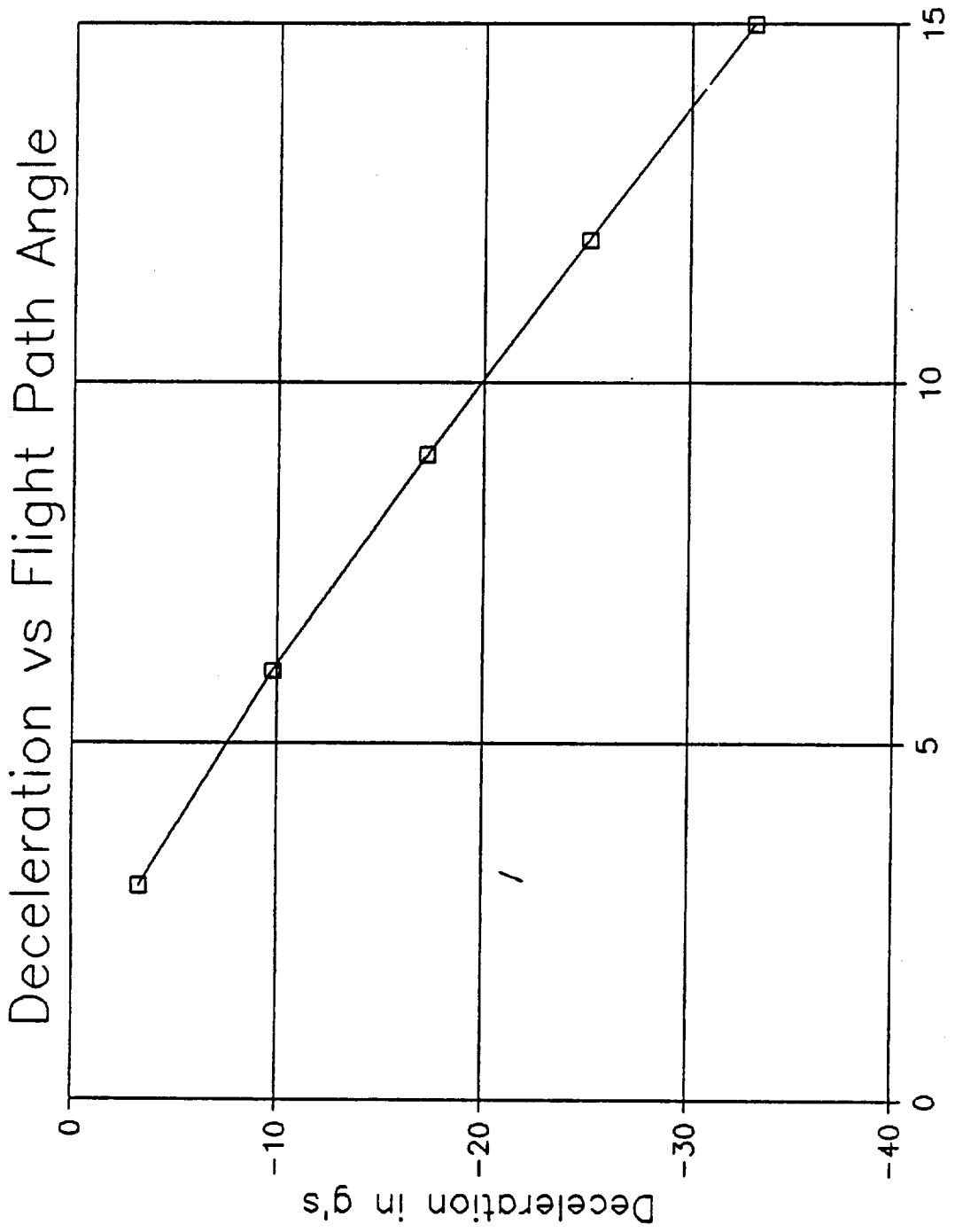

Figure 25. Deceleration Measured in Earth g's as a Function of Initial Flight Path Angle for reentry with L/D equal to 0.25.

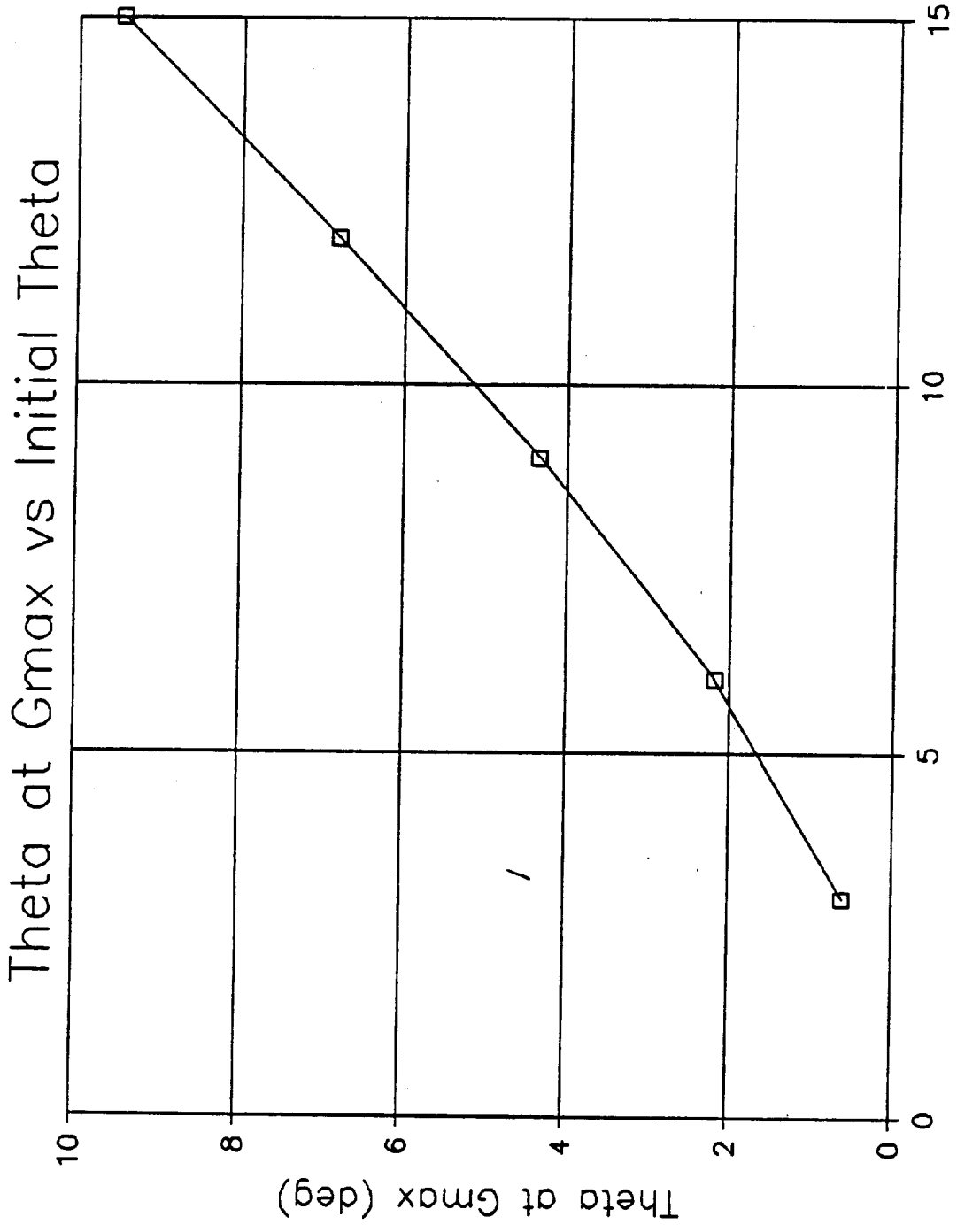

Figure 26. Flight Path Angle at Maximum Deceleration as a Function of Initial Flight Path Angle for Reentry with L/D equal to 0.25.

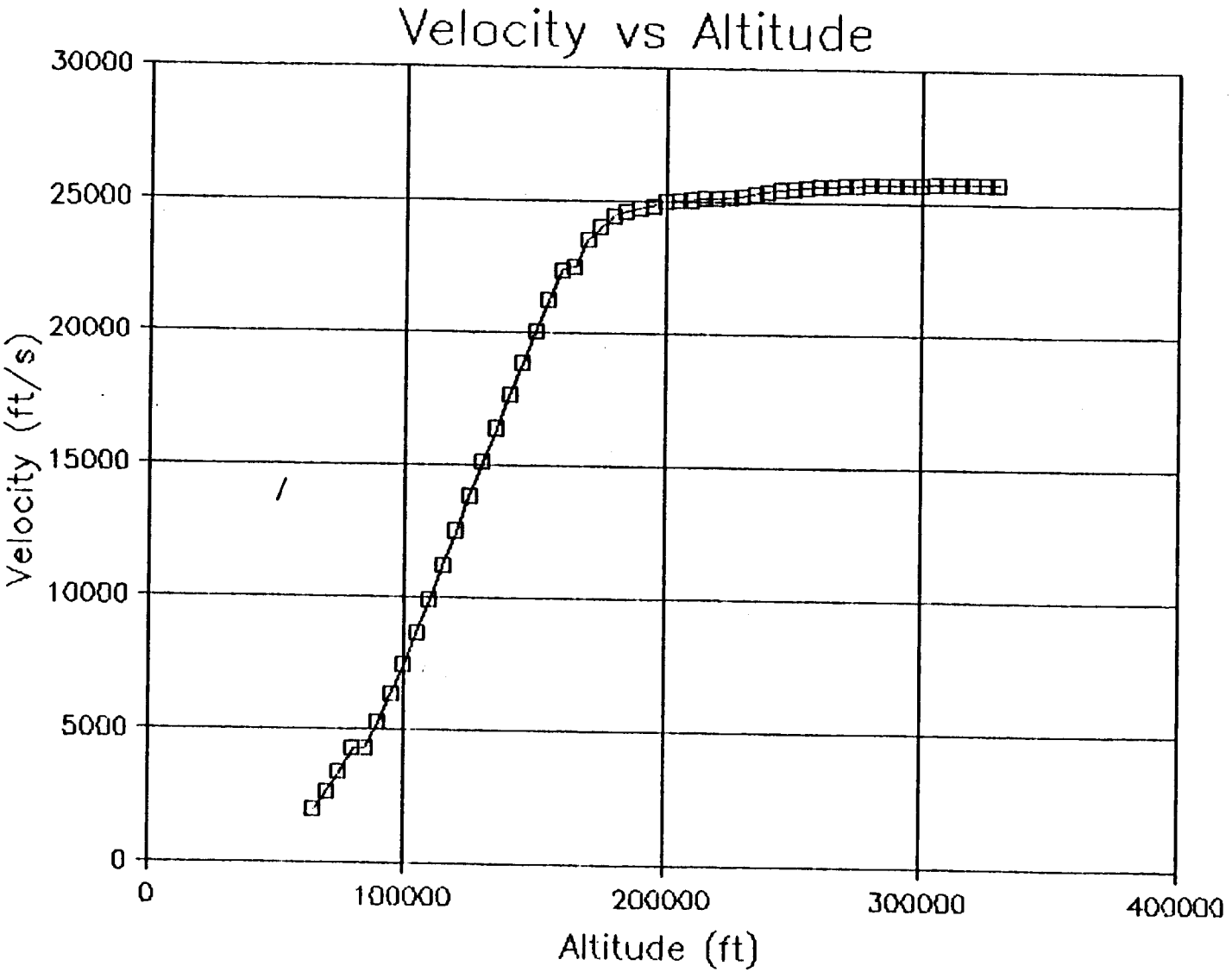

Figure 27. Velocity as a Function of Altitude for Reentry with L/D equal to 0.25 at an Initial Flight Path Angle Equal to three Degrees.

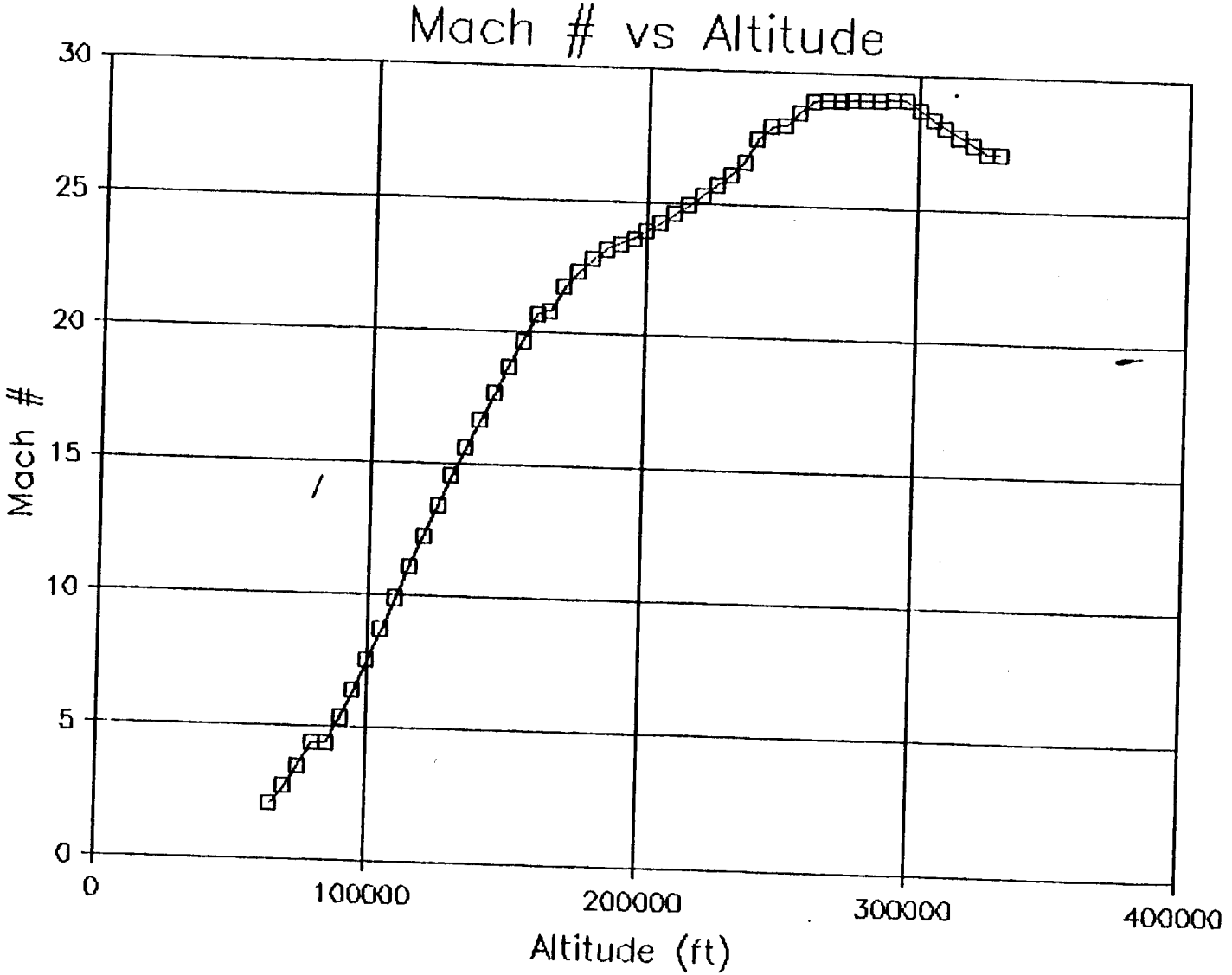

Figure 28. Mach Number as a Function of Altitude for Reentry with L/D equal to 0.25 at an Initial Flight Path Angle Equal to three Degrees.

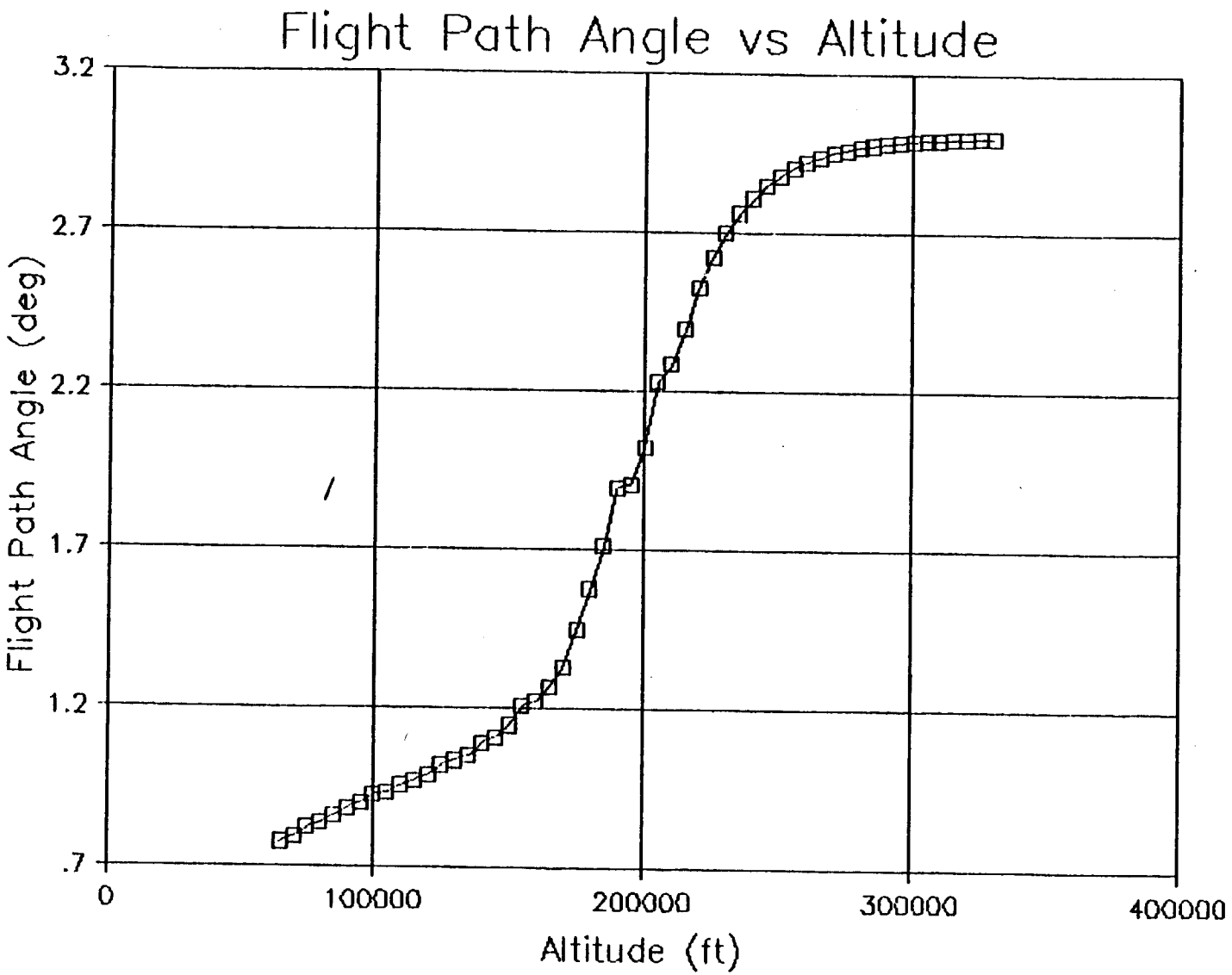

Figure 29. Flight Path Angle as a Function of Altitude for Reentry with L/D equal to 0.25 at an Initial Flight Path Angle Equal to three Degrees.

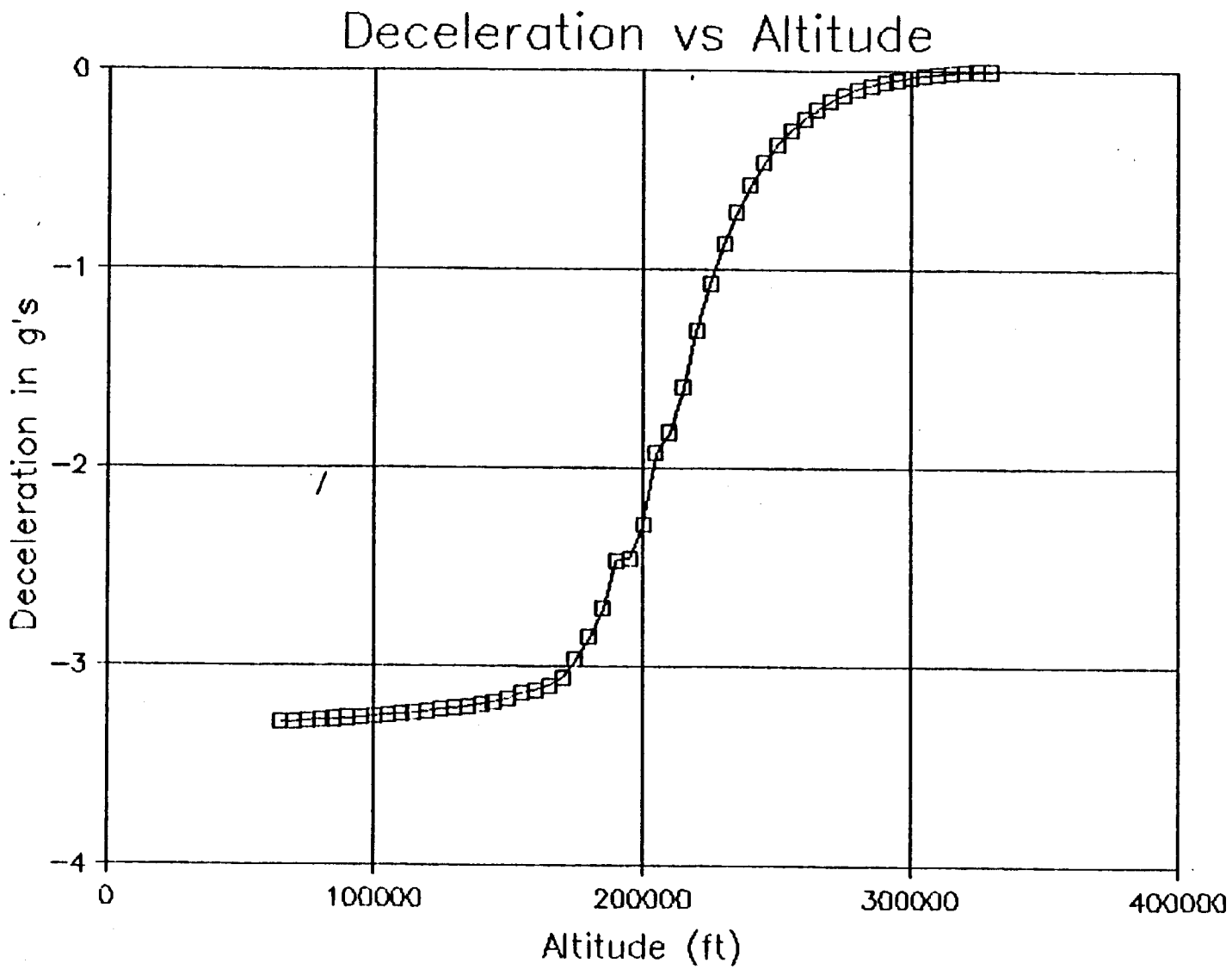

Figure 30. Deceleration Measured in Earth g's as a Function of Altitude for Reentry With L/D equal to 0.25 at an Initial Flight Path Angle Equal to three Degrees.

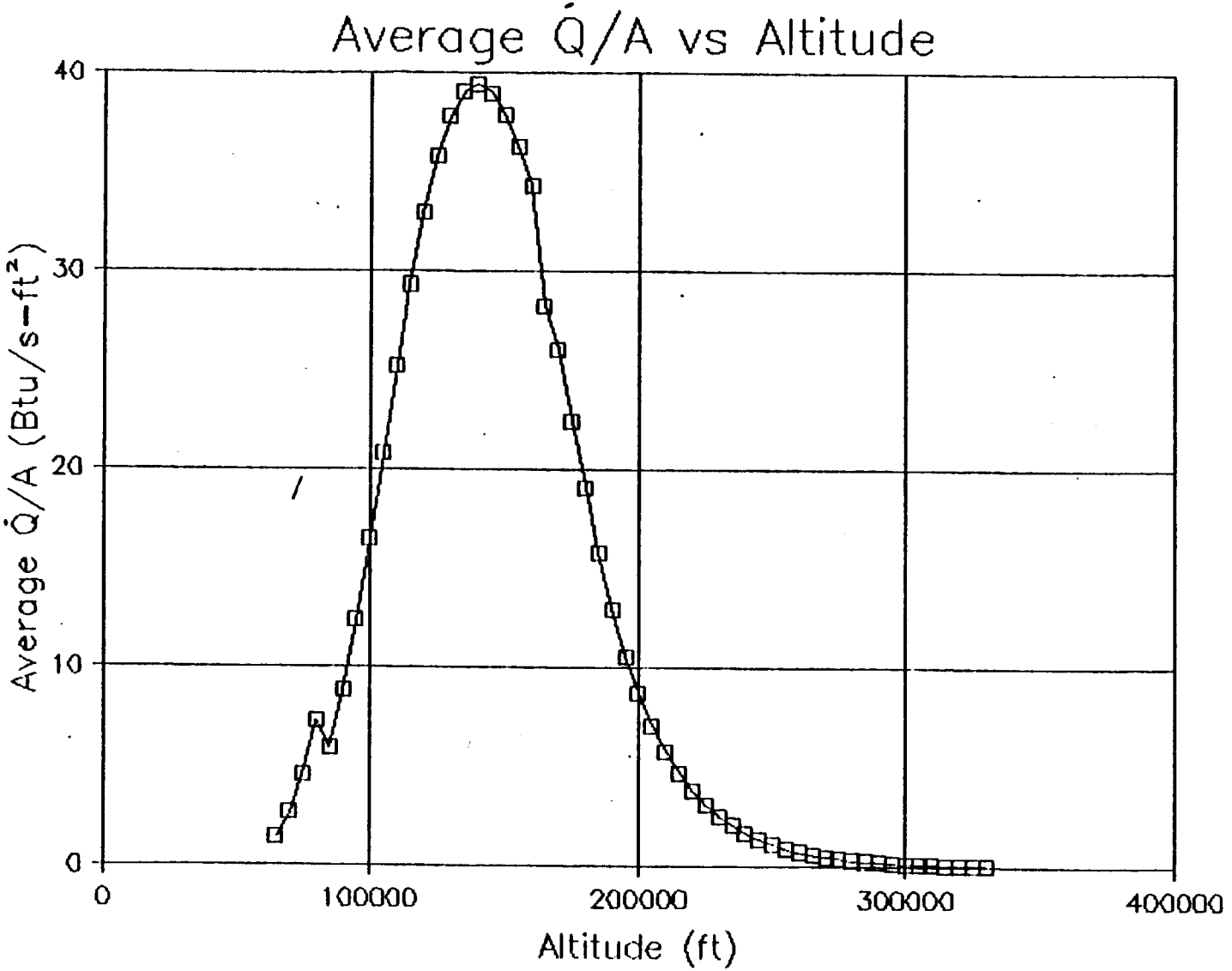

Figure 31. Average Heat Flow Rate Per Unit Area as a Function of Altitude for Reentry with L/D equal to 0.25 at an Initial Flight Path Angle Equal to three Degrees.

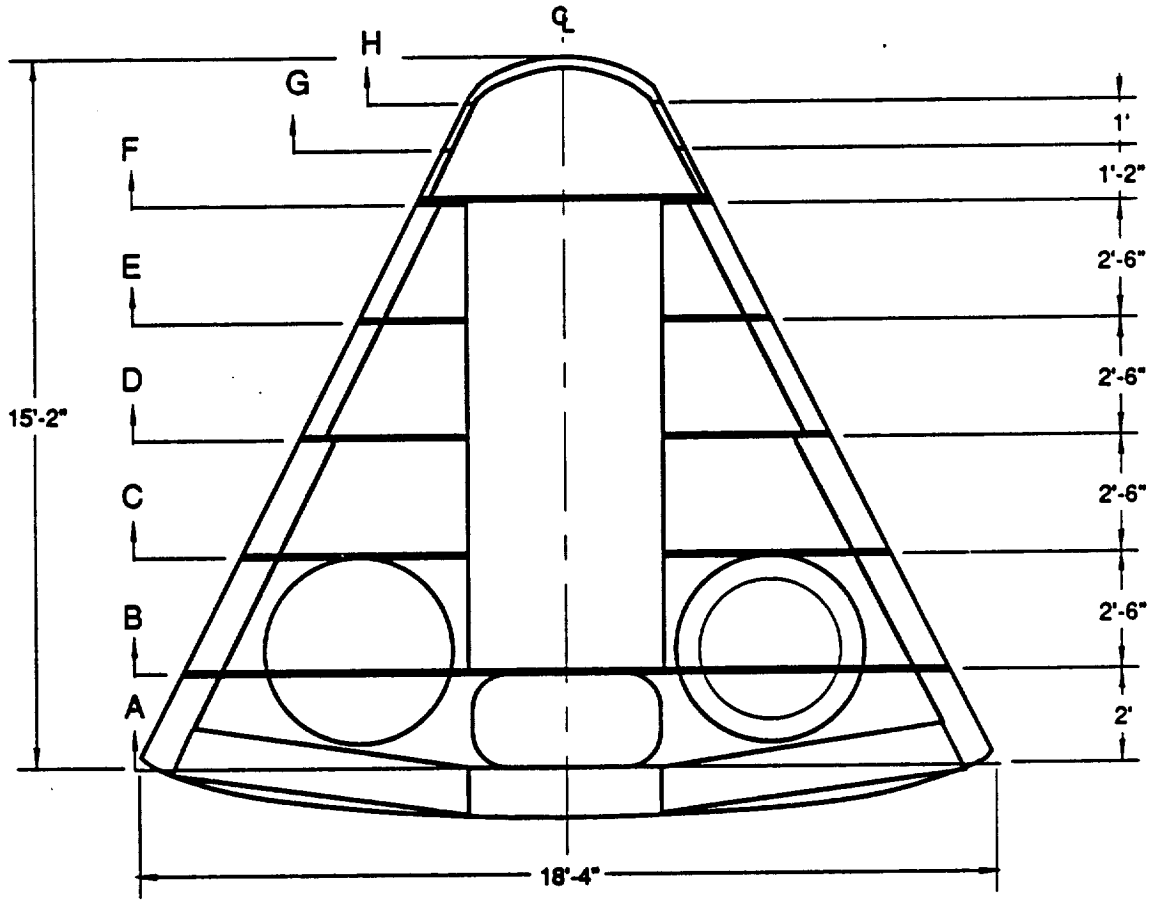

Figure 32A. Capsule Structural Design With Dimensions: Side View and Sectional Views.

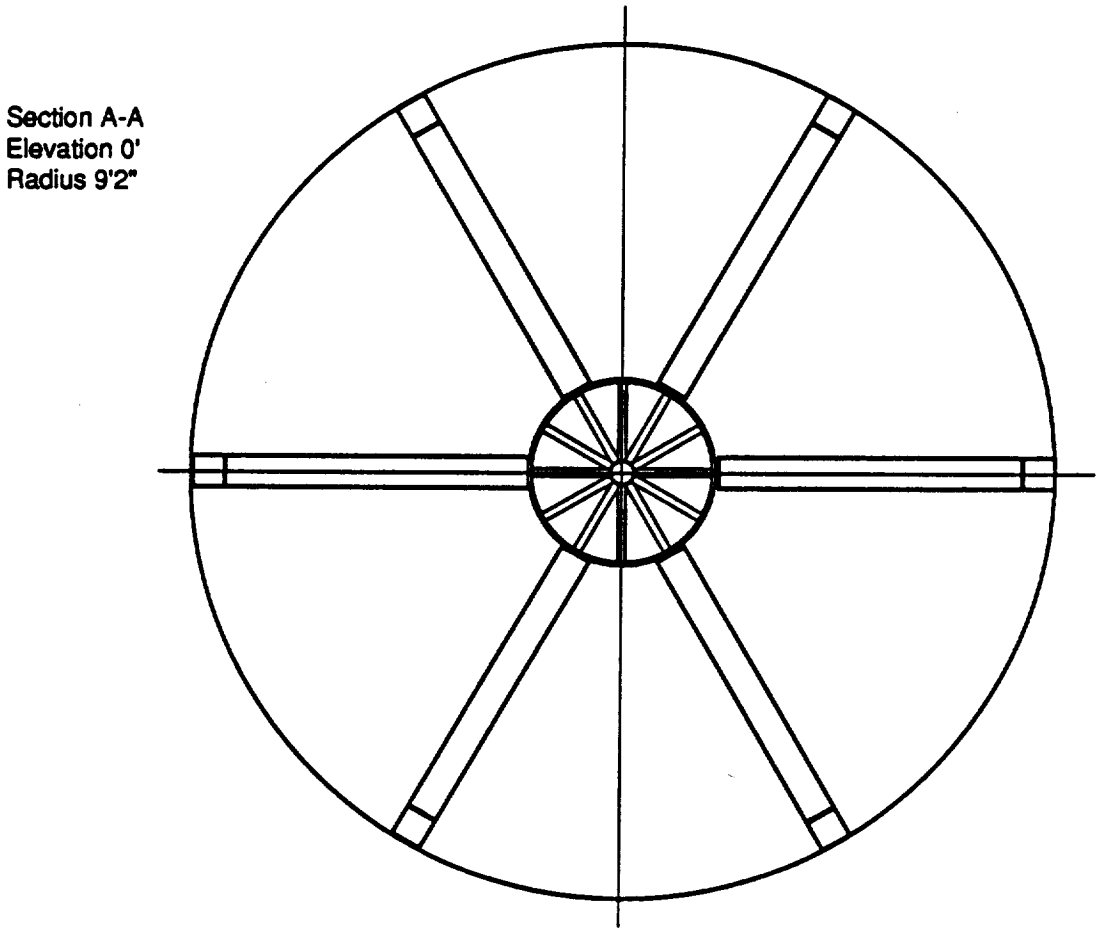

Figure 32B. Capsule Structural Design With Dimensions: Side View and Sectional Views.

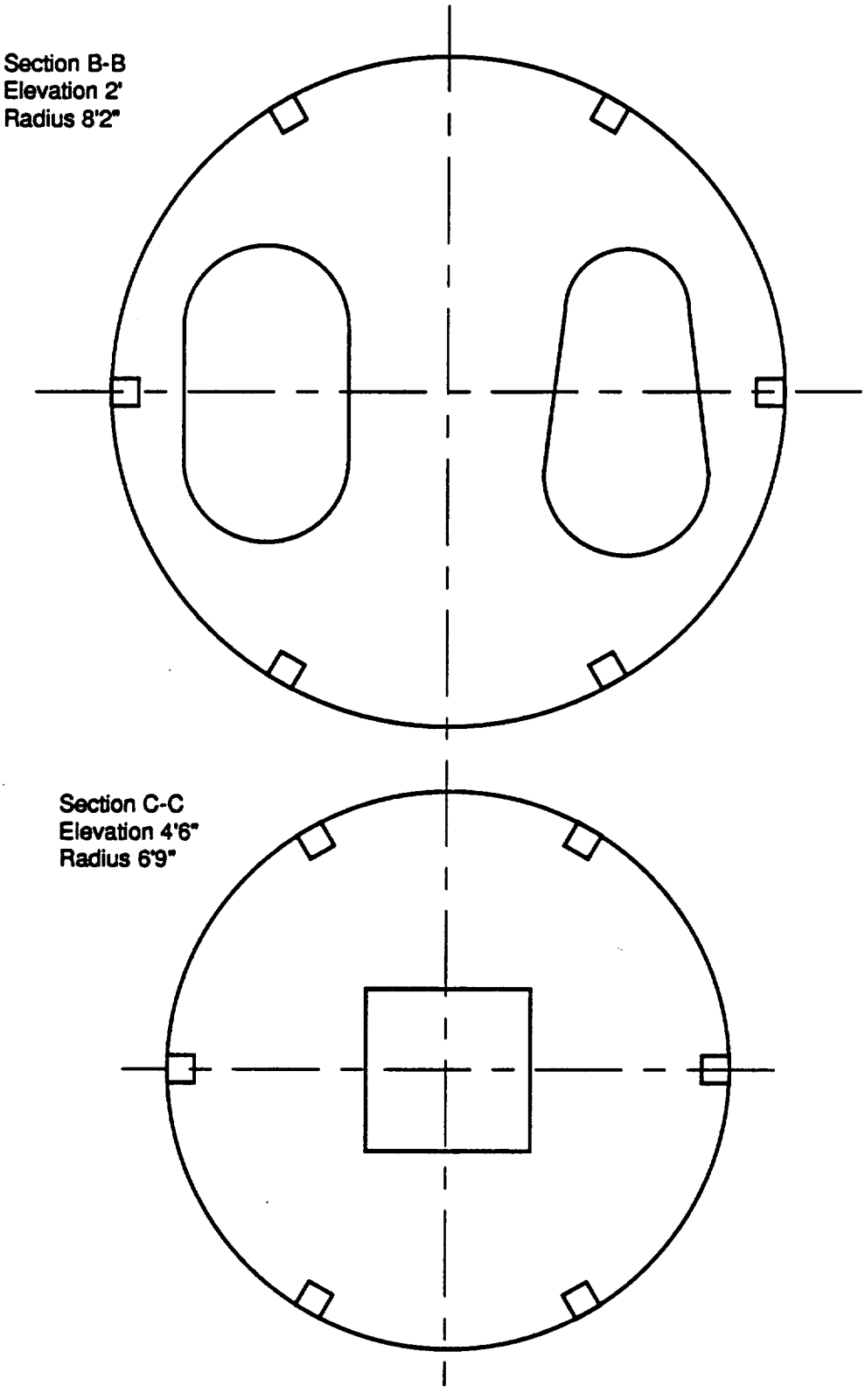

Figure 32C. Capsule Structural Design With Dimensions: Side View and Sectional Views.

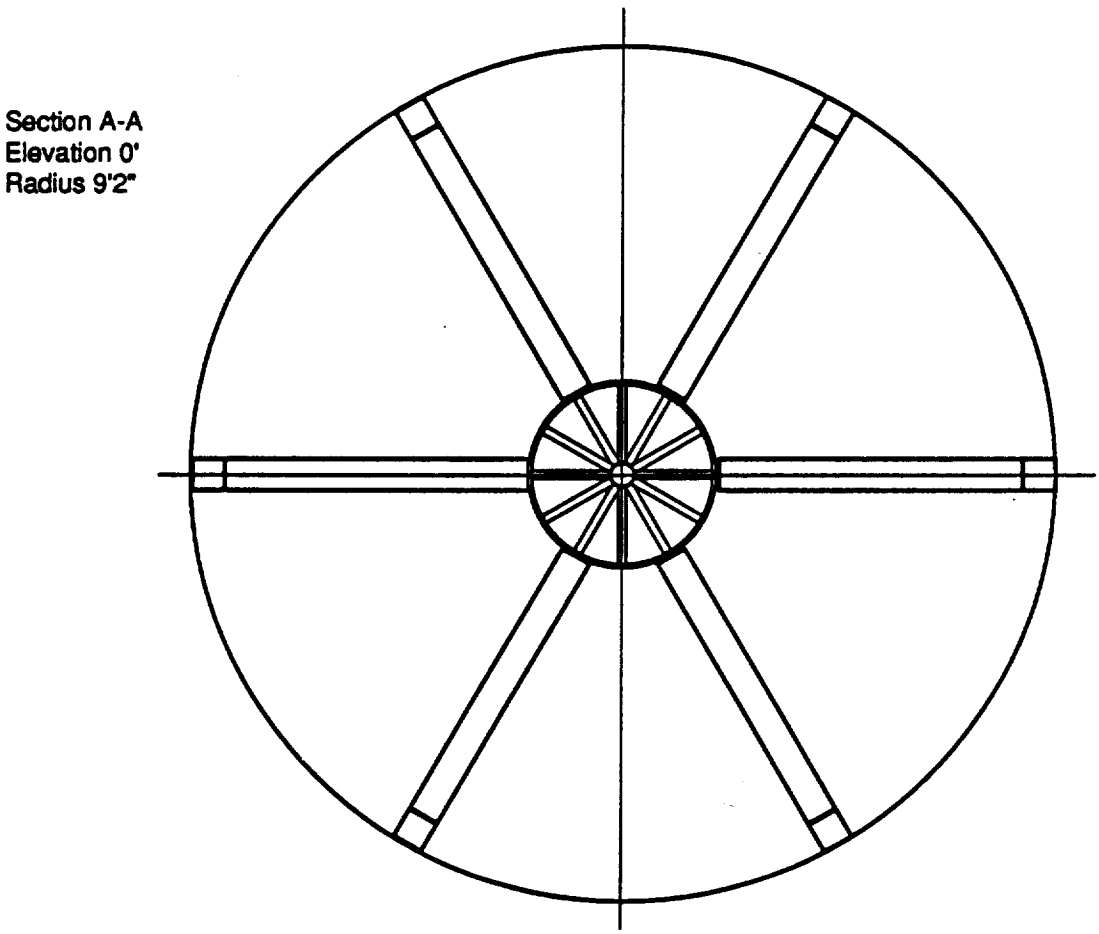

Figure 32B. Capsule Structural Design With Dimensions: Side View and Sectional Views.

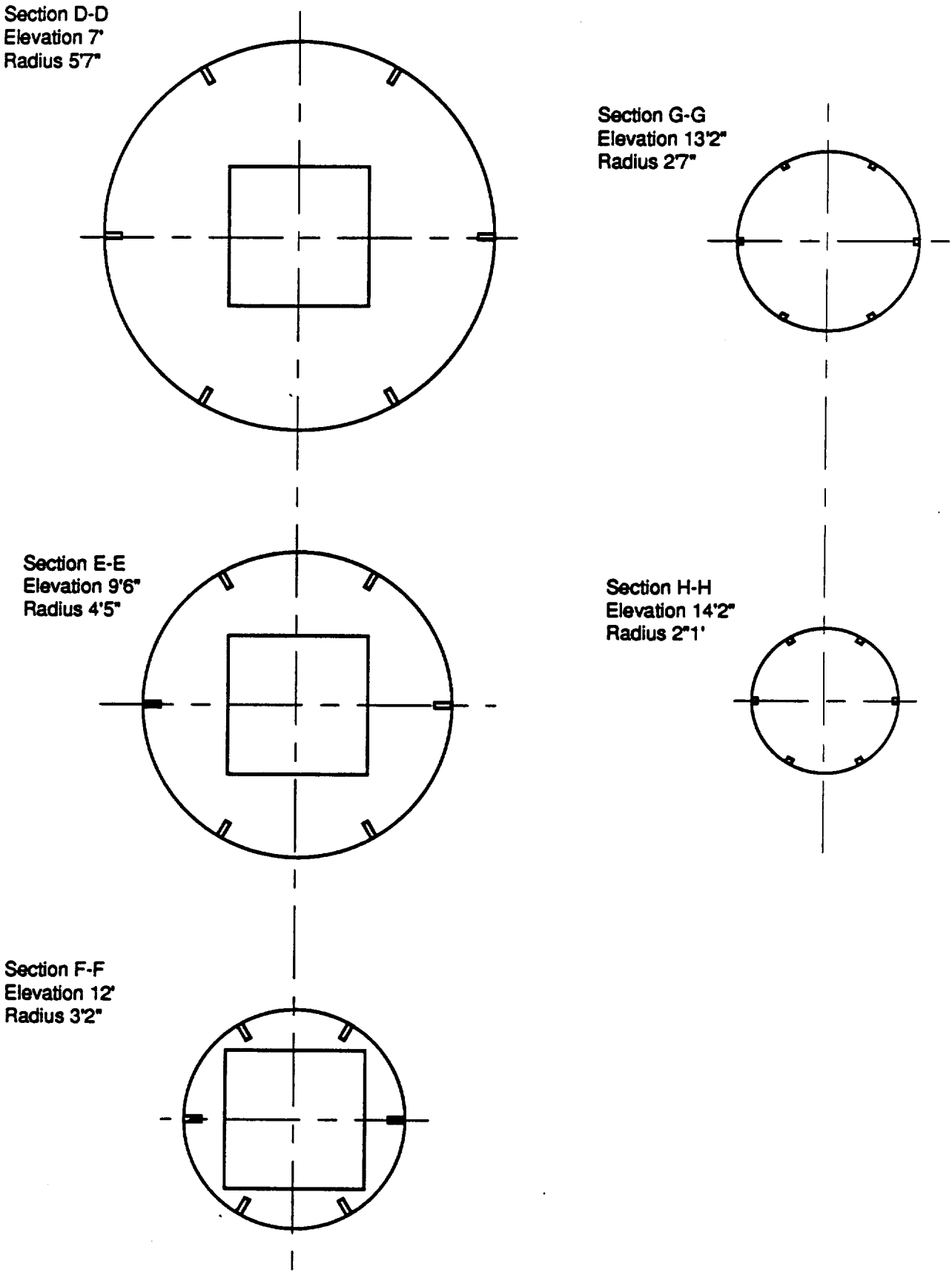

Figure 32D. Capsule Structural Design With Dimensions: Side View and Sectional Views.

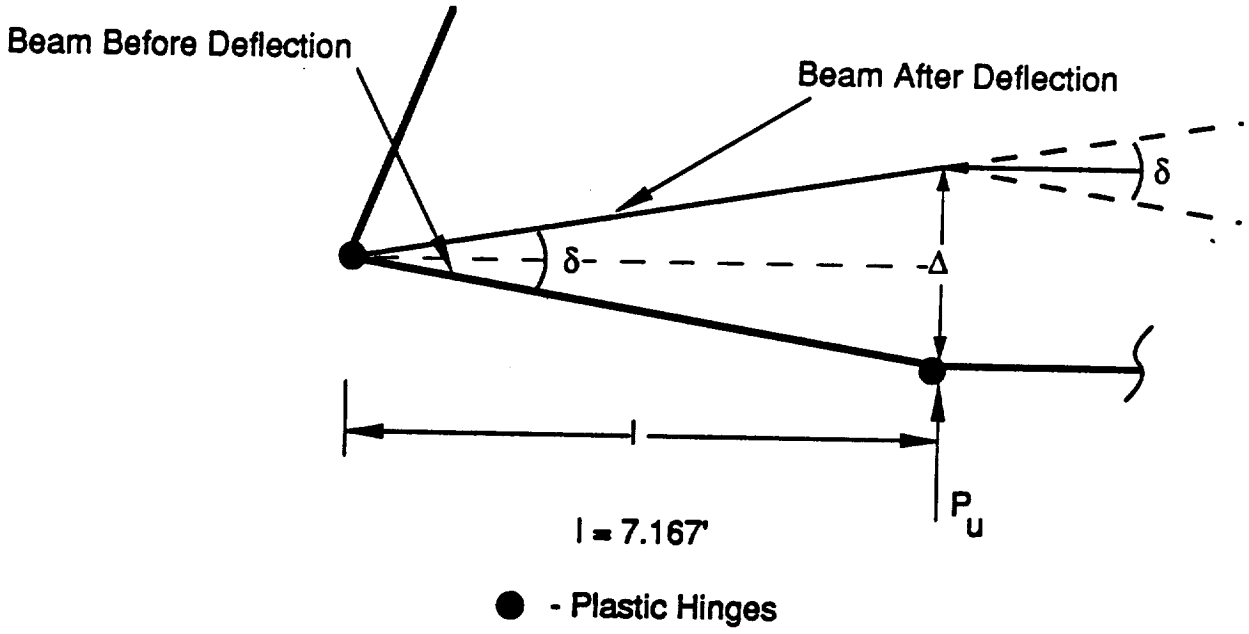

Figure 33. Plastic Hinge Diagram.

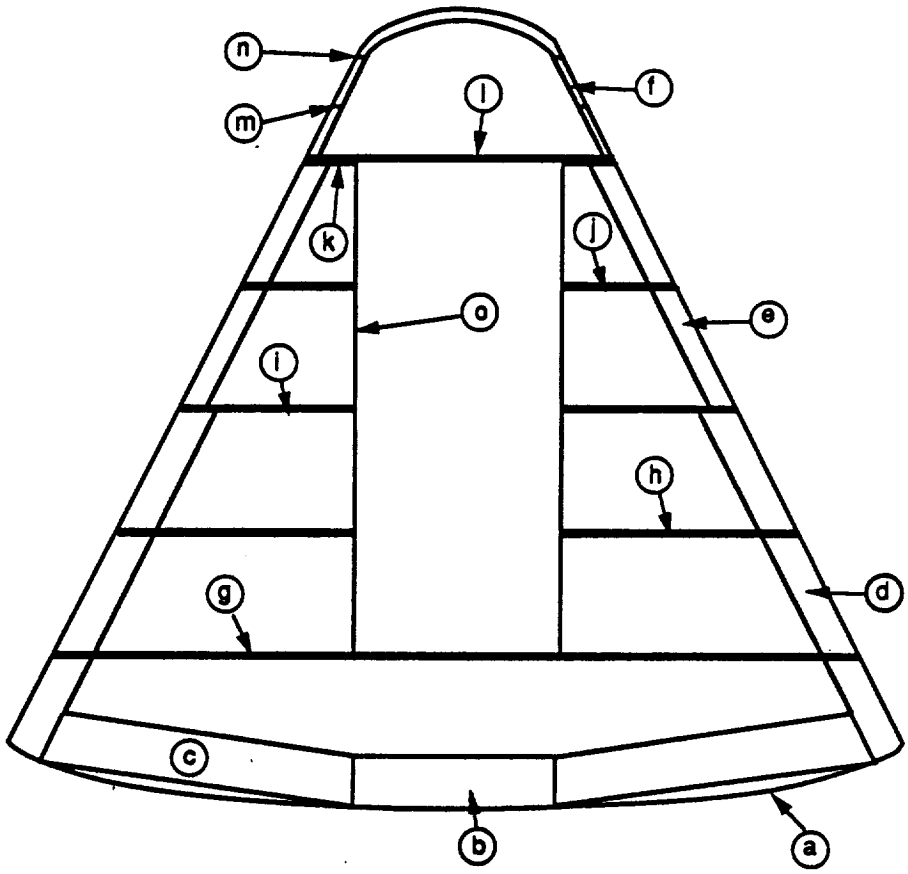

Figure 34. Capsule Structural Parts Identification.

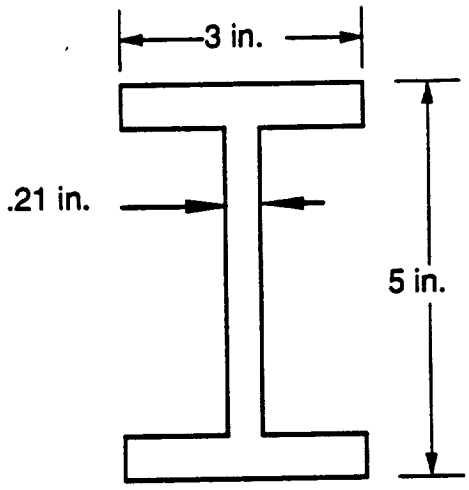

Extrusion No. S 851-C
3.43 lb/ft
$I = 12.26\ in^4$
Cross Sectional Area = $2.92\ in^2$

Figure 35. Extrusion No. S 851-C Dimensions and Properties.

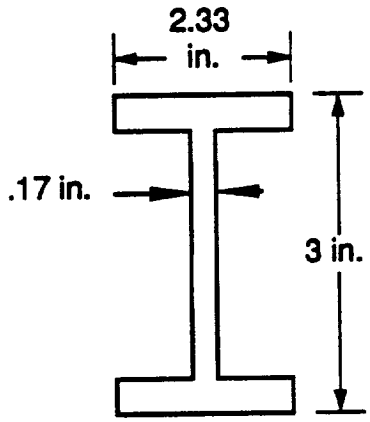

Extrusion No. S 851-A
1.96 lb/ft
$I = 2.52\ in^4$
Cross Sectional Area = $1.67\ in^2$

Figure 36. Extrusion No. S 851-A Dimensions and Properties.

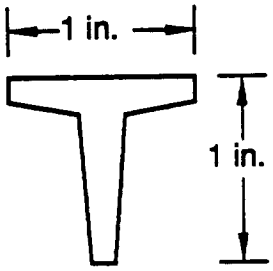

Extrusion No. 853-F
0.31 lb/ft
$I = .023\ in^4$
Cross Sectional Area = $0.27\ in^2$

Figure 37. Extrusion No. 853-F Dimensions and Properties.

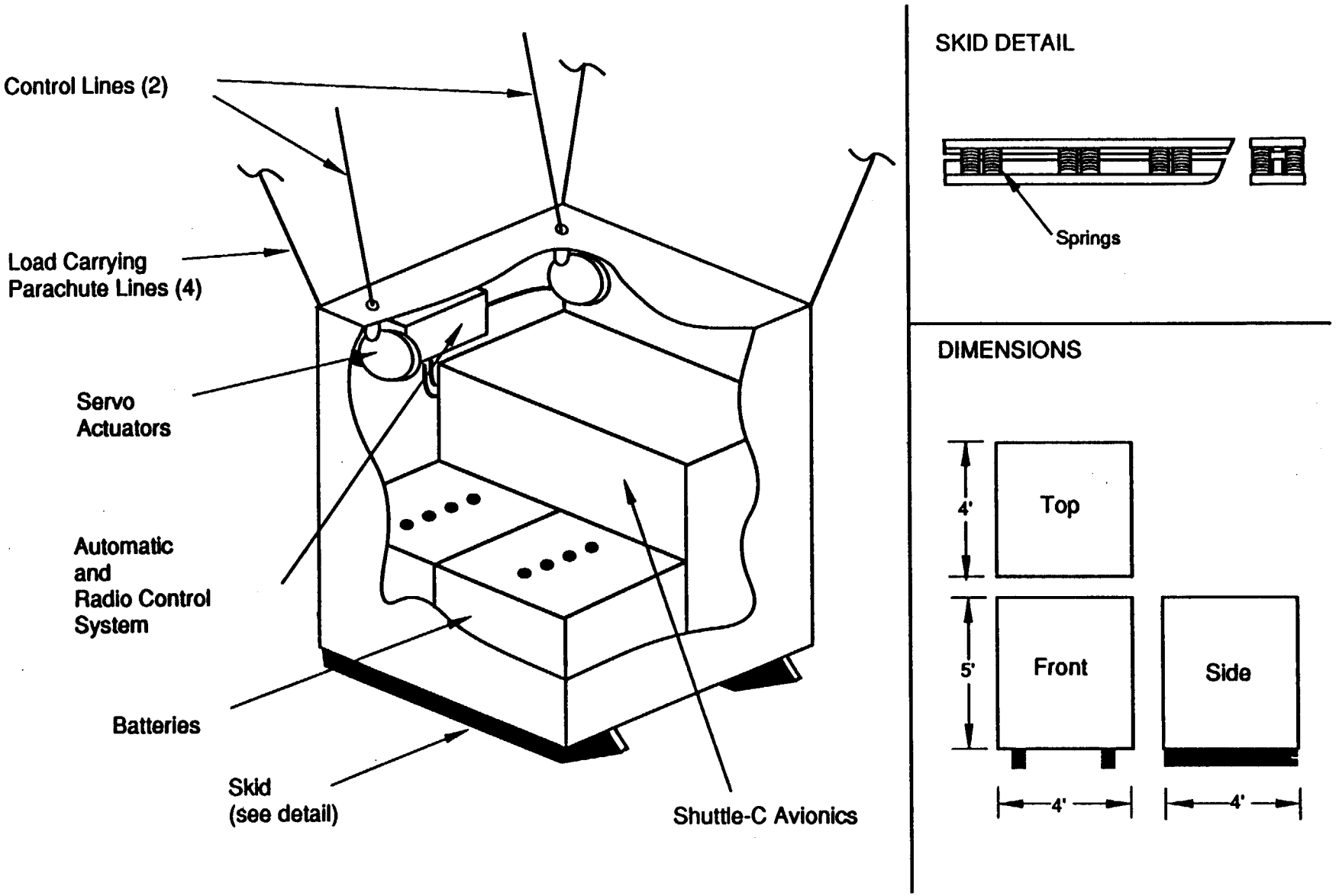

Figure 38. Avionics Module Cutaway View With Skid Detail and Dimensions.

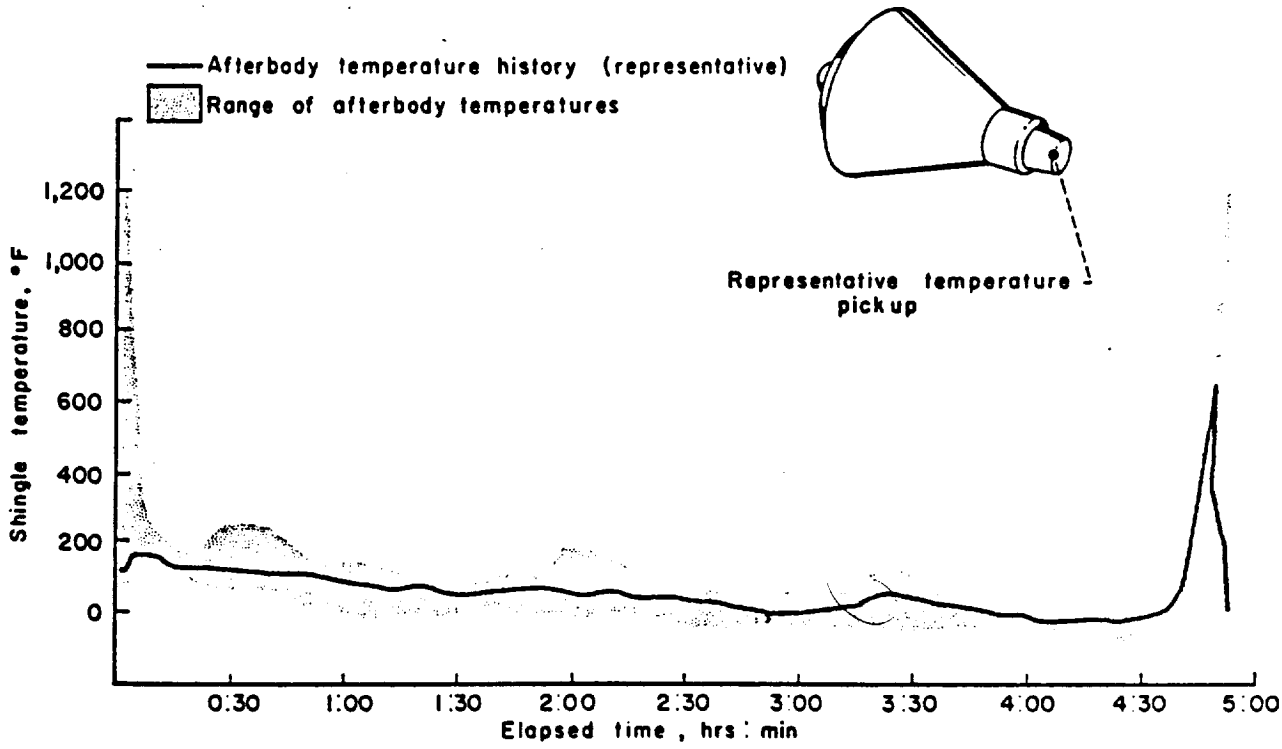

Figure 39. Temperature Ranges for the Mercury Capsules Tower Section Over a Five Hour Mission. Peak Temperature During Reentry At 4:45 hrs.

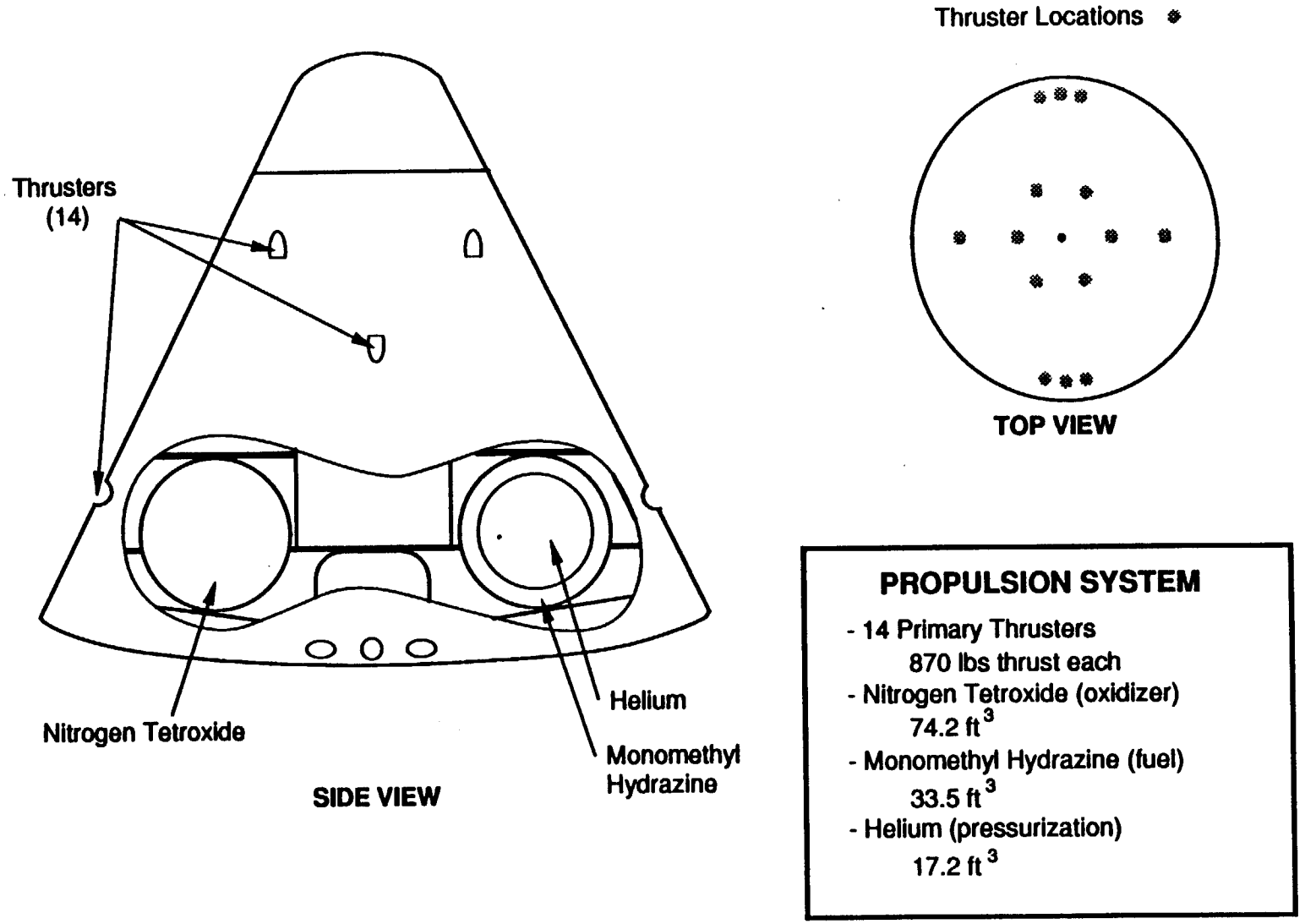

Figure 40. Thruster and Tank Locations of the Capsule Reaction Control System.

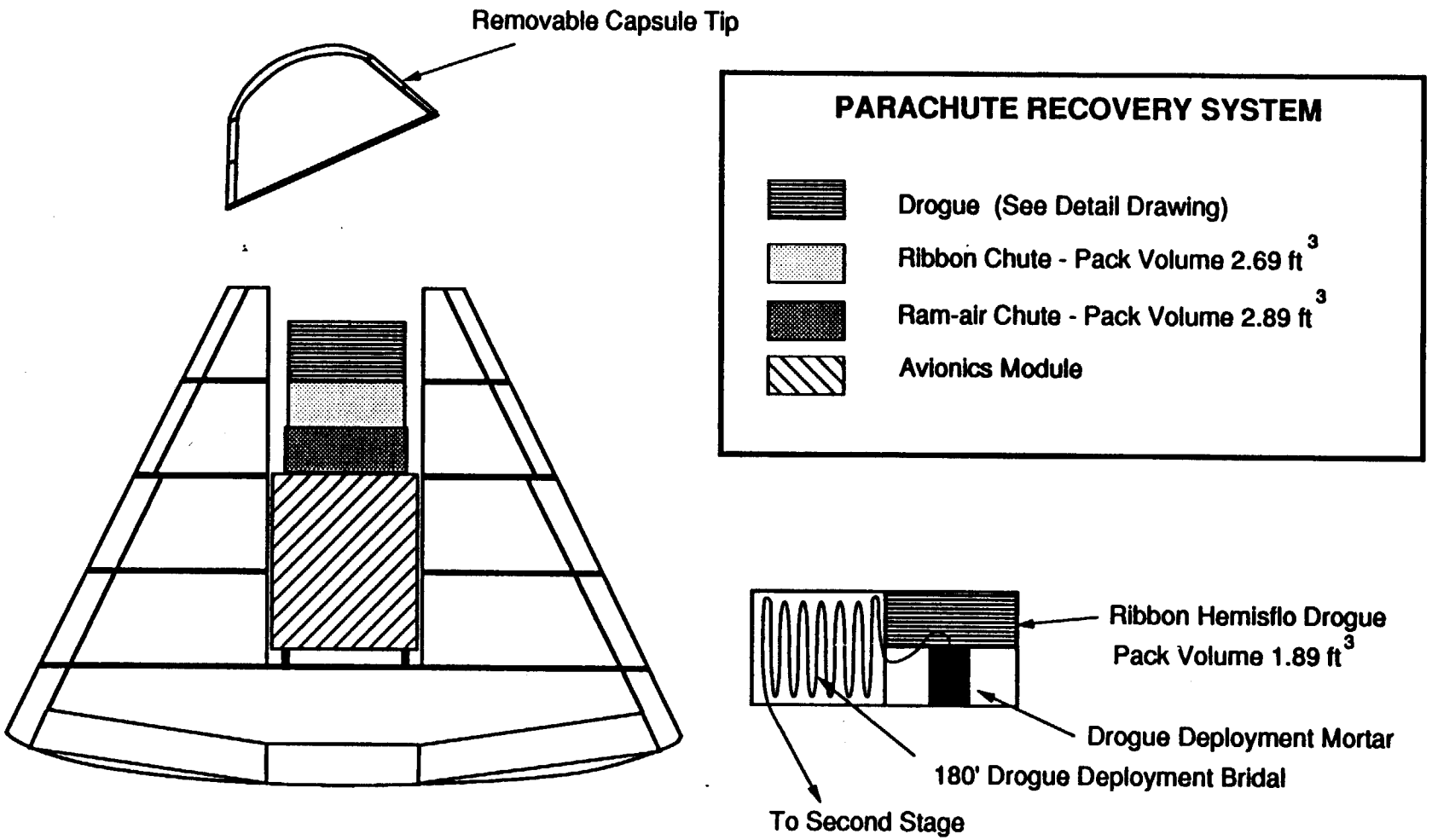

Figure 41. Location of the Three Stage Parachute Recovery System in the Reentry Capsule.

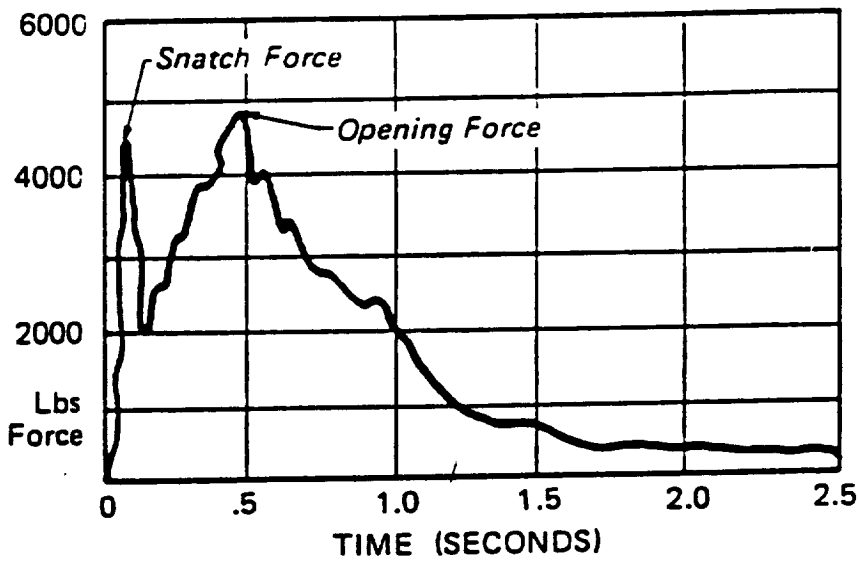

Figure 42. Snatch and Opening Forces as a Function of Time.

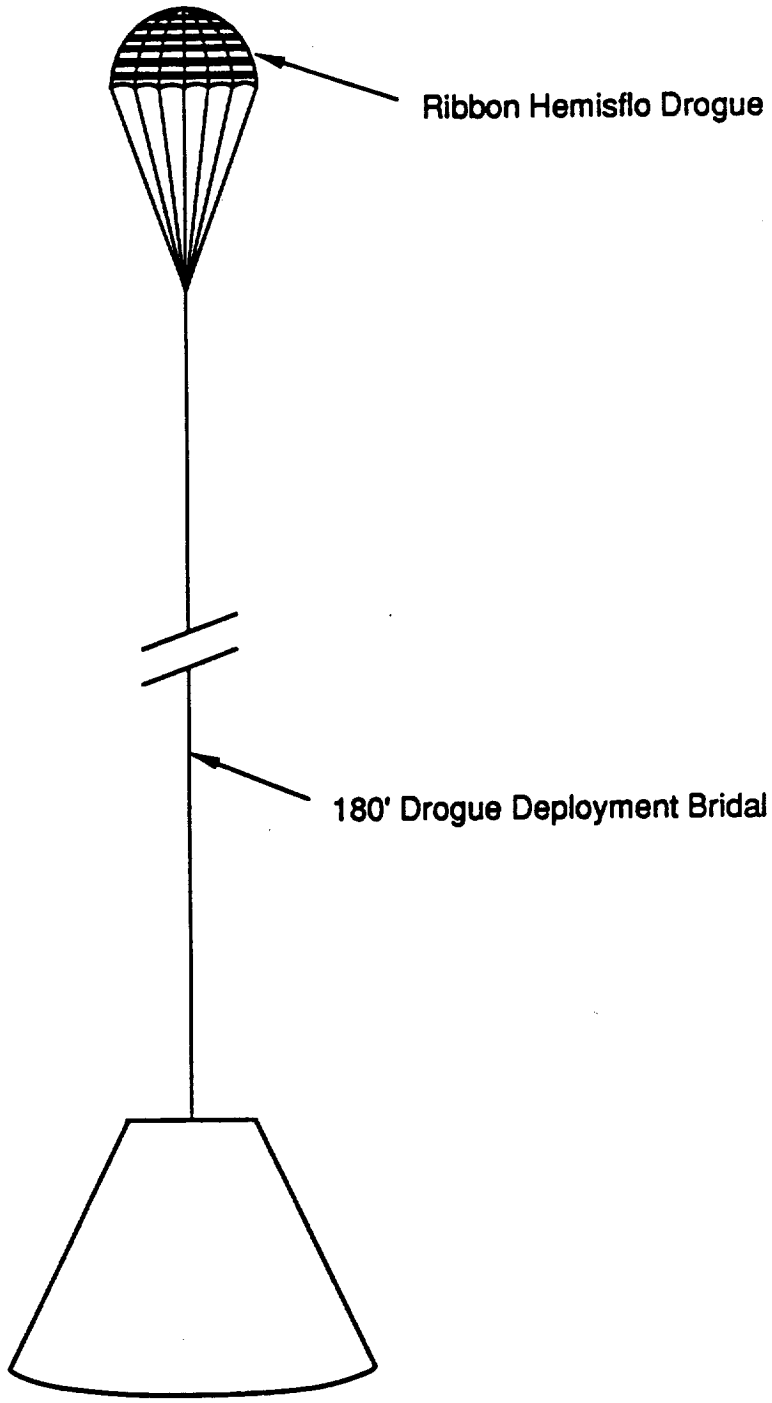

Figure 43. Ribbon Hemisflo Drogue and Attaching Bridal.

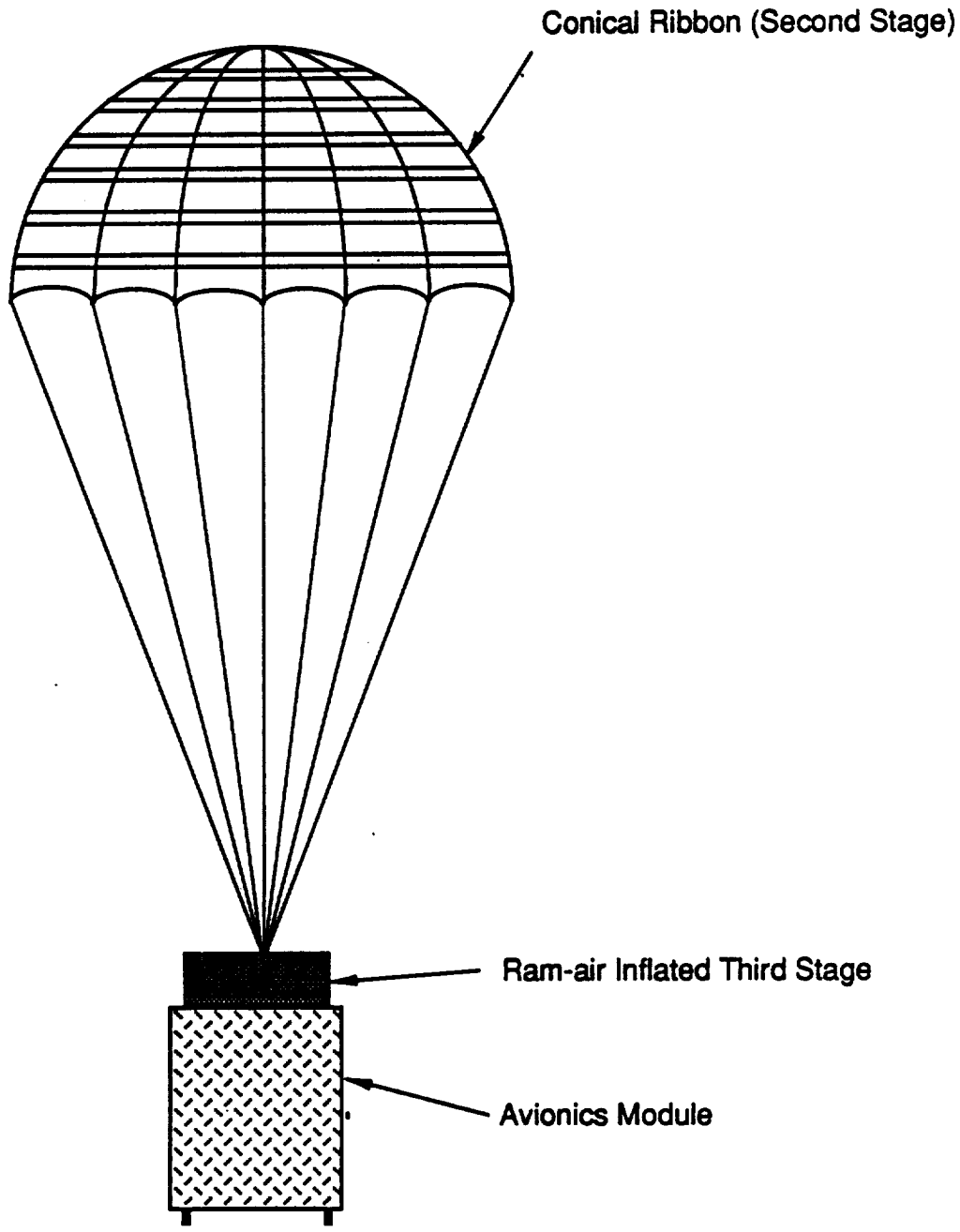

Figure 44. Conical Ribbon Parachute.

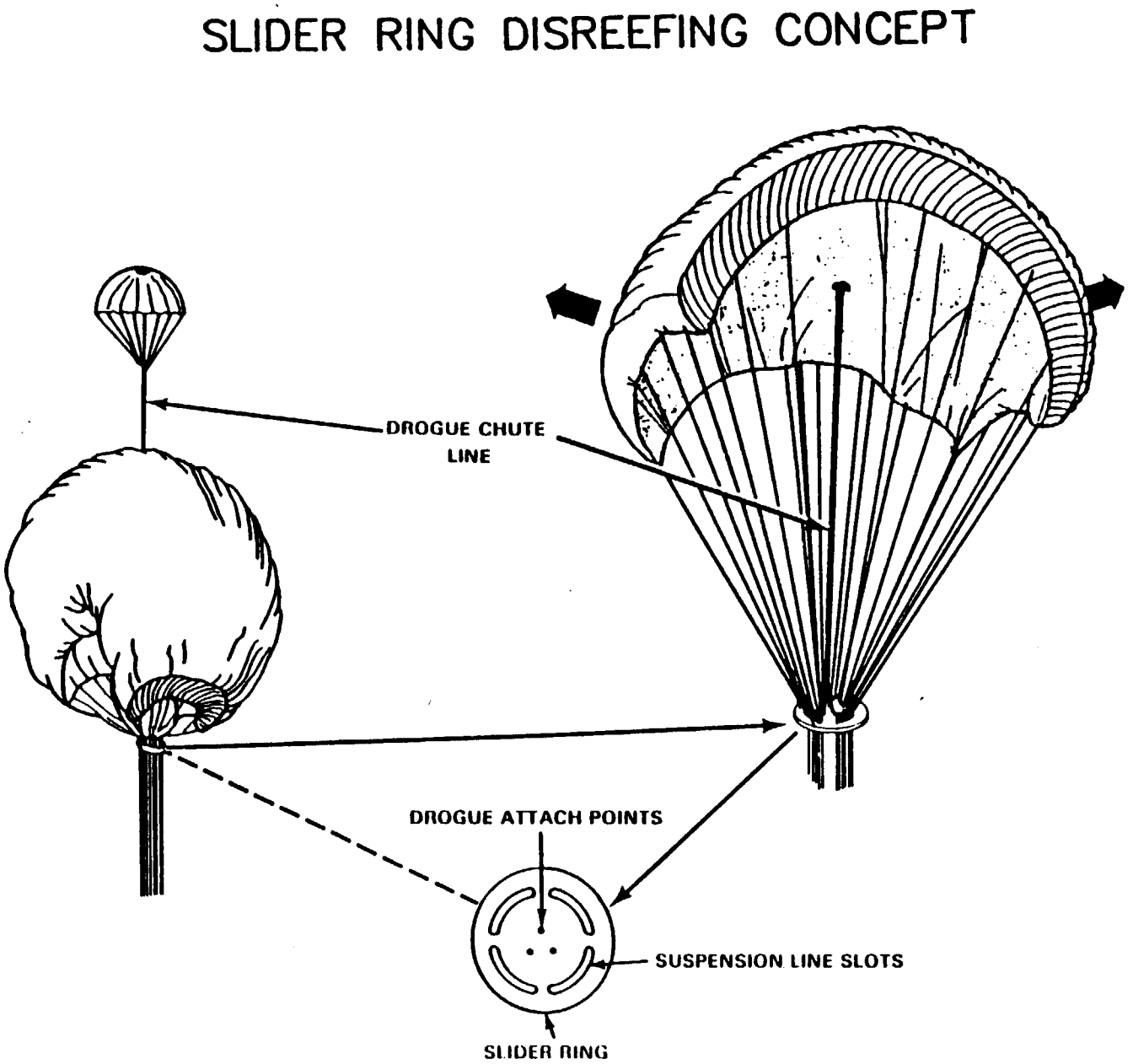

Figure 45. Parachute Reefing System.

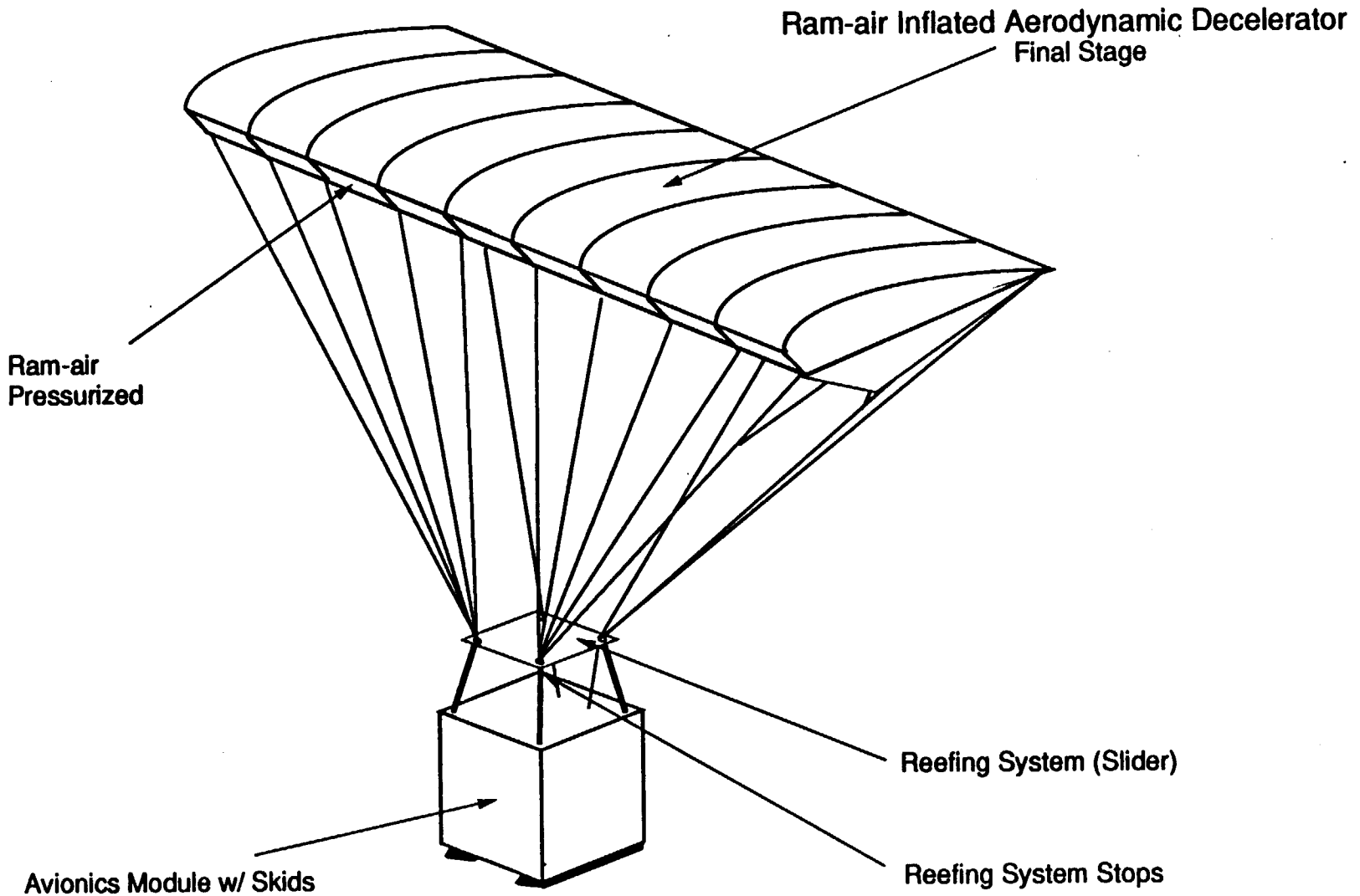

Figure 46. Inflated Ram-air Aerodynamic Decelerator.